PARAMETRIC OPTIMIZATION OF PERFORMANCE MEASURES OF WIRE ELECTRO-DISCHARGE MACHINING FOR TITANIUM MATRIX COMPOSITE

Thesis submitted by

SOUTRIK BOSE

Doctor of Philosophy (Engineering)

Department of Mechanical Engineering,

Faculty Council of Engineering & Technology

Jadavpur University

Kolkata, India

2022

JADAVPUR UNIVERSITY

KOLKATA-700032, INDIA

<u>**INDEX NO. 251/18/E**</u>

1. **Title of the thesis:**   PARAMETRIC OPTIMIZATION OF PERFORMANCE MEASURES OF WIRE ELECTRO-DISCHARGE MACHINING FOR TITANIUM MATRIX COMPOSITE

2. **Name, Designation & Institution of the Supervisor/s:**

Prof. (Dr.) Titas Nandi

Professor
Department of Mechanical Engineering
Jadavpur University, Kolkata, INDIA

3. **List of publication:**

1. **Soutrik Bose**, Titas Nandi, Microstructural characterization and measurement of laser responses of lens developed novel titanium matrix composite, *The European Physical Journal Plus*, 2021; 136(9): 978: 1-23. https://doi.org/10.1140/epjp/s13360-021-01951-6

2. **Soutrik Bose**, Titas Nandi, Novel approach in experimental and statistical investigations on titanium matrix composite, *Bulletin of Materials Science*, 2021; 44(1): 46: 1-11. https://doi.org/10.1007/s12034-020-02330-0

3. **Soutrik Bose**, Titas Nandi, Experimental investigation of WEDM on titanium hybrid composite reinforced with boron powder: a novel approach, *The European Physical Journal Plus*, 2020; 135(11): 914: 1-34. https://doi.org/10.1140/epjp/s13360-020-00904-9

4. **Soutrik Bose**, Titas Nandi, Statistical and experimental investigation using a novel multi-objective optimization algorithm on a novel titanium hybrid composite developed by lens process, *Proceedings of the Institution of Mechanical Engineers, Part C: Journal of Mechanical Engineering Science*, 2020; 235(16): 2911-2933. https://doi.org/10.1177/0954406220959101

5. **Soutrik Bose**, Titas Nandi, A novel optimization algorithm on surface roughness of WEDM on titanium hybrid composite, *Sādhanā*, 2020; 45(1): 236: 1-10. https://doi.org/10.1007/s12046-020-01472-5

6. **Soutrik Bose**, Titas Nandi, Improvement in performance measures by desirability coupled with Lean Six Sigma tool on titanium matrix composite: a novel approach, *International Journal of Six Sigma and Competitive Advantage*, 2022; 13(1-3): 38-54. DOI:10.1504/IJSSCA.2021.120226

7. **Soutrik Bose**, Titas Nandi, Parametric optimization of WEDM on hybrid titanium matrix composite using response surface methodology, *Multiscale and Multidisciplinary Modeling, Experiments and Design*, 2021; 4(3): 187-194. https://doi.org/10.1007/s41939-020-00088-w

8. **Soutrik Bose**, Nabankur Mandal, Titas Nandi, Selection and Experimentation of the Best Hybrid Green Composite Using Advanced MCDM Methods for Clean Sustainable Energy Recovery: A Novel Approach, *International Journal of Mathematical, Engineering and Management Sciences*, 2020; 5(3): 556-566. https://doi.org/10.33889/IJMEMS.2020.5.3.046

9. **Soutrik Bose**, Nabankur Mandal, Titas Nandi, Comparative and Experimental study on Hybrid Metal Matrix Composites using Additive Ratio Assessment and Multi-Attributive Border Approximation area Comparison methods varying the different Weight Percentage of the Reinforcements, *Materials Today: Proceedings*, 2020; 22(4): 1745-1754. https://doi.org/10.1016/j.matpr.2020.03.007

10. **Soutrik Bose**, Titas Nandi, Selection of Aluminum Hybrid Metal Matrix Composite Material Using Additive Ratio Assessment Approach and Comparing with the Experimental Results Varying Different Weight Percentage of the Reinforcements, *Advances in Unconventional Machining and Composites*, 2019; 687-695. https://doi.org/10.1007/978-981-32-9471-4

4. List of Patents: NIL

5. List of Presentations in National/ International Conferences/ Workshops:

1. **Soutrik Bose**, Titas Nandi, Parametric Optimization of WEDM on Hybrid Titanium Matrix Composite using Response Surface Methodology, *2nd International Conference on Future Learning Aspects of Mechanical Engineering (FLAME 2020)*, 5th -7th August'2020, Department of Mechanical Engineering, Amity School of Engineering and Technology, Amity University Uttar Pradesh, Noida.

2. **Soutrik Bose**, Titas Nandi, Optimization on Box-Behnken model of WEDM on Ti-TiB$_2$ hybrid composite developed by LENS process, *International Conference on Energy and Sustainable Development (ICESD 2020)*, 14th-15th February'2020, Department of Mechanical Engineering, Jadavpur University, Kolkata.

3. **Soutrik Bose**, Titas Nandi, Investigation on wire electro-discharge machining of titanium based alloys and composites varying different process parameters, *International Conference on Advancements in Mechanical Engineering (ICAME 2020)*, 16th-18th January'2020, Department of Mechanical Engineering, Aliah University, Kolkata.

"Statement of Originality"

I **Soutrik Bose** registered on **3rd May, 2018** do hereby declare that this thesis entitled "**PARAMETRIC OPTIMIZATION OF PERFORMANCE MEASURES OF WIRE ELECTRO-DISCHARGE MACHINING FOR TITANIUM MATRIX COMPOSITE**" contains literature survey and original research work done by the undersigned candidate as part of Doctoral studies.

All information in this thesis have been obtained and presented in accordance with existing academic rules and ethical conduct. I declare that, as required by these rules and conduct, I have fully cited and referred all materials and results that are not original to this work.

I also declare that I have checked this thesis as per the "Policy on Anti Plagiarism, Jadavpur University, 2019", and the level of similarity as checked by iThenticate software is **8 %**.

Soutrik Bose

Signature of Candidate: *Soutrik Bose .*

Date: 26/07/22

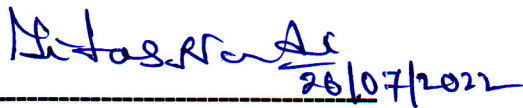Certified by Supervisor:

Titas Nandi
26/07/2022

Prof. (Dr.) Titas Nandi

PROFESSOR
Mechanical Engineering Deptt.
(Signature with date, seal)
Kolkata-700 032

III

CERTIFICATE FROM THE SUPERVISOR/S

This is to certify that the thesis entitled "**PARAMETRIC OPTIMIZATION OF PERFORMANCE MEASURES OF WIRE ELECTRO-DISCHARGE MACHINING FOR TITANIUM MATRIX COMPOSITE**" submitted by **Shri Soutrik Bose**, who got his name registered on **3rd May, 2018** for the award of Ph.D. (Engineering) degree of Jadavpur University is absolutely based upon his own work under the supervision of **Prof. (Dr.) Titas Nandi**, Professor, Department of Mechanical Engineering, Jadavpur University, and that neither his thesis nor any part of the thesis has been submitted for any degree/ diploma or any other academic award anywhere before.

-- 26/07/2022

Signature of the Supervisor

and date with Office Seal

PROFESSOR
Mechanical Engineering Deptt.
Jadavpur University
Kolkata-700 032

IV

Dedicated to My
Family &
My Teachers

Acknowledgement

I deeply thank my parents, Sumita Bose and Swadesh Bose, for their unconditional trust, timely encouragement, and endless patience. It was their love, prayers and blessings that raised me up again when I got exhausted. I am grateful to my brother, Sourojeet Bose, for his silent support and good wishes which guided me throughout my journey.

I would like to express my deepest sense of gratitude to my wife, Ankita, for her love, patience, understanding, inspiration and believe in me, in spite of all the ups and downs of my life. The completion of this thesis would not have been possible without her sacrifice.

Finally, I would like to highlight the fact that due to God's grace, we have our daughter Ayangsha, whose innocent smile and ignorance boosted my fatherly instinct in every possible ways, which endured this long process with me, offering love, compassion, empathy, perseverance and support.

Last but not the least, I would like to thank to those people and colleagues who contributed in de-motivating, backstabbing, assigning excess duties and creating hindrance in every possible ways, which ironically motivated me to complete my dissertation in time.

Date: **26/07/22**

Place: **KOLKATA**

SOUTRIK BOSE

Contents

List of Tables

List of Figures

Nomenclature

Symbols

Al_2O_3	Alumina
Ar	Argon
CC	Closeness Co-efficient
CR	Cooling Rate (K/s)
d	Wire Diameter
D	Laser Beam Diameter
E	Energy input/area (J/mm^2)
H	Hardness (HV)
IP	Peak Current (A)
KW	Kerf Width (mm)
l	Lower value of triplet M
m	Median value of triplet M
u	Upper value of triplet M
M	Triplet
M_1 and M_2	Triangular Fuzzy Numbers (TFNs)
Mi	Degree of Possibility
MRR	Material Removal Rate (mm^3/min)
O_2	Oxygen
OC	Over Cut (mm)
P	Laser Power (W)
P	Power (W)
PD	Pulse Duration (μs)
SiC	Silicon Carbide
SR	Surface Roughness (μm)

Ti	Titanium
TiB	Titanium boride
TiB$_2$	Titanium di-boride
TiC	Titanium carbide
Toff	Time off (µs)
Ton	Pulse-on Time (µs)
V	Laser Scan Speed (mm/s)
Vc	Cutting Velocity (mm/min)

Greek letters

$\breve{Z}$	Output Response
$\breve{a}_o$, $\breve{a}_{\bar{i}}$, $\breve{a}_{\bar{i}\bar{i}}$, $\breve{a}_{\bar{i}j}$	Regression Coefficients
$\breve{m}$	Experimental Factors
$\breve{i}$	Linear Effect
$\breve{j}$	Quadratic Effect
$\breve{x}_{\bar{i}}$ & $\breve{x}_{\bar{j}}$	Interactive Effects
$\breve{e}$	Random Error
$\breve{d}_{\bar{i}}$	Individual Desirability of response
$\breve{w}_{\bar{i}}$	Criteria Weights
$\breve{D}$	Overall Desirability
$\breve{r}$	Importance
$\breve{n}$	Number of responses
$\breve{r}_{\bar{i}}$	Target Value
$\breve{i}^{th}$	Response
$\breve{X}_{\bar{i}}(\breve{k})$	Function obtained after the generation of DGRA
$\breve{Y}_{\bar{i}}(\breve{k})$	Function attained from experimental runs
$\min \breve{Y}_{\bar{i}}(\breve{k})$	Minimum assessment
$\max \breve{Y}_{\bar{i}}(\breve{k})$	Maximum assessment
$\breve{i}$	Run-orders in DGRA
$\breve{k}^{th}$	Response
$\breve{\zeta}_{\bar{i}}$	DGRC
$\Delta_{o\bar{i}}(\breve{k})$	Offset value flanked by reference

$\breve{\xi}$	Characteristic Coefficient
$\Delta_{\min}$	Least value of $\Delta_{o\tilde{i}}(\breve{k})$
$\Delta_{\max}$	Highest value of $\Delta_{o\tilde{i}}(\breve{k})$
$\breve{\delta}_{\tilde{i}}$	DGRG
$\mu_M(x)$	Membership function
D	Decision Matrix of FTOPSIS
$\hat{m}$	Number of alternatives
n	Number of criteria
k	Members of Decision Matrix
A_i	Alternative
w_j^k	Criteria Weights in FAHP
r_{ij}	Normalized Decision Matrix
$\tilde{m}$	Values of Extent Analysis
M_g	Triangular Fuzzy Numbers (TFNs)
$S_{\tilde{i}}$	Synthetic Extent Value
λ_m	Maximum Eigen-value
V	Weighted Normalized Fuzzy Decision Matrix
D_i^+	Intervals between FPIS
D_i^-	Intervals between FNIS

Acronyms

AHP	Analytical Hierarchy Process
AI	Artificial Intelligence
ALMD	Annular Laser Metal Deposition
AM	Additive Manufacturing
ANFIS	Adaptive Neuro-Fuzzy Inference System
ANN	Artificial Neural Network
ANOVA	Analysis of Variance
ASTM	American Society for Testing and Materials
BBD	Box-Behnken Design
CAD	Computer Aided Design
CCD	Central Composite Design
CI	Confidence Intervals
CI	Consistency Index
CNC	Computer Numeric Control
COA	Centre of Area
CR	Consistency Ratio
CR	Cooling Rate
DED	Direct Energy Deposition
DGA	Desirable Genetic Algorithm
DGRA	Desirable Grey Relational Analysis
DGRC	Desirable Grey Relational Coefficient
DGRG	Desirable Grey Relational Grade
DM	Decision Makers
DMD	Direct Metal Deposition
DOE	Design of Experiments
EDM	Electric-Discharge Machining
EWR	Electrode Wear Ratio
FAHP	Fuzzy Analytical Hierarchy Process
FEM	Finite Element Method
FNIS	Fuzzy Negative Ideal Solution
FPIS	Fuzzy Positive Ideal Solution
FTOPSIS	Fuzzy Technique for Order Preference by Similarity to Ideal Solution

GA	Genetic Algorithm
GEC	Genetic and Evolutionary Computation
GP	Genetic Programming
GRA	Grey Relational Analysis
GRNN	General Regression Neural Network
HV	Hardness Value
ISM	Induction Skull Melting
LENS	Laser Engineering Net Shaping
LMD	Laser Metal Deposition
LTW	Laser Transmission Welding
M	Triplet
MCDM	Multi-Criteria Decision Making
MOGA	Multi-Objective Genetic Algorithm
MOO	Multi-Objective Optimization
MOPSO	Multi-Objective Particle Swarm Optimization
NC	Numeric Control
Nd:YAG	Neodymium: Yttrium Aluminum Garnet
NSGA	Non-dominated Sorting Genetic Algorithm
PI	Prediction Intervals
R&D	Research & Development
RI	Random Index
RSM	Response Surface Methodology
SEM	Scanning Electron Microscope
SLM	Selective Laser Melting
StdErr	Standard Error
SVM	Support Vector Machine
TFN	Triangular Fuzzy Number
TMC	Titanium Matrix Composite
TOPSIS	Technique for Order Preference by Similarity to Ideal Solution
PSO	Particle Swarm Optimization
WEDM	Wire Electro-Discharge Machining
WW	Wire Wear

Abstract

Conventional machining of hybrid titanium matrix composite (TMC) is very intricate due to its superior characteristics of corrosion resistance, superior strength-to-weight ratio, fatigue and abrasion resistance. It is expansively necessary for aerospace, bio-medical and automobile industries. In recent diverse modern multi-disciplinary industries like automotive, aerospace and biomedical there is a comprehensive usage of titanium matrix composite (TMC) for its exceptional strength and resistant properties. The prime scope of this investigation deals with the development of a novel TMC by laser engineering net shaping (LENS) process and recent state-of-the-art of advancement of tribo-mechanical and metallurgical properties like Young's modulus (550 GPa), co-efficient of thermal expansion ($8.6x10^{-6}$ /K), hardness (396 HV), yield strength in compression (945-1020 MPa), ultimate compressive strength (1020-1096 MPa) and elongation (25-32.5%). Laser process parameters like laser power (P), scan speed (V) and energy input/area (E) are varied. The microstructure and characterization depict an outstanding interfacial bonding between TiB_2 and Ti where the best parametric combination is identified. A novel optimization algorithm named as desirable genetic algorithm (DGA) is proposed in this research. The objective functions determined by desirability function are further incorporated in genetic algorithm in MATLAB R2018a to improve the optimized solution. Multi-objective optimization (MOO) is developed by Box-Behnken design (BBD) and mathematical model is projected considering response surface methodology (RSM) on output responses like cooling rate (CR) and hardness (H), and legitimated by confirmation tests. ANOVA is incorporated for seeking the contributing effects and significance of the parameters. Optimal solution achieved after DGA, when P is 350.956 W, V is 12.371 mm/s, E is 49.475 J/mm^2, CR is -3146515.795

K/s and H is 395.097 HV, and combined overall desirability is 0.838. Optimization is additionally enhanced by 20.049% of CR and 0.229% of H when evaluated with DGA.

Further the investigation deals with the development of another new-fangled optimization algorithm termed desirable grey relational analysis (DGRA) which is a combination of desirability and grey relational analysis. Here, the predicted responses obtained from desirability function are further analyzed with the experimental results obtained from WEDM by varying power (P), time off (Toff) and peak current (IP) which are regarded as chief input process parameters. Comparative analysis is projected by FTOPSIS along with FAHP for criteria weights between experimental and proposed MOO algorithm. RSM is conducted on BBD model (3 factor / 3 levels) DOE on output responses like material removal rate (MRR), surface roughness (SR), kerf width (KW) and over cut (OC). Satisfactory outcomes are obtained authenticated by confirmatory test. To obtain the significance of these models, ANOVA is again incorporated. Optimal solution is obtained by desirability approach to achieve the most excellent output responses which are additionally improved by 1.75%, 0.73% and 1.02% when contrasted with desirability to FTOPSIS, FTOPSIS to DGRA, and desirability to DGRA respectively.

Keywords: Laser engineering net shaping; Wire electro-discharge machining; Desirable grey relational analysis; Desirable genetic algorithm; Microstructure; Multi-objective optimization

CHAPTER 1

1. Introduction

A composite is developed from more than two essential constituents with appreciably diverse physical and chemical characteristics combined to manufacture a component with enhanced and better uniqueness compared to the individual elements. These composites possess greater strength, much lighter and cheaper than other conventional materials. Composites have wider applications in aerospace, automotive industries, space, defense and in underwater because of its improved mechanical, physical and tribological properties like elevated specific strength, resistance to corrosion and wear, improved strength-to-weight, high stiffness, abrasion, impact resistance, etc. Composites are classified under: reinforced concrete, fibre-reinforced polymers, composite wood, ceramic matrix composites, metal matrix composites, advanced hybrid composites. Ceramic comprises of an inorganic metal and non-metal mainly bonded in covalent or ionic bonds. This word is referred to a product obtained through the action of fire upon earthy product. The most primitive ceramics created by humans were pottery objects made of clay combined with silica which was heat-treated, hardened and sintered. Afterwards, ceramics were fired for creation of soft multi-colored products, diminishing porosity by using glassy, amorphous coatings on pinnacle of crystalline substrates. Recently, semiconductors are widely manufactured by new ceramic materials. Ceramics have towering melting point, lofty hardness, elevated thermal conductivity, and elevated corrosion and wear resistance. The combination of two or more of these materials together produce a new material called composite material which has better and enhanced characteristics than the monolithic alloys. Ceramics are defined as non-metallic and inorganic materials manufactured from minerals or chemically processed powders. Ceramics are characteristically crystalline amalgams produced amid metallic and non-metallic elements like alumina (Al_2O_3), silica, silicon carbide (SiC). Wide applications of ceramics are in

engine components, medical components, computer peripheries, electronic gadgets, cutting tools, etc.

Titanium based composites are strong, light and durable advanced hybrid composites with outstanding properties like corrosion resistance, fatigue resistance, etc. These hybrid composites are highly used in various industries like automobile, aerospace, biomedical, chemical, food etc as indicated by *Gu et al.* [1]. Currently, titanium is extensively used in medical grounds for its exceptional bio-compatibility with advanced growth in bones and other tissues. Titanium is used for its vast applications in miscellaneous medical equipments like, dental, hips, bones, and knees replacement enucleation and a range of other surgical instruments as obtained by *Elias et al.* [2]. However, machining of titanium alloys and composites by conventional methods is very complicated because tool wear occurs at elevated speed and temperature which affects highly to other machining characteristics like surface finish as obtained by *Younas et al.* [3]. In addition, *Kumar et al.* [4-7] pointed out other limitations like high initial cost, ease of availability and manufacturability. The microstructure and mechanical characteristics of titanium by altering different environmental conditions was studied by *Saji et al.* [8] and *Fleck et al.* [9].

Niu et al. [10] reinforced Ti with TiB_2 by using induction skull melting (ISM) and inferred superior characteristics in the developed titanium matrix composite (TMC). Nevertheless, for widespread prospects of better applications of TMCs, enhanced performance with low manufacturing cost must be incorporated. Their properties have to be improved with suitable processing technology, resulting in the best replacements of other expensive metallic materials for intricate designing of complex shapes. Hence, this exploration has led to the development of TMC by laser engineering net shaping (LENS) process. LENS engages powdered metals and ceramics for production of accurate functional parts. It generates multifaceted, net-shape

components in an extremely superior method unwaveringly from powders with minimal processing, enhancing the production rate. LENS provides a line-by-line, net-shaping mechanism for manufacturing of complicated components obtained from computer aided design geometry. The most imperative deposition factor is powder feed rate. LENS inhabits ceramic and metal powders for fabricating complex and broken shapes. A layer-by-layer methodology is incorporated for manufacturing computer aided design (CAD) specified precision parts. The powdered metal is positioned to the tip of the laser beam's focal point by nozzle-deposition technique. Nozzle deposition technique [11] is used to supply the powder at the focus of the laser beam. An important advantage of LENS process is to manufacture complicated and graded hollow components coalescing different materials using multiple powder feeders. LENS is employed for re-commissioning of damaged components which were earlier considered unrestorable, thereby developing enhanced microstructure formation of TMCs [10, 11]. *Attar et al.* [11] developed TMC and inferred powder feed rate to be the most imperative deposition parameter throughout LENS process. LENS process provides an advantage of producing complex and intricate hollow components with the help of multiple powder feeders. *Hu et al.* [12, 13] examined an assortment of 98.4 wt.% of pure titanium with 1.6 wt.% of boron roughly about 4 hrs in LENS under different processing conditions and obtained improved characteristics of TMCs. Increment of laser power transformed non-uniform distribution of Ti-TiB at 125 W to a partial and fine 3D network at 175 W to a full 3D network with excellent mechanical properties at 200 W. *Attar et al.* [14] constructed Ti-TiB hybrid composites by LENS in an assortment of powdered mixture of 98 wt.% pure titanium with 2 wt.% boron and inferred a coarse microstructure because of elevated cooling rate, but very little research has been made so far for the development of Ti-TiB$_2$ composite using LENS process. Machining titanium with maximum

4

precision and in minimum time is a major concern in biomedical research. Titanium is highly chemically responsive towards various tool materials at elevated temperature. Therefore, work hardening, high temperature generation, excessive cutting pressure and vibrations are serious issues for proper machining as inferred by *Khan et al.* [15]. Hence, proper tool material of the wire must be selected for appropriate machining of titanium alloys and composites.

1.1. Laser Engineering Net Shaping (LENS)

LENS provides an effective alias of direct metal deposition (DMD) where energy deposition is directed under the categorization of additive manufacturing (AM) process as designated by American Society for Testing and Materials (ASTM). DMD merges powder from the feeding nozzle with the help of laser as designed by CAD and other numeric control technologies. An elevated laser beam power is employed for creating a melt pool on the substrate and concurrently powder feeding is carried over the melt pool for consolidation. The metal powder is then supplemented from the nozzle over the melt pool by traversing the laser beam. By this method, independent delivery of the powder and the laser beam is operated irrespective of the orientation position. This LENS process is susceptible to powder flow behavior as the powder is sent by the nozzle which in turn provides a consolidated pathway of preferred volume and surface quality of texture [10, 11]. This latent process assures manufacturing suppleness of multifaceted silhouette deposition of wide variety of challenging materials. Appropriate process parameters are to be selected for acquiring the optimality condition and solution of performance measures. Various powder materials can be supplied for fabrication of functional graded objects of different hybrid alloys and composites. Nozzle deposition technique [11] and powder feed rate [11] are the two important parameter of LENS process. A competent powder delivery system distributes uniformly the powder with high accuracy to the laser-substrate interaction zone [11]. A powder

delivery is hence the most vital component for uniform transportation of stream efficiently to the interaction zone of laser- melt pool-substrate. LENS process is cost effective and time saving. The powder is carried from powder feeder by transport or carrier gas or by gravity-driven technology. The particles of the powder progress through an assortment of various channels/ chambers which are inside the nozzle, thus having collisions with nozzle wall to provide a stream of powder particles which are directed at a laser spot. Transformation of phase by melting and solidification takes place after that for fabrication with XY table movement. The deposition head consisting of powder delivery nozzle shifts up vertically following each layer. The complete process is conceded in an inert environment for protecting the melt pool from oxidation. Fig. 1.1 provides the graphical representation diagram of components of LENS method where laser beam is scanned on the substrate. The basic components of this process are computer numeric control (CNC), CAD model, laser system, powder feeder and feedback control system. Interaction of beam with substrate results in generation of localized melt pool. Subsequently, the delivery of powder is carried by the nozzle over the interaction zone. Then this zone fuses with the incoming powder resulting in bond formation with the substrate. Development of LENS process occurred at Sandia National Laboratories at nineties to which resulted in excellent improvement by employing multiple material processing and utilizing blended powder feeders. The process of LENS is more commercialized and successful amongst all direct energy deposition (DED) processes. Advantages of LENS are:

➢ Horizontal, vertical and inclined orientation can be obtained by deposition technique with the assistance of additional axis of work stage.

➢ Variety of blended powder can be processed.

➢ System envelope size is not a constraint, so manufacturing of intricate and graded void

components coalescing diverse materials by means of multiple powder feeders can be done.

➢ The process is relatively appropriate for repairing and coating applications on flat and round surfaces.

➢ Functional grading can be accomplished in-situ, with the help of different powder combination.

➢ Higher deposition rates are obtained than the powder bed fusion process.

➢ Minimal heat affected zone is obtained.
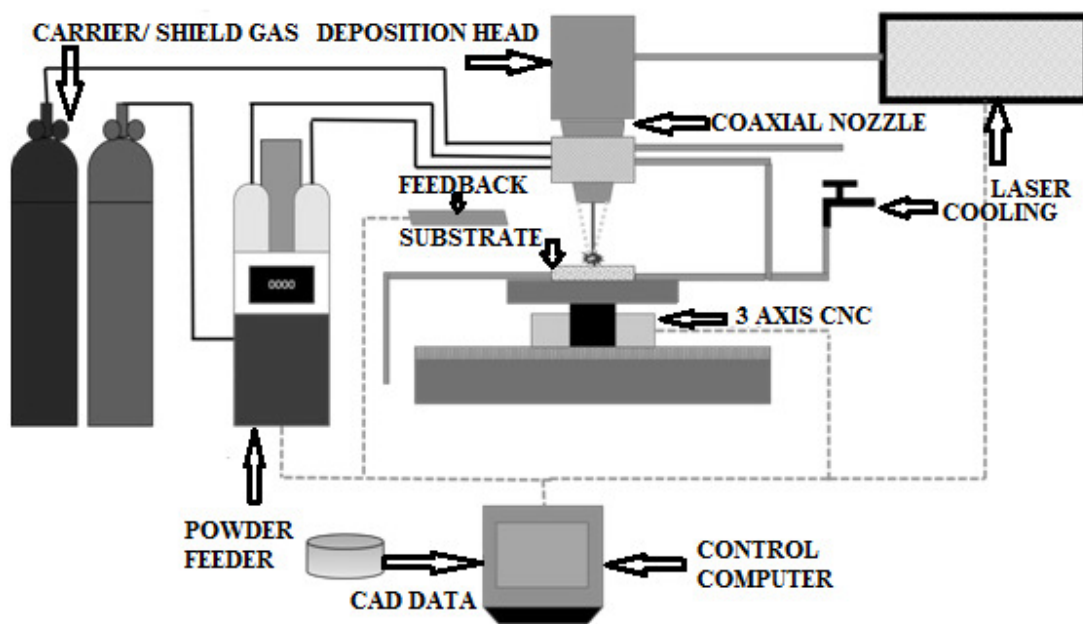
Fig. 1.1. Components of LENS process

Disadvantages of LENS are:

➢ Efficiency of process with proper powder utilization is a challenge.

➢ The resolution of deposition is lower than some other AM processes.

➤ The deposition of unsupported structures is an issue while using a limited axis work stage.

➤ Inter-track porosity and high dilution ratio are some common defects.

➤ Requirement of post-processing operations are mandatory for improvement in surface finish and geometrical accuracy.

➤ Powder particle size may result in a hazardous work environment.

1.2. Wire electro-discharge machining (WEDM)

WEDM as depicted in Fig. 1.2, employs a wire as the tool electrode with electro-thermal mechanism for precision manufacturing. Both the workpiece and wire electrode (tool) are inundated in dielectrics. Dielectrics act as electrical insulator and then machining occurs with the incidence of the electrical discharge. Therefore, a gap is created on the wire advancement towards the workpiece and higher voltage is generated breaking the dielectric and generating the electrical discharge initiating a spark between the wire-workpiece interfaces. The dielectric becomes an ionized gas and turns into plasma bubble. The plasma bubble collapses, vigouring the cutting material to disperse into the dielectric, creating small craters leading to wire failure and rupture. This process continues approximately around 2,40,000 times per second removing the metal and a precision cut is formed. A flushing flow of dielectric acts as a coolant of the wire removing the scattered particles. As the wire erodes, a WEDM machine continuously supplies un-sullied wire from a reel and dumps the used eroded wire to trash bin for recycling. WEDM is an advanced EDM of unconventional machining group. Materials which are electrically conductive are machined with the help of electro-thermal system by a succession of distinct discharges in the gap of workpiece and electrode inundated in dielectrics. There is an occurrence of excessive lofty temperature where discharge transpires causing removal of molten surface materials of the workpiece. The dielectric flushes the unwanted fragments from the arena of the

machining zone. WEDM is commonly used for precision manufacturing. Different wire electrodes like copper, brass and zinc-coated brass of different wire diameter are used in today's manufacturing environment, having a competence to manufacture intricate shapes. Wire tension is carried in the contactless machining arena resulting in the purging of residual stresses. WEDM uses electrical as well as thermal responses for precision machining of conductive materials. WEDM is successfully projected for conductive materials which are harder, tougher, possessing elevated strength and resistant to temperature, like heat treated steels and advanced ceramic composites. WEDM uses different input process parameters like power, peak current, pulse-on time, time-off, pulse duration, pulse width, servo voltage, wire tension on wire cutting speed, wire feed, wire wear rate (WWR) and injection pressure to investigate upon various output performance measures like material removal rate (MRR), surface roughness (SR), kerf width (KW), over cut (OC) and optimized accordingly by various optimization techniques.
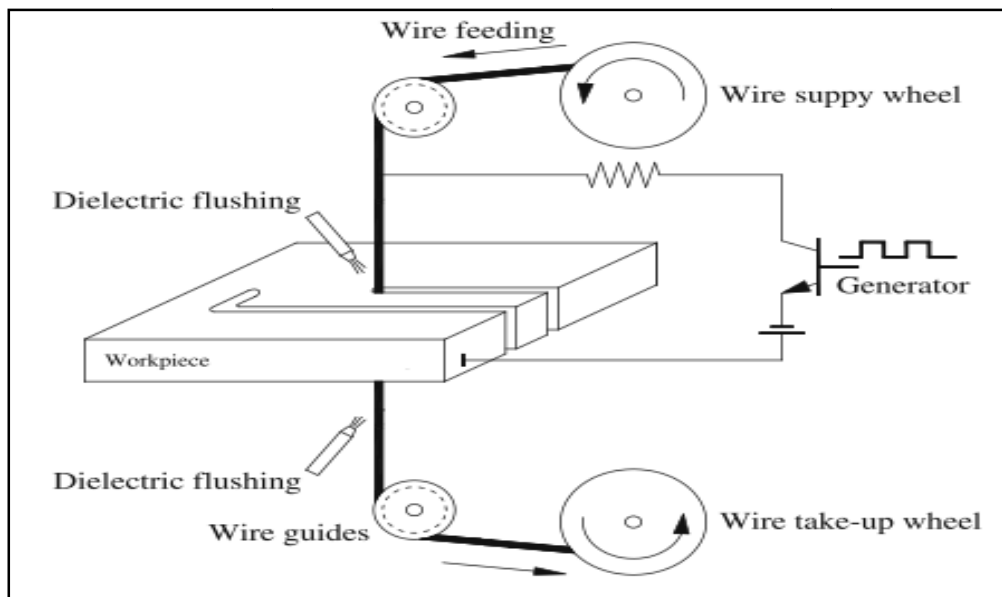
Fig. 1.2. Schematic diagram of WEDM

WEDM has major application in modern industries in metal cutting as it achieves a better dimensional accurateness and fine surface finish compared to other non-traditional processes. The operating cost is also lesser compared to other processes. The complicatedness which bumped into die sinking EDM is evaded by WEDM, because the multifaceted design tool is reinstated by poignant relative movement of the conductive wire and guides. WEDM provides the best substitute for machining exotic, conductive, elevated strength and temperature resistive advanced ceramic composites with an aim of creating obscure products. Nowadays, CNC is commenced into WEDM which is itself most important boon in machining era.

1.2.1. Basic principle of WEDM process

WEDM generates an impulse voltage between the gap of electrode wire and workpiece, all the way through a servo system, and machining occurs by generation of innumerable sparks inundated in dielectrics. The basic principle is creation of a difference in voltage by power supply between the electrode and workpiece as depicted in Fig. 1.2. During the approach of the tool towards the workpiece, there is an increment in strength of the gap's electric field till the separation of the tool in the dielectric, resulting in machining of workpiece. A plasma channel is occurred due to the ionization of the dielectric. At cathode point the electrode wire is connected and at anode the workpiece is connected. When the tool approaches towards the workpiece at some threshold point, the insulating liquid breaks down and small discharges are generated. A temperature range of 8000^0C-$12,000^0C$ exists between the gaps. The plasma channel is fragmented during the power off time reducing the temperature and flushing away the molten particles. When discharge occurs, there is a collapsibility of plasma channel and occurrence of vapor bubble which explodes inside the dielectric. The evicted material is reddened away but

some portions of the melt re-solidify over workpiece surface termed as recast layer. Three basic conditions that WEDM works correctly:

1. The gap must be maintained in an optimum range. Here, the impulse power breaks creating discharging of sparks and the battered workpiece also flushed away. Larger gap results in improper breaking and indecent spark discharging. And smaller gap results in short circuit where no spark discharging will happen.

2. The process must be carried in an insulated liquid like deionized water which will act as a discharging medium and should also afford proper flushing and cooling.

3. The discharge timing must be very minimal because the released heat is not sufficient to affect the workpiece with limiting energy.

1.2.2. Components of WEDM setup

The WEDM components are:

(i) *Power supply*: It creates sufficient voltage difference between the wire and the workpiece to melt and vaporize the material from the wire surface. The frequency of the pulse is around 1 MHz resulting in abridged crater and improved surface finish.

(ii) *Dielectric medium*: Deionized water and in some research papers kerosene are used as dielectric medium. Deionized water is preferable due to its accessibility, enviable thermal properties, squat viscosity and almost freed from polluted environment. Small viscosity results in competent flow whereas lofty cooling rate gives emaciated recast layer.

(iii) *Positioning system*: It is a computer numeric two-axes controlled system where wire approaches to workpiece but it must be capable to sense any short circuit created by the gap and the debris.

(iv) *Wire drive*: This mechanism serves two functions; one being continuous delivery of fresh wire and the other to keep the wire in proper tension. While traversing towards the machining zone, the diamond wire guides protect the fresh wire. Again while travelling the spool, the wire pass all the way through a succession of tensioning rollers.

1.2.3. Dielectric used in WEDM

Deionized water and kerosene are used as dielectric medium in WEDM system. In some researches kerosene with little amount of SiC abrasives are also used. But the most favorable dielectric is the deionized water because it is readily available, it has low viscosity, it is non fire hazard, it has high cooling rate and high MRR. Due to high cooling rate, there is a slender white layer produced over the workpiece surface. This dielectric helps in machining as well as flushing of the unwanted debris. After proper filtration, the deionized water is recycled to reduce the cost. Resins may be used to keep a constant resistivity of this dielectric.

1.2.4. Wire electrode

In WEDM a slender single-strand metal wire (diffused zinc coated brass) is supplied towards the workpiece, inundated in dielectric medium of deionized water. During machining wear of the electrode is high, but this does not affect the performance as fresh wire with appropriate tension is supplied continuously from a spool as a straight wire. Here, wire diameter of 0.25 mm is used in WEDM process. Nowadays, stratified wires are used as wire electrodes, where copper is the parent material and a thin layer of zinc is made on it, for carrying more current and higher MRR.

1.2.5. Process parameters of WEDM

Different process parameters of WEDM are:

(i) *Power (P)*: Power is the main process parameter in WEDM which supplies current and voltage to create spark erosion.

(ii) *Peak current (IP)*: It is the highest current obtainable for every pulse from power supply which is the average of the amperage that is supplied to the electrode for discharge in the spark gap deliberated in a complete cycle.

(iii) *Pulse-on time (Ton)*: This is the duration of the electric discharge that arises between the gap of tool and workpiece where material is removed.

(iv) *Time off (Toff)*: In this time duration, there is no spark in the machining gap, rather the eroded debris are removed from the machining zone as well as cooling takes place during this time interval.

(v) *Pulse frequency*: Pulse frequency is the number of times per second for the current to be turned on/off. This sparking frequency has greater influence on the surface finish. Larger spark gaps are created by lower frequency for rapid material removal with irregular surface finish and elevated frequencies with miniature gaps create smooth surface finish.

(vi) *Wire velocity*: It is an important criterion in WEDM process. High wire velocity results in non-uniform discharge and more wastage of wire resulting in higher operating cost. Lower wire velocity results in frequent breakage of wire hampering productivity. So optimum wire velocity is a must criterion in WEDM for efficient machining operation.

(vii) *Gap voltage*: It is the voltage across the gap during the current flow.

(viii) *Wire tension*: It is the tension created during wire feeding which is essential for proper machining.

(ix) *Flushing pressure*: It is kept at optimum level so that the dielectric can redden away the battered particles from the machining zone, otherwise it will create short circuit between the electrodes resulting wire rupture.

1.2.6. Prime Performance Measures

(i) *Material Removal Rate (MRR)*: MRR involves in the productivity of all manufacturing industries. It is the rate of removed quantity of the workpiece material when machining time is considered (mm^3/min); hence the characteristic efficiency of the machine is determined. From Fig. 1.3, it is pragmatic that superior MRR is accomplished with deionized water when contrasted to kerosene. It is primarily because of the adherence of carbon to the tool surface which defends the tool electrode's erosion in case of deionized water. But with kerosene, dense abrasives get accrued in between the gap of the electrode causing instability in the discharge. The increment of MRR for deionized water is due to the increment of the discharge current (power) as the removal of the material is easily obtained by increasing the density of the current [16]. The MRR increases and reaches a threshold value with the enhancement of pulse on time duration but then diminishes. For higher MRR; Peak current (IP), Time on (Ton) and Pulse Duration (PD) are the main input process parameters and the other factors are less significant according to past literature [4-7]. This is mainly due to the increment of plasma channel and sufficient current density for proper stable discharge to the threshold value and decreases beyond due to occurrence of large carbon content forming large amount of recast layer. At high PD, increase in the localized temperature decomposes the carbon leading to lower the MRR value. It is also

unswervingly proportional to the discharge pulse energy which is again dependent upon the servo voltage and capacitance. Thus, at elevated voltage wider gap is formed, leading to high discharge. The capacitance establishes the frequency, larger crater forms at the lower frequency. MRR is also affected largely by hardness. Lower hardness and melting temperature cause higher MRR which is determined by *Niu et al.* [10]. According to *Lin et al.* [16], higher MRR is obtained with the increment in PD. MRR also augments with the amplification in IP. The MRR enhances linearly with the PD with deionized water, but enhances non-linearly upto the optimum zone and then reduces when kerosene is used. Electrode wear ratio (EWR) amplifies with PD with kerosene rather than deionized water as obtained by *Chen et al.* [17]. This research also provides a comparative correlation using kerosene and deionized water with silicon carbide (SiC) abrasive concentration as dielectrics.
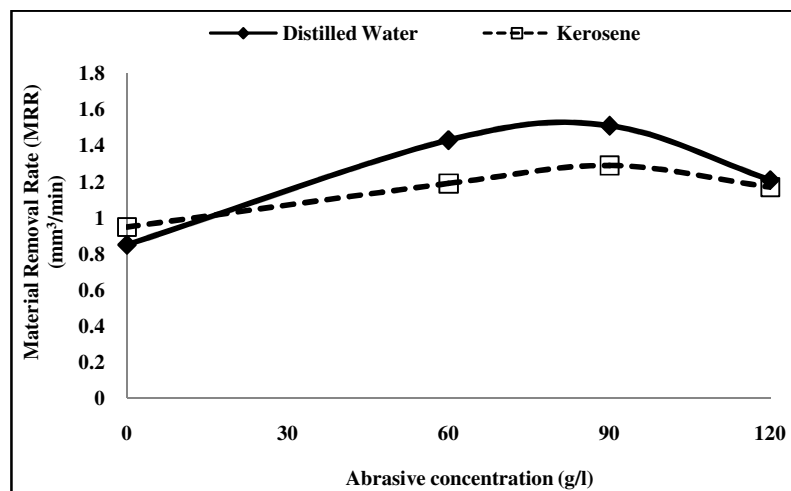
Fig. 1.3. MRR obtained in different dielectrics [17]

It is observed from Fig. 1.3, the maximum value of MRR is obtained after using 90g/l SiC concentration in the dielectric fluid. MRR decreases beyond this value due the occurrence of

greater amount of abrasive particles and large carbon content which forms large amount of recast layer on further increment of SiC concentration.

(ii) *Surface Roughness (SR)*: SR is another important parameter which has a great impact on the performance characteristics of the machined components. It mainly varies with the discharge current followed by PD. Low discharge current and PD results in better SR. Proper selection of tool material is essential as SR depends on it. PD highly affects SR. From Fig. 1.4, it is evident that the experimental SR directly depends on PD; higher the PD more is the SR, and it has been validated by the past research works [3-7, 16-18]. Increasing PD enhances the feed rate thus allowing greater discharge energy penetrating into the surface of work-piece material forming deep crater wear. SR augments with the discharge current for any material of the WEDM electrode. SR hence enhances with the discharge current. The best 'Ra' value obtained experimentally is 1.31 µm (IP, 3A, PD, 4 µs).
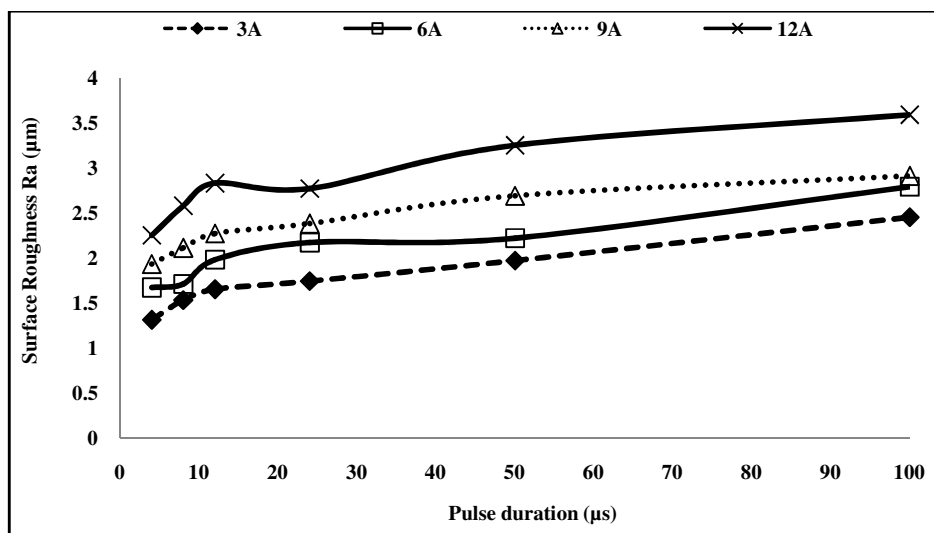
Fig. 1.4. Experimental SR with variation of peak current and pulse duration on WEDM [17]

16

Improved surface finish can be accomplished at elevated values of servo speed because of rapid erosion of particles. An augmentation in servo voltage amplifies SR because of more number of collisions between ions and electrons resulting in higher MRR. Therefore, for the sake of better surface finish, low standard value of servo voltage is required. Superior the pulse-off time, lower is the value of SR. The higher pulse-off time supplies better cooling effect and sufficient time to flush the unwanted debris. High dielectric pressure results in total removal of particles resulting in better surface finish. Low wire speed causes more melting of material due to higher energy and hence high MRR is obtained causing high SR. High wire speed causes instability in machining as less energy density occurs resulting in lower melting of material causing irregularities in the surface. Therefore, to obtain better surface finish, optimum wire speed is necessary [16, 17]. Low wire tension is the root cause of amplified vibration during the machining, and high wire tension may result in breakage. The wire feed rate is another important dependant parameter affecting SR. Superior surface finish may be achieved with inferior machine feed as obtained by *Alias et al.* [18].

1.2.7. Process characteristics

In WEDM, various complicated shapes like micro holes, press tools, micro electrodes, etc are fabricated by removing a bulk of material guiding the wire through U and V drive systems. However, there are some process responses that are responsible for generating good quality products which are given below:

(i) *Surface finish*: The surface generated after WEDM process should be smooth enough for excellent precise product. It will be better if the surface roughness value is kept lower than 5 µm.

(ii) *White layer*: To minimize the white layer thickness, deionized water is carried as dielectric medium for its enhanced cooling rate.

1.2.8. WEDM applications

WEDM has vast applications in today's manufacturing industries like:

➤ Used vastly in automotive, aerospace, die making, medical, optical, dental, jewellery and other R&D areas. In this research WEDM on titanium based hybrid composite is selected basically highlighting its applications on bone replacement, artificial knee-joint fabrication, dental, medical, aerospace wings, impeller and automobile valve pins manufacture.

➤ WEDM reduces the overall fabrication and machining time and also reduces operating cost than the other conventional and unconventional machining processes.

➤ Machining of extrusion dies and powder metallurgy compacted dies. Used in precision gauges, keyways, gears, shafts, axles, prototype production, punches and dies.

1.2.9. Advantages of WEDM

➤ Contactless machining of the workpiece, hence mechanical and residual stresses are eliminated.

➤ Electrode fabrication is not required.

➤ WEDM can be used in most of the electrically conductive metals and alloys heedless of their mechanical properties.

➤ Machining is user friendly and does not need extreme precautions and attention.

CHAPTER 2

2. Literature Review

Development of titanium matrix composite (TMC) necessitates an incredibly cautious concentration in current sustainable manufacturing environment. These hybrid composites are durable, strong, light and flexible with outstandingly improved properties like resistance to fatigue and corrosion, which has vast usage in diverse modern industries like biomedical, aerospace and automobile [3, 15]. Conventional techniques are extremely complicated to machine and manufacture these composites due to porosity at soaring temperature and rough surface finish ensuing in unwarranted wear [4-7]. *Niu et al.* [10] employed ISM on titanium (Ti) with TiB_2 reinforcements, and acquired better characteristics in TMC. Results inferred ISM is socially feasible to fabricate TiB_2/TiAl composite, but the research gap lies on the question of better feasibility of the development of Ti-TiB_2 composite using LENS process. Reinforcements of TiB_2 were mixed proportionately with Ti [10] and obtained improved mechanical properties in developed TMC. However, for prevalent projection of superior relevance with improved efficiency ought to be integrated. Apposite processing technology is pragmatic for enhancement of tribo-mechanical properties, following the unsurpassed substitution of additional costly metals intended for complicated designs. Consequently, laser engineering net shaping (LENS) method is therefore proposed for the growth of TMC. LENS populates powders of ceramics, metals and other alloys to manufacture complex broken shapes. A line-by line, net-shaped method, is integrated for development of meticulous parts as obtained from CAD geometry. Nozzle-deposition system is implemented for the positioning of the powdered metal at tip of the laser beam focus. Powder feed rate [11] was the major essential parameter in this deposition technique for the TMC development by LENS. Major advantage of LENS is mass production multifaceted and obscure hollow components by using multiple powder feeders. *Hu et al.* [12, 13] obtained an

assortment of mixture (98.4 wt.% pure titanium + 1.6 wt.% boron) for approximately 4 hrs and then engaged for LENS under different processing conditions. Increment of laser power transformed non-uniform distribution of Ti-TiB at 125 W to a partial and fine 3D network at 175 W to a full 3D network with excellent mechanical properties at 200 W. *Attar et al.* [14] manufactured Ti-TiB hybrid composites through LENS from a combination of hybrid mixture (98 wt.% pure titanium + 2 wt.% boron powder) and inferred a coarse microstructure because of enhanced rate of cooling, but very little research has been made so far for the development of Ti-TiB$_2$ composite using LENS process.

Enormous preliminary cost, complexity in manufacturability and lenience in availability are significant restrictions and concerns while developing these hybrid composites [19]. Mathematical model founded by Box-Behnken Design (BBD) of response surface methodology (RSM) was incorporated using desirability function [4-7] coupled with Taguchi method, and multi-objective optimization (MOO) was identified. RSM was also coupled with TOPSIS [20, 21] for better optimal solution but the research gap lies on maximizing productivity at nominal cost by using such empirical decision making approaches which needs proper validation. Results from analysis of variance (ANOVA) endowed with the parametric significant interactive and quadratic effects. *Yu et al.* [22] employed ANOVA of multi response optimization of laser cladding and obtained the influence of the trend using contour and surface plots. There was an improvement in the response targets, and it was pragmatic that the optimized cladding layer was more effective than the other cladding layers in microstructural characterization. Selective laser melting (SLM) [23] on TMC was performed and obtained superior wear resistance and refined microstructure. TiB whiskers were found to be properly synthesized due to excellent bonding. Improved grain refinement was observed by microstructural analysis and improved

microhardness was obtained on the increment of TiB_2 contents. Worn depth and wear rate was also decreased with the enhancement of TiB_2 contents. *Cheng et al.* [24] investigated microstructure and mechanical properties of Ti-6Al-4V by incorporating laser metal deposition technique. Martensitic microstructure and improved strength was obtained because of elevated cooling rate by a novel annular laser metal deposition (ALMD) technique. *Chen et al.* [25] deliberated the effects on various laser parameters based on eminence of prediction model derived from support vector machine (SVM) of coating characteristics by laser cladding of TiC ceramic powders. The results inferred that laser spot diameter, laser power and pre-placed powder thickness provided essential contribution. *Shivakoti et al.* [26] also proposed a predictive model using RSM coupled with desirability and analyzed the optimal condition by incorporating Nd:YAG laser. Various process parameters of laser were considered like lamp current, scanning speed and pulse repetition rate. Sensitivity analysis was carried on the experimental runs and also on the predictive models. Optical microscopic and scanning electron microscope (SEM) images were also examined for quality facets of laser marking on gallium nitride. Similar parametric MOO was examined on laser beam welding NiTinol sheets by desirability coupled with metaheuristic techniques [27]. Various possessions of process parameters on mechanical properties were investigated. *Gao et al.* [28] investigated parametric optimization on laser-arc welding based on hybrid fiber. A novel optimization algorithm combining genetic algorithm (GA) with Kriging was projected for determining the optimal weld geometry. Micro-hardness and microstructures were analyzed varying various process parameters of laser welding. Taguchi L25 array of experiments were conducted depending on four-factor and five-levels. The novel model was developed for optimal solution for maximizing penetration depth, minimizing bead width and ensuring bead reinforcement at a desired value. Metallographic characterizations with

experimental investigations were carried by *Kumar et al.* [29] on Ti-6Al-4V components using fiber based laser beam for welding by using RSM and GA. The correlation of laser process parameters with performance measures were computed via regression models. The significance and contributions of process parameters were identified along with the optimal solution. It was inferred that power and speed offered in welding contributed to the maximum. Direct effect of laser power during welding was noted while inverse effect was observed for welding speed. *Wang et al.* [30] proposed a hybrid intelligent technique for optimization and simulation of laser transmission welding (LTW) and validated with the experimental results. Finite element method (FEM) in combination with RSM and GA was analyzed on the thermal model for improvement of the veracity of the predicted results in minimum experimental time. Desirability was integrated with the developed optimization algorithm for achieving the optimality for enhancement of the efficiency and quality of the welding. Results inferred that the proposed novel integrated optimization tool executed excellently in optimum performance of LTW method. Parametric optimization was investigated by back propagation neural network couple with Taguchi method and GA. This proposed statistical method BPNN-GA [31] showed improved results in the efficiency and stability of the laser beam. *Weisheit et al.* [32] provided a thorough understanding of the advancement of titanium aluminide by direct laser cladding. Excellent mechanical properties were inferred from the microstructure and characterization.

TMCs show evidence of superior microstructure and characterization during LENS [32, 33]. Porosity occurrence [34, 35] and lofty fluctuations in cooling rate [36] result in heterogeneity. *Qiu et al.* [35] affirmed that optimization is extremely vital to acquire multi-response parametric solution for successful production of TMCs by LENS. *Sterling et al.* [36] obtained lofty fluctuations in thermal heating and cooling that resulted in anisotropy of the LENS samples for

the presence of porosity. The researchers used LENS process for the fabrication of Ti based composites for biomedical purpose, with superior ductility and strength as compared to the conventional counterparts. *Manjaiah et al.* [37] endowed with detailed information on diverse optimization processes and pointed on surface integrity of WEDM on TMC. The cutting speed was unswervingly proportional to IP. SR increased with increase in IP and PD but got decremented with pulse interval. Coated wires were obtained to be more favorable than the uncoated wires due to the decrement of oxide formation [36, 37]. *Manjaiah et al.* [37] presented combined information in the application of electric-discharge machining (EDM) and WEDM on TMC and identified the research gaps. The review also provided knowledge on the different optimization processes and highlighted the analysis of surface integrity like surface roughness, surface topography, surface metallurgy, layer formation and residual stress generation in WEDM on titanium based composites.

Bose et al. [38-40] proposed two new MOO algorithms termed as desirable genetic algorithm (DGA) [38] and desirable grey relational analysis (DGRA) [39, 40] for improvement in the optimized solution process parameters and performance measures in machining of hybrid TMC. Several investigations have been carried out for the enhancement of performance criteria by integrating advanced miscellaneous statistical methods like GA [41-43], artificial neutral network (ANN) [44-48], etc; however the optimal parametric combination of laser performance measures are yet to be explored. It is pragmatic from the past researchers that very less investigators have recognized the optimal solution of the laser performance measures after LENS process. Hence, the prime scope of this investigation is to develop a novel TMC with enhanced tribo-mechanical properties and to obtain the optimal parametric combination by varying important laser process parameters on various performance measures like cooling rate (CR) and

hardness (H). A novel MOO algorithm named as desirable genetic algorithm (DGA), where the objective functions obtained from desirability function, are further incorporated in GA in MATLAB R2018a for improvement in the optimized solution of the laser parametric combinations. ANOVA is incorporated for determining the reasonability of the mathematical model and the significance of the parameters.

Machining of titanium matrix composite (TMC) require a very vigilant attention in modern sustainable manufacturing arena. TMCs are strong, flexible, light and durable with exceptionally superior properties like corrosion and fatigue resistant and used in different aerospace, biomedical and automobile industries [49]. *Mouralova et al.* [50, 51] obtained a comparison on the surface and sub-surface topography of WEDM on structural materials like titanium and aluminium, and obtained greater productivity and superior characteristics of titanium at the effect of manufacturing cost. Manufacturing and machining of these hybrid composites by conventional techniques are enormously difficult due to the occurrence of uneven surface finish at lofty temperature resulting in excessive wear [4-7]. Large initial cost, ease of availability and manufacturability are the important limitations which are the prime concern while machining these TMCs [4]. RSM had been used in desirability function [5] of BBD on WEDM on pure titanium where Ton, Toff and IP were obtained as the key factors for obtaining the optimized output responses like dimensional deviation, MRR and wire wear (WW) ratio. The authors further examined the recast layer and surface crack density [6] and obtained the contribution of the same factors on SR by MOO using Taguchi method coupled with RSM and desirability. For sustainable manufacturing, grey relational analysis [52, 53] was projected to combine with various optimization techniques like analytical hierarchy process (AHP) for criteria weights [3, 15] coupled with RSM and regression analysis [53, 54]. The effects of machining parameters

with the cutting conditions (cryogenic, dry and wet) were examined for MOO. ANOVA results provided the significance and contributing effects of various interactive and quadratic effects of the parameters. TOPSIS [54, 55] was considered to be the appropriate decision making technique for determining the optimized condition because of its simplest computational procedure where infinite number of criteria and alternatives can be considered with easy implementation algorithm. *Majumder et al.* [56] carried WEDM on nitinol, a smart shape memory alloy and predicted the various surface roughness responses using general regression neural network (GRNN) coupling with fuzzy MOORA. Pulse-on time and discharge current were obtained to be the main contributing factors and ANOVA results showed the significance of the interactive parameters. A novel MOO algorithm known as MOPSO-TOPSIS [57] was proposed for machining Cu-MWCNT composite coated on 6061Al electrode. MOPSO was used for determination of non-dominated optimal solutions and TOPSIS was used for identification of the most desirable optimal solution. This novel technique may be used for MOO of TMC as similar contribution of process parameters were obtained and authenticated with the help of confirmatory tests. FTOPSIS [58-60] technique provides successful solutions in realistic problems where the decision makers provide opinions based on linguistic data. The judgment was acted on the decision of different decision makers (DM) which had been articulated by means of crisp numbers. However, in different realistic factual life circumstances, penchant model of an individual was inexact and DM was inept to place crisp numbers for comparison of judgments. Therefore, this limitation can be overcome by using FTOPSIS [58-60] which is a combination of TOPSIS [20, 21, 54, 55] and fuzzy theory [60, 61]. The added advantage is obtaining the criteria weights by FAHP [61, 62] based on their goals and importance, therefore obtaining the fuzzy ranking.

Nourbakhsh et al. [63] investigated experimentally on WEDM on titanium based alloys and composites. A Taguchi L18 DOE was applied. Cutting speed was unswervingly proportional to the peak current and pulse interval. SR incremented with the augmentation of pulse width and decremented with the pulse interval. *Hsieh et al.* [64] attained outstanding experimental results on $Ti_{35.5}Ni_{49.5}Zr_{15}$ and $Ti_{50}Ni_{49.5}Cr_{0.5}$ alloys and inferred about highest feeding rate without wire rupture in the process of WEDM. SR got enhanced with rising pulse duration of the machined TiNiX. As the pulse duration decreased, the oxide formation also got diminished. Therefore, the favorable condition was to incorporate coated wires instead of using the uncoated wires to obtain uniformity, as obtained by *Kuriakose et al.* [65]. The authors obtained uniform surface roughness with moderate discharge energy pulse. It was also obtained by *Han et al.* [66] that superior surface finish occurred with the apposite pulse energy in reversed polarity machining. *Sharma et al.* [67] performed BBD-RSM to examine the DOE. Cutting rate improved with the increment in pulse-on time and with the enhancement of peak current; and got decremented with the enhancement of the pulse-off time and the servo voltage affecting the surface roughness in a similar fashion. For improvement in the optimal solution of WEDM machining of the novel TMC, *Bose et al.* [68, 69] developed the novel MOO algorithm DGRA and improved the production with minimum machining time and cost. Further, *Bose et al.* [70-72] developed a novel method in selection of excellent and new hybrid green composite with the help of advanced MCDM techniques, compared with the experimental results and obtained excellent industrial applications for clean and sustainable energy recovery. The authors used ANOVA to obtain the significant input process parameters and concluded the dependency of input parameters on output responses of WEDM. Various researchers [73-84] have carried out their efforts for the development of WEDM performance of titanium based alloys and composites by

proposing various statistical techniques like ANN, MOGA-II, ANFIS, NSGA-II, desirability method, GRA, FTOPSIS, FAHP, PSO, etc, but still the limitation lies on the fabrication of complex shapes by the above methods and obtaining the optimal result. Hence, LENS process is suggested for better feasibility of the development of TMC which is socially viable and entirely accepted in social environment.

Yildiz et al. [85] introduced hybrid novel algorithms based on Nelder-Mead coupled with whale optimization for design and real-life manufacturing applications. The scope was to accelerate the convergence speed globally for solving such real-time manufacturing problems. The researchers [86] again coupled with another novel optimization named Harris hawks for solving such complex problems. A metamodel annealing with simulation [87] was projected for MOO of design strictures and a case study was optimized on highway guardrails for investigation of its performance having minimum weight and minimum value of acceleration severity index. Results inferred that this hybrid optimization algorithm is an extremely effective approach for real-life designing manufacturing problems. Several researchers [88, 89] used self adaptive techniques of meta-heuristic algorithms for reliability based optimization of design problems in aerospace and automobile sectors. The novel algorithm was very useful for solving the complex problems of aerodynamic analysis of the unmanned aerial vehicle and comparative performance were obtained based on hyper volume indicator. Recently various novel optimization algorithm [90-99] were developed in the automobile sectors namely moth-flame algorithm coupled with RSM, mine blast algorithm, equilibrium algorithm coupled with response surface-based metamodel, multi-verse optimization coupled with Harris hawks and grasshopper, salp swarm for structural design of automobile components, spotted hyena for reduction of weight in automobile brake components. A new modified adaptive differential evolution [100] was proposed for MOO of a

cam mechanism with offset deciphered roller follower. The simulation results indicated the robustness and effectiveness of this novel algorithm [101, 102] for real-life design and structural problems.

From the precedent literature it is apparent that very few researchers have identified the optimal solution in the proposed arena and there is an immense scope of improvement in the optimal solution by MOO of machining of WEDM on this developed TMC by LENS. Table 2.1 depicts the summary of prime literature reviews with research gaps. Therefore, this thesis aims to discover the influence of different process parameters on various performance measures like enhanced MRR, minimum SR, minimum KW and minimum OC of a developed novel material of titanium-titanium diboride (Ti-TiB$_2$) by LENS process and are compared with the past works. A novel composite is developed by LENS process by identifying the optimal process parameters. The other major scope is to explore the optimality set of WEDM on this developed TMC by using a novel DGRA optimization algorithm. BBD mathematical model with 3 factors 3 levels DOE is premeditated using RSM design matrix. A 17 grouping of run-orders with 5 center points is used in a full quadratic mathematical model. This research aims to enhance the mechanical properties and the microstructure depicts an excellent interfacial bonding of TiB$_2$ with Ti. To investigate the conformity of the experimental and predicted results, these results have been compared with an advanced MCDM method known as FTOPSIS coupled with FAHP for criteria weights. These experimental and predicted results are further compared and correlated with FTOPSIS coupled with FAHP for criteria weights for analyzing the conformity for various industrial applications. The reasonability of the developed mathematical model is confirmed by ANOVA. Sensitivity analysis has also been conceded for studying the robustness and sensitivity of four decision makers' preference on optimal machining condition.

Table 2.1. Summary of prime literature reviews with research gaps

AUTHORS (YEAR)	RESEARCH FINDINGS	RESEARCH GAPS
Niu et al. [10] (2012)	TiB_2 as reinforcements in ISM process and obtained improved mechanical properties	Optimal solution is not identified
Attar et al. [11] (2017)	Relative study of raw titanium manufactured by different laser process	Development by LENS process
Qiu et al. [35] (2015)	Production of hefty Ti–6Al–4V structures through undeviating laser deposition	Microstructural characterization
Sterling et al. [36] (2016)	Exhibited the LENS samples and inferred feeble fatigue properties	Porosity presence
Hu et al. [12, 13] (2018)	Mixture powder of titanium with 1.6 wt.% boron	Proper MOO analysis
Attar et al. [14] (2014)	LENS of TMC with 2 wt.% boron	Development of Ti-TiB_2 composite using LENS
Manjaiah et al. [37] (2014)	Consolidated information on the application of EDM and WEDM on titanium based composite	Novel optimization method is to be incorporated
Nourbakhsh et al. [63] (2013)	Experimentally investigated WEDM on titanium based alloys and composites by Taguchi L18 DOE	BBD and CCD are to be examined
Kumar [42] (2019)	Measurement of responses and process parameters optimization	GA and MOGA can be coupled with desirability
Younas et al. [3] (2019)	MOO for sustainable turning Ti6Al4V alloy using GRA and AHP	GRA + desirability is yet to be developed
Khan et al. [15] (2020)	MOO on turning of Ti-6Al-4V under various environmental conditions by GRA	Work hardening, high temperature generation, excessive cutting pressure are serious issues for proper machining
Ananthakumar et al. [20] (2019)	RSM with TOPSIS is used for optimization of plasma arc cutting of Monel 400™	FTOPSIS may be used with RSM for better result analysis
Jin et al. [23] (2021)	Refined microstructure and enhanced wear resistance with excellent mechanical characteristics are obtained on TMCs by selective laser melting (SLM)	Worn depth and wear rate are the challenges in the developed matrix
Cheng et al. [24] (2021)	Microstructure of Ti-6Al-4V components by annular laser metal deposition	Improved strength was obtained at the cost of martensitic microstructure
Kumar et al. [29] (2017)	Laser Power and speed contributed to the maximum speed	Direct effect of laser power with inverse effect was observed
Abidi et al. [41] (2018)	MOGA-II was conceded on micro-electrical discharge machining	MOGA-II may be coupled with desirability for comparative analysis

Kumar [43] (2018)	Investigations experimentally for MOO of SR using GA	Better optimal solution is yet to be identified
Mouralova et al. [49-51] (2018)	Analysis of surface morphology of WEDM on titanium alloys and composites	Uneven surface finish at high temperature following excessive wear
Kavimani et al. [53] (2019)	MOO in WEDM process through hybrid methods	Proper optimization analysis is needed
Ramesh et al. [54] (2016)	Measurement and optimization of SR and tool by coupling with GRA, TOPSIS and RSM methods	Gap lies in the comparative analysis coupling with RSM+GRA+FTOPSIS
Shandilya et al. [73] (2020)	MOO on machining of Inconel-825 using WEDM	Comparative analysis of WEDM with TMC and Inconel-825 is needed
Yildiz [85, 86] (2019)	Novel Whale–Nelder–Mead to solve problems based on design and manufacturing	Desirability may be coupled with these MOO methods
Yildiz [91, 92] (2020)	Moth-flame optimization and mine blast algorithm and response surface methodology	Desirability may be coupled with these MOO methods
Yildiz [96, 97] (2020)	Spotted hyena optimization algorithm for automobile components	Desirability may be coupled with these MOO methods

ANOVA provides the dependency of linear, quadratic and interactive effects of all the process parameters over the performance measures where peak current is the most contributing factor influencing the DGRA of MOO. Improved tribo-mechanical and biocompatible properties are obtained in the developed novel TMC when compared to pure titanium to make complex shapes for various industrial and biomedical applications.

2.1. Objectives of the research

Within the scope of the literature review, enough information is not available about the development and fabrication of LENS of Ti-TiB$_2$ taking pure titanium as base material reinforcing with a varying weight percentage of titanium diboride, and machining with WEDM. Therefore, the objectives of the present research work are:

- This research includes three major stages: (i) Developing a novel Ti-TiB$_2$ hybrid composite for various automotive, aerospace, and biomedical applications; (ii) Using the LENS process for the composite development and optimizing the process parameters; and (iii) Using WEDM to machine the TMC and to obtain the optimal process parameters for the best performance using a novel optimization algorithm.

- To obtain the better mechanical, metallurgical, and tribological properties of the hybrid TMC. This research aims to provide the current state-of-the-art of enhancement of tribo-mechanical properties.

- To investigate various output performance measures like cooling rate (CR) and hardness (H) while the development of TMC by LENS process.

- To analyze the microstructural characterization of the hybrid composite using SEM micrographs.

- To acquire the optimal process parameters while machining the samples by WEDM.

- To investigate various output performance measures like MRR, SR, KW, and OC and optimization can be done accordingly by different optimization techniques.

- New process models implementing novel optimization algorithms are to be developed to decrease inaccuracy caused by machine vibration, chatter, and wire deflection.

2.2. Novelty of the research

- In this present investigation, the objective functions obtained from desirability function are further incorporated in genetic algorithm (GA) in MATLAB R2018a for improvement in the optimized solution. This combination of desirability with GA outcomes the novelty in MOO named as desirable genetic algorithm (DGA) where the predicted responses are also considered along with the experimental responses. Main

advantage of incorporating this novel DGA technique is more accuracy and robustness. The actual and predicted responses are in near proximity with one another. This novel DGA method has additional superiority in accomplishing the MOO solution.

➢ Novel multi-objective optimization algorithm called desirable grey relational analysis (DGRA) is proposed for determination of optimal solution on the performance measures of the WEDM. The novelty lies in its dual optimization technique where predicted responses obtained from desirability function is coupled with GRA, which has not yet been covered by the past researchers. The main advantage of DGRA lies in the consideration of the predicted responses as obtained from desirability method with the actual experimental responses; therefore the numbers of total responses are incremented even in single and multi-objective optimization problems. As a result, in this method more accuracy is obtained along with enhanced percentage of improvement.

➢ A novel titanium matrix composite (TMC) is developed by laser engineering net shaping (LENS) process. This research provides the current state-of-the-art of enhancement of tribo-mechanical properties like corrosion, wear, fatigue resistant and biocompatible properties when compared to pure titanium and other titanium alloys, to make complex shapes for various industrial applications, and other biomedical applications specifically in bones, hips, dental problems, knee replacement enucleation and has an assortment of different surgical instruments.

CHAPTER 3

3. Materials and Research Methodology

The hybrid composite is developed using LENS (MR7, Optomec, United States of America) process following three major steps namely pre-processing, development and post-processing. In pre-processing, pure titanium raw powder (98 wt.%) as base material is reinforced with boron powder (2 wt.%) as secondary phase reinforcement for the composite development. After proper mixing of the powders, the mixture is dried in a vacuum oven at around 90^0C for removal of any moisture content. In LENS process, a 500 W fiber laser doped by ytterbium with continuous wave is used for the composite development in LENS. LENS merges powder from the feeding nozzle with the help of laser as designed by CAD and other numeric control technologies. An elevated laser beam power is employed for creating a melt pool on the substrate and concurrently powder feeding is carried over the melt pool for consolidation. The metal powder is then supplemented from the nozzle over the melt pool by traversing the laser beam. Independent delivery of the powder and the laser beam is operated irrespective of the orientation position. This LENS process is susceptible to powder flow behavior as the powder is sent by the nozzle which in turn provides a consolidated pathway of preferred volume and surface quality of texture. The powder is carried from powder feeder by transport or carrier gas or by gravity-driven technology. The particles of the powder progress through an assortment of various channels/ chambers which are inside the nozzle, thus having collisions with nozzle wall to provide a stream of powder particles which are directed at a laser spot. Transformation of phase by melting and solidification takes place after that for fabrication with XY table movement. The deposition head consists of powder delivery nozzle shifts up vertically following each layer. The complete process is conceded in an inert environment for protecting the melt pool from oxidation. The sample powders are maintained in a box containing argon (Ar) and oxygen (O_2)

smaller than 10 ppm and laser power from 150 - 400 W, with a scan speed of 10-15 mm/s when the powder feed rate is maintained at 2.3 g/min. The best parameter obtained is 350 W laser power with 10 mm/s scan speed.

Raw powders [pure Ti (98 wt.%) + B (2 wt.%)] in LENS

Proper mixing and drying in a vacuum oven (90^0C) to release locked-in moisture contents

Composite development (500 W continuous wave ytterbium-doped fiber laser)

Dried powder is kept in an atmosphere of (Ar + O_2 < 10 ppm) using optimum laser power 350W at scan speed of 10 mm/s, when powder feed rate = 2.30 g/min

Post-fabrication + polishing using a solution of 100 ml HNO_3 + 100 ml HF + 300 ml H_2O solution

Composite is developed and ready for WEDM machining

Fig. 3.1. Flowchart of the composite development

Fig. 3.1 indicates the complete flow chart of composite development. Eq. (1) [11] portrays the energy input/area (E):

$$E = \frac{P}{V.D} \qquad (1)$$

P illustrates laser power, V represents scan speed, and D reveals laser beam diameter (which is 0.5 mm). The mixture powder absolutely melts with the optimum incident energy lying between 50 and 70 J/mm^2. When entire powder melting is accomplished, the deposits emerge to familiar towering temperatures because of extreme heat upsurge. The consecutive overheating and quick cooling may pilot to the creation of internal stresses. Post-fabrication grinding and polishing is necessary to remove the tiny surface cracks and porosity apparently because of the liberation of locked-in residual stresses. Further investigation is performed on the characterization of microstructure, hardness, and other mechanical properties. Post-processing includes polishing to remove the miniature surface cracks and porosity to release the entrapped residual stresses. The polished samples are etched by 100 ml HNO$_3$ + 100 ml HF + 300 ml H$_2$O solution. For examining in particular the uniformity in microstructure and deposits' quality, standard light microscope (Olympus BX51M, Japan) is used. Scanning electron microscope (SEM, Phenom proX, Phenom-World B.V., Netherlands) is used for detecting microstructural characterization.

The dimension of the developed sample is 11 mm in diameter and 16 mm in height as depicted in Fig. 3.2(a). Machined sample after WEDM is portrayed in Fig. 3.2(b).
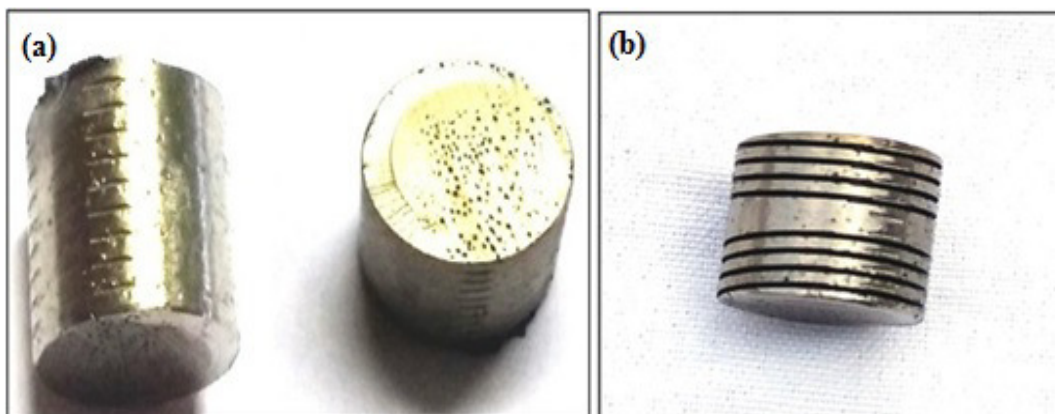
Fig. 3.2(a) Developed TMC after LENS process; and **(b)** after WEDM

This novel developed TMC possesses enhanced tribo-mechanical properties as illustrated in table 3.1. An apparent comparison of enhanced and superior tribo-mechanical properties with other akin aerospace alloys and composites has been recognized when contrasted with the precedent investigators [3, 11, 14, 15]. The developed TMC (Ti-TiB$_2$) acquires improved tribo-mechanical characteristics like enhanced strength-to-weight ratio at eminent temperature, improved resistant to wear, fatigue, corrosion, excellent strength and bio-compatibility. The novel characteristics developed in this TMC are: Young's modulus (550 GPa), co-efficient of thermal expansion (8.6x10^{-6} /K), Hardness (396 HV), Yield strength in compression (945-1020 MPa), Ultimate compressive strength (1020-1096 MPa) and Elongation (25-32.5%). Vicker's microhardness measurements are conceded (500 gm load for 10 s) at an average of 10 measurements. These results can compared with the TMC developed by *Attar et al.* [11, 14] where parameters obtained were: Young's modulus (529-540 GPa), co-efficient of thermal expansion (8.6x10^{-6} /K), Hardness (392 HV), Yield strength in compression (940-1010 MPa), Ultimate compressive strength (1016-1092 MPa) and Elongation (26.5-36.4 %).

Fig. 3.3(a) depicts the schematic diagram of the TMC developed after LENS process which signifies very fine and excellent distribution of TiB$_2$ particles adjacent to the bigger Ti powders. Fig. 3.3(b) represents the formation of TMC developed by selective laser melting (SLM) process [23] which portrays semi-reacted TiB$_2$ particles with unreacted TiB$_2$ and in-situ creation of needle-shaped TiB (whiskers) with partially formation of TiB owing to a weak interfacial bonding [14]. SLM uses powder-based deposition technique where high laser energy is mandatory for complete melting owing to a greater difficulty of proper formation of these intermetallic compounds as these TMCs have high melting point causing increment in viscosity.

This limitation can be surmounted by using LENS process as it is a nozzle-deposition technique with powder feed rate as an additional parameter.
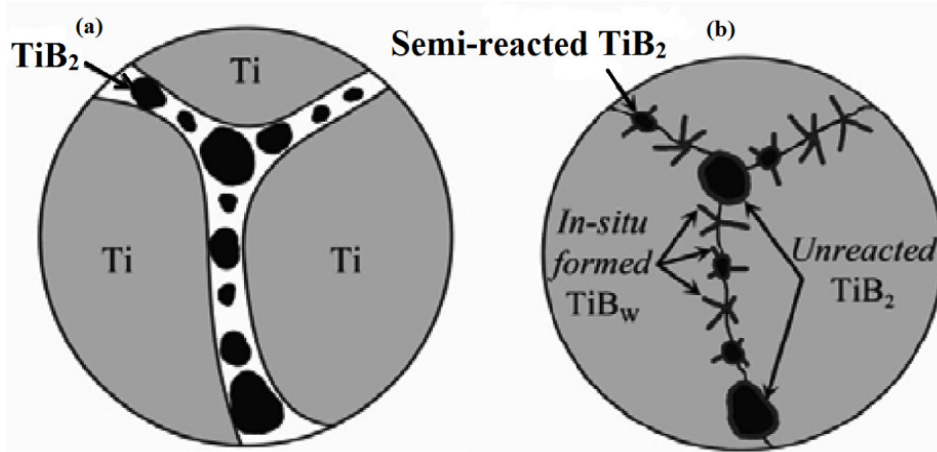
Fig. 3.3. TMC formed after **(a)** LENS process and **(b)** after SLM

Table 3.1. Comparative properties of TMC with other alloys [3, 11, 14, 15]

Mechanical Property	Material						
	Ti-TiB$_2$ (Ti-2.0 wt.%B)	Ti-1.6 wt.%B	Pure Ti	Ti6Al4V	Ti6Al6V-2Sn	Ti-10V-2Fe-3Al	Inconel 718
Density (g/cm^3)	4.41	4.48	4.5	4.43	4.54	4.65	8.22
Hardness (HV)	396	392	180-184	285-342	361	303	361-438
Young's modulus (GPa)	550	529-540	116	114	110	110	200
Yield strength (MPa)	945-1020	940-1010	140	880	980	900	1170
Ultimate strength (MPa)	1020-1096	1016-1092	220	950	1050	970	1350
Ductility (%)	25-32.5	26.5-36.4	54	14	14	9	16
Fracture toughness (MPa m$^{1/2}$)	78	72	70	75	60	-	96.4
Thermal conductivity (W/mK)	6.8	6.8	17	6.7	6.6	7.8	11.4

CHAPTER 4

4. Theoretical and statistical foundations

4.1. Mathematical model design by RSM

RSM [3-7] is mainly competent flourishing statistical technique in lieu of a compilation of mathematical techniques, stratagems of designs based on statistics and strategies of experimental design and statistical inferences. It is used for improvement of quadratic and interactive effects in the midst of the different variables. The output responses in terms of performance measures are considered in this experimental and statistical investigation. The experimental performance measures output responses which are considered for the present statistical and experimental investigation. Eq. (2) represents the fitness function of a second-order polynomial:

$$\breve{Z} = \breve{a}_o + \sum_{\breve{i}=1}^{\breve{m}} \breve{a}_{\breve{i}} \breve{x}_{\breve{i}} + \sum_{\breve{i}=1}^{\breve{m}} \breve{a}_{\breve{i}\breve{i}} \breve{x}_{\breve{i}}^{\,2} + \sum_{\breve{i}=1, \breve{j}>1}^{\breve{m}} \breve{a}_{\breve{i}\breve{j}} \breve{x}_{\breve{i}} \breve{x}_{\breve{j}} + \breve{e} \tag{2}$$

$\breve{Z}$ represents the output response; $\breve{a}_o$, $\breve{a}_{\breve{i}}$, $\breve{a}_{\breve{i}\breve{i}}$, $\breve{a}_{\breve{i}\breve{j}}$ symbolize regression coefficients; $\breve{m}$ represents the experimental factors; $\breve{i}$ corresponds to linear effect; $\breve{j}$ corresponds to quadratic effect; $\breve{x}_{\breve{i}}$ & $\breve{x}_{\breve{j}}$ signifies the interactive effects on variables; $\breve{e}$ represents random error.

For the development of the material, design expert 11 software based on RSM-BBD, has been conceded on sixteen (16) run-orders for experimentation having four (4) center points. A 3-factor/3-level design of experiments (DOE) is anticipated for obtaining the MOO solution of CR and H as acquired experimentally from LENS process. Low, medium and high levels, characterized by -1, 0, and +1, are incorporated in the DOE for obtaining the objective function. Table 4.1 specifies the detailed DOE of the developed TMC with their predicted and actual results.

Table 4.1. RSM-BBD design of experiments of composite development

Run Order	Space Type	A: Laser power (W)	B: Scan speed (mm/s)	C: Energy input/area (J/mm^2)	R1: Cooling Rate (K/s)	Pred R1 (K/s)	R2: Hardness (HV)	Pred R2 (HV)
1	IBFact	275	10	80	-2912981.669	-2892557.9	392	392.25
2	IBFact	400	12.5	80	-2921796.193	-2913517	397	396.375
3	IBFact	400	12.5	20	-2898138.021	-2903599	396	396.625
4	IBFact	150	15	50	-8850853.189	-8822150.2	390	390.125
5	IBFact	275	10	20	-2866357.76	-2832193.9	393	392.5
6	IBFact	275	15	80	-4874821.303	-4908985.2	394	393.5
7	IBFact	400	15	50	-3515644.346	-3489759.6	397	397.125
8	IBFact	400	10	50	-2327964.069	-2356667	396	395.875
9	IBFact	275	15	20	-4922132.983	-4942556.7	394	393.75
10	Center	275	12.5	50	-4135723.086	-4111679.7	392	393
11	Center	275	12.5	50	-4113077.143	-4111679.7	393	393
12	Center	275	12.5	50	-4090493.371	-4111679.7	393	393
13	IBFact	150	12.5	80	-7324544.229	-7319083.3	389	389.375
14	IBFact	150	10	50	-5802567.97	-5828452.7	389	388.875
15	IBFact	150	12.5	20	-7293929.657	-7302208.9	390	389.625
16	Center	275	12.5	50	-4107425.371	-4111679.7	393	393

For machining of the developed TMC by WEDM again RSM-BBD methodology of 17 grouping of experimental run-orders in a full quadratic mathematical model with 5 center points is carried in design expert 11 software. A 3-factor/3-level DOE is projected in this research for obtaining the optimal solution of MRR, SR, KW and OC after machining with WEDM on TMC obtained after LENS. Table 4.2 indicates the detailed experimental designs of the mathematical model for machining Ti-TiB$_2$ hybrid composite and their corresponding actual and predicted results.

Table 4.2. RSM-BBD design of experiments of WEDM

		A	B	C	R1		R2			R3		R4	
Std	Run	Power (W)	Time Off (μs)	Peak Current (A)	Material Removal Rate (mm³/min)	Predicted MRR (mm³/min)	Surface Roughness (μm)	Actual Value SR Transform	Predicted value	Kerf Width (mm)	Predicted KW (mm)	Over Cut (mm)	Predicted OC (mm)
		P	Toff	IP	MRR	Pred. MRR	SR	SRT=1/sqrt(SR)	Pred. SRT	KW	Pred. KW	OC	Pred. OC
10	1	7	30	5	3.5136	3.5202	0.895	1.0570	1.0639	0.36	0.3608	0.11	0.1108
7	2	6	25	10	3.1812	3.1827	1.378	0.8519	0.8593	0.33	0.3288	0.08	0.0788
2	3	8	20	8	4.0262	4.0125	0.942	1.0303	1.0345	0.41	0.4100	0.16	0.1600
17	4	7	25	8	3.3388	3.3866	0.857	1.0802	1.0675	0.34	0.3480	0.09	0.0980
1	5	6	20	8	3.423	3.4253	0.697	1.1978	1.1980	0.35	0.3520	0.1	0.1020
14	6	7	25	8	3.43	3.3866	0.878	1.0672	1.0675	0.35	0.3480	0.1	0.0980
9	7	7	20	5	3.876	3.8917	0.771	1.1389	1.1422	0.38	0.3792	0.13	0.1292
15	8	7	25	8	3.416	3.3866	0.911	1.0477	1.0675	0.35	0.3480	0.1	0.0980
16	9	7	25	8	3.416	3.3866	0.899	1.0547	1.0675	0.35	0.3480	0.1	0.0980
11	10	7	20	10	3.542	3.5377	1.213	0.9080	0.9002	0.35	0.3488	0.1	0.0988
12	11	7	30	10	3.6584	3.6404	1.576	0.7966	0.7941	0.34	0.3412	0.09	0.0912
13	12	7	25	8	3.332	3.3866	0.845	1.0879	1.0675	0.35	0.3480	0.1	0.0980
5	13	6	25	5	3.2328	3.2153	0.743	1.1601	1.1566	0.36	0.3592	0.11	0.1092
8	14	8	25	10	3.7592	3.7799	1.592	0.7926	0.7953	0.37	0.3712	0.12	0.1212
3	15	6	30	8	3.2472	3.2609	0.923	1.0409	1.0367	0.36	0.3600	0.11	0.1100
4	16	8	30	8	4.0052	4.0029	0.988	1.0061	1.0058	0.38	0.3780	0.13	0.1280
6	17	8	25	5	3.9858	3.9811	0.968	1.0164	1.0097	0.39	0.3908	0.14	0.1408

4.2. Desirability

The desirability [4-7] approach is vastly recommended for its simplified form of algorithm where individual response's weightage and importance are extremely flexible with each other. It is also immensely suggested due to the flexibility in the individual weightage of performances and its importance. It converts individual response to utility values delimited by the domain $0 < \breve{d}_{\bar{i}} < 1$ ($\breve{d}_{\bar{i}}$ represents individual desirability of response). Superior desirability of a response depends on the higher value. Criteria weights $\breve{w}_{\bar{i}}$ resemblances the shape of desirability function. $\breve{Z}$

signifies output response, $\breve{D}$ showcases overall desirability where individual response is prearranged depending on the importance $\breve{r}$ which is comparative to other responses as designated in Eq. (3). Importance of 3 signifies neutral importance, greater than 3 portray superior importance, and 1 represents lowest importance.

For a goal to be maximum, desirability is identified using Eq. (3):

$$
\breve{d}_{\bar{i}} = \begin{cases} 0 & ; \quad \breve{Z}_{\bar{i}} < Low_{\bar{i}} \\ \left(\dfrac{\breve{Z}_{\bar{i}} - Low_{\bar{i}}}{High_{\bar{i}} - Low_{\bar{i}}} \right)^{\bar{w}_{\bar{i}}} & ; \quad Low_{\bar{i}} < \breve{Z}_{\bar{i}} < High_{\bar{i}} \\ 1 & ; \quad \breve{Z}_{\bar{i}} > High_{\bar{i}} \end{cases}
\tag{3}
$$

Table 4.3 signifies the importance with limits and goals for the matrix development. Laser process parameters like P, V and E are in range, assigned as 3 and kept as neutral; and the main performance measures like CR is given the maximum importance of 5 whereas H is assigned an importance of 4 for better comparison. The goal of H is to be maximum and the magnitude of CR is to minimum but due to the '-ve' sign the goal has to be maximized for better optimized solution.

Table 4.3. Goals and importance of matrix development

Name of Parameter	Goal	Lower	Upper Limit	Importance
A:Laser Power	range	150	400	3
B:Scan Speed	range	10	15	3
C:Energy input/area	range	20	80	3
Cooling Rate	maximize	-8.85E+06	-2.33E+06	5
StdErr(Cooling Rate)	minimize	17559.5	30414	3
Hardness	maximize	389	397	4
StdErr(Hardness)	minimize	0.119678	0.267609	3

Table 4.4 represents the goals, importance values and their lower and upper limits for machining by WEDM. P, Toff and IP is in range and assigned as 3 as these are the neutral input process parameters; and both MRR and SR are assigned an importance of 5 for giving maximum importance as these are the main performance measures. MOO is carried for WEDM of Ti-TiB$_2$ hybrid composite is acquired using D-optimality also called desirability approach. The lower and upper limits of goals with their importance are assigned to all parameters and responses as depicted in table 4.4. All the input process parameter goals are set in range with importance as 3(+++). The objective is to achieve maximum MRR, therefore, goal of MRR is assigned to maximize with top priority of 5(+++++); minimum SR, therefore, goal of SR is allotted to minimize with top priority of 5(+++++); KW and OC also to be kept minimum, so the goal is assigned to minimize with an importance of 4(++++); and all the standard errors to be kept minimum with least importance.

Table 4.4. Numerical optimization goals and importance by WEDM

Name	Goal	Lower Limit	Upper Limit	Importance
A:Power	is in range	6	8	3
B:Time Off	is in range	20	30	3
C:Peak Current	is in range	5	10	3
MRR	maximize	3.1812	4.0262	5
StdErr(MRR)	minimize	0.0174479	0.0348209	1
SR	minimize	0.792553	1.1978	5
StdErr(1/Sqrt(SR))	minimize	0.00634902	0.0126708	1
KW	minimize	0.33	0.41	4
StdErr(KW)	minimize	0.00165345	0.0032998	1
OC	minimize	0.08	0.16	4
StdErr(OC)	minimize	0.00165345	0.0032998	1

For the criteria of minimum goal, the boundary value of 0 and 1 reinstates their position under the identical boundary conditions. Eq. (4) signifies $\breve{D}$:

$$\breve{D} = \left(\prod_{\breve{i}=1}^{\breve{n}} \breve{d}_{\breve{i}}^{\breve{r}_{\breve{i}}} \right)^{\frac{1}{\sum \breve{r}_{\breve{i}}}} \tag{4}$$

$\breve{n}$ indicates the number of responses and $\breve{r}_{\breve{i}}$ represents the target value in $\breve{i}^{th}$ response.

4.3. Desirable Genetic Algorithm (DGA)

For finding the best solution associated to problems based on the relevance of philosophy of evolutionary biology, a method is invented known as genetic algorithm (GA). GA employs genetic inheritance, selection by natural instincts, crossover, mutation and reproduction. GA incorporates genetic programming (GP) based on methodologies like genetic and evolutionary computation (GEC) [41-43]. It is employed by computer simulations by MATLAB software for MOO problems. For optimization problems, individuals are characterized by abstract representations termed as chromosomes, which are members in space. In this present investigation, the objective functions obtained from desirability function are further incorporated in GA in MATLAB R2018a for improvement in the optimized solution. This combination of desirability with GA outcomes the novelty in MOO named as desirable genetic algorithm (DGA) where the predicted responses are also considered along with the experimental responses. Main advantage of incorporating this novel DGA technique is more accuracy and robustness. The actual and predicted responses are in near proximity with one another. This novel DGA method has additional superiority in accomplishing the MOO solution. Here, an iterative progression is proposed which develops an effective individual set, termed as population, towards an objective function, known as fitness function. Alternative encodings are developed by binary strings. It is extremely simplified and possesses stylized biological simulation. Fig. 4.1 entails the detailed flow chart of DGA. A population of individuals is randomly generated based on probabilistic

distribution generally uniform in multiple steps called generations. From the current population, every generation and individuals are randomly selected based on certain fitness application by means of crossover ratio which is then tailored by mutation for obtaining a new population. A swap over of genetic objects called as crossover indicating structural mechanism that attributes machine learning for searching MOO problem. Selection criteria resemblances the relevance of complete fitness decisive factors to decide about the reproduction. Replication is the dissemination of former to subsequent generation individuals. Mutation is the amendment of chromosomes for solitary individuals.
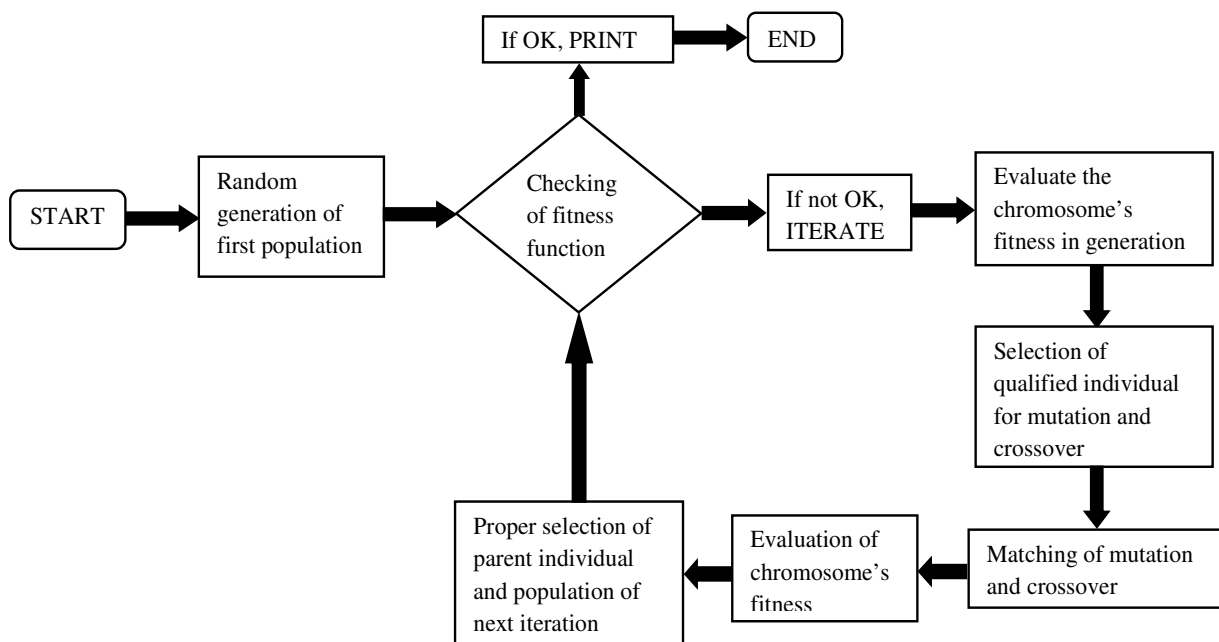
Fig. 4.1. Flowchart of novel desirable genetic algorithm

47

4.4. Desirable Grey Relational Analysis (DGRA)

Prof. Deng in 1982 invented grey relational analysis (GRA) [52, 53] which is based on grey logic system where information based on continuum quality and quantity appear from black to white, through grey. Here, the information associated with the quantity and quality constitutes a continuum from zero to complete information, resembling from black through grey and to conclude with white. Therefore, for such multifaceted multi response optimization problems, an assortment of MCDM techniques are used in statistical analysis for attaining the most excellent and optimal set of results with maximum productivity and minimum cost. Therefore, in this research a novel optimization algorithm called DGRA is proposed for the enhancement and improvement of optimized results after obtaining from desirability function. The prime novelty lies in its dual optimization technique where predicted responses obtained from desirability function are coupled with GRA, which has not yet been covered by the past researchers. Taguchi method coupled with DGRA is adopted to recognize the most imperative influencing process and performance parameters. The predicted responses acquired from desirability function are considered along with the actual experimental responses which are then coupled with GRA, therefore increasing the number of responses in single and MOO problems. The main advantage of DGRA lies in the consideration of the predicted responses as obtained from desirability method with the actual experimental responses; therefore the numbers of total responses are incremented even in single objective optimization and MOO problems. As a result in this method more accuracy is obtained along with enhanced percentage of improvement. Hence, added accuracy is attained in this technique with superior percentage of improvement. DGRA steps are highlighted below:

Step 1: Normalization: The normalization is rated between 0 to 1 where all the predicted and experimental responses are considered. Higher the improvement for MRR and lower the improvement for SR, KW and OC as depicted by Eq. (5):

$$\breve{X}_{\bar{i}}(\breve{k}) = \begin{cases} \dfrac{\breve{Y}_{\bar{i}}(\breve{k}) - \min \breve{Y}_{\bar{i}}(\breve{k})}{\max \breve{Y}_{\bar{i}}(\breve{k}) - \min \breve{Y}_{\bar{i}}(\breve{k})} \; ; \; Higher\,the\,better \\[3mm] \dfrac{\max \breve{Y}_{\bar{i}}(\breve{k}) - \breve{Y}_{\bar{i}}(\breve{k})}{\max \breve{Y}_{\bar{i}}(\breve{k}) - \min \breve{Y}_{\bar{i}}(\breve{k})} \; ; \; Lower\,the\,better \end{cases} \tag{5}$$

$\breve{X}_{\bar{i}}(\breve{k})$ is the function obtained after the generation of DGRA, $\breve{Y}_{\bar{i}}(\breve{k})$ attained from experimental runs, $\min \breve{Y}_{\bar{i}}(\breve{k})$, $\max \breve{Y}_{\bar{i}}(\breve{k})$ represents minimum and maximum assessment of $\breve{Y}_{\bar{i}}(\breve{k})$ and $\breve{i}$ signifies the run-orders for $\breve{k}^{th}$ response.

Step 2: Computation of Desirable Grey Relational Coefficient (DGRC): It is computed by Eq. (6):

$$\breve{\zeta}_{\bar{i}}(\breve{k}) = \frac{\Delta_{\min} + \breve{\xi}\Delta_{\max}}{\Delta_{o\bar{i}}(\breve{k}) + \breve{\xi}\Delta_{\max}} \tag{6}$$

$\breve{\zeta}_{\bar{i}}$ portrays DGRC, $\Delta_{o\bar{i}}(\breve{k})$ represents the offset value flanked by reference (considered as 1.00), $\breve{\xi}$ signifies characteristic coefficient (selected at 0.5) [52, 53], $\Delta_{\min}$ signifies least value and $\Delta_{\max}$ portrays highest value of $\Delta_{o\bar{i}}(\breve{k})$.

Step 3: Computation of Desirable Grey Relational Grade (DGRG): The multi-objective values are converted to equivalent single objective value by Eq. (7):

$$\breve{\delta}_{\bar{i}} = \frac{1}{\bar{n}} \sum_{\breve{k}=1}^{\bar{n}} \breve{\zeta}_{\bar{i}}(\breve{k}) \tag{7}$$

$\breve{\delta}_i$ signifies DGRG whose range is in between 0 to 1, $\breve{n}$ represents the run-orders, where highest DGRG value corresponding to best possible parameters and performance measures and considered as rank 1.

4.5. FTOPSIS

TOPSIS coupled with fuzzy logic [55] is correlated for the measurement of distance of alternatives from ideal solutions. Positive ideal solution (PIS) maximizes superior the improvement and lowers the improved type criteria in case of negative ideal solution (NIS). Here, judgment based on several decision makers (DM) is articulated with crisp numbers. However, in different realistic circumstances, preference model of an individual is inexact and DM is inept to place crisp numbers for contrasting the judgments, inferring the system to be inexact and DM is incapable for providing the crisp numbers. Therefore, this limitation can be overcome by using FTOPSIS [58-60] which is a combination of TOPSIS [20, 21, 54, 55] and fuzzy theory [60, 61] methodology. A Triangular Fuzzy Number (TFN) is identified by a triplet M = (l, m, u) signifying lower, median and upper values of M as shown in Fig. 4.2.
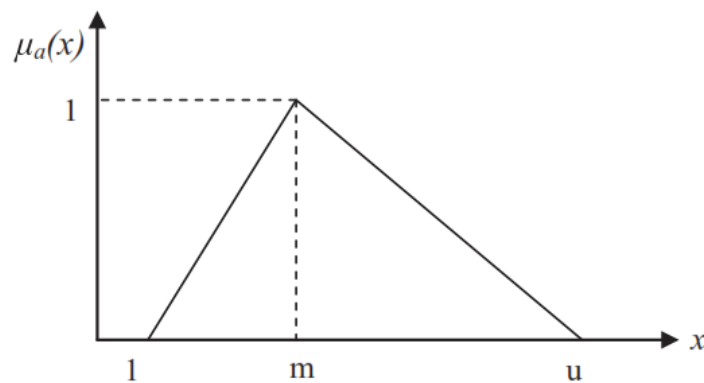

Fig. 4.2. Triangular Fuzzy Number (M)

The membership function $\mu_M(x)$ is shown in Eq. (8):

$$\mu_M(x) = \begin{cases} 0, & if \ x < l \\ \dfrac{x-l}{m-l}, & l \leq x \leq m \\ \dfrac{x-u}{m-u}, & m \leq x \leq u \\ 0, & if \ x > u \end{cases} \tag{8}$$

The distance between two TFN $M_1 = (l_1, m_1, u_1)$ and $M_2 = (l_2, m_2, u_2)$ can be calculated using vertex method as given by Eq. (9):

$$d(M_1, M_2) = \left[\frac{1}{3} \left\{ (l_1 - l_2)^2 + (m_1 - m_2)^2 + (u_1 - u_2)^2 \right\} \right]^{\frac{1}{2}} \tag{9}$$

The implementation of FTOPSIS is shown:

Step 1: Formation of decision matrix, D as depicted by Eq. (10):

$$D = \left[x_{ij} \right]; i = 1, 2, \ldots, \widehat{m}; \ j = 1, 2, \ldots, n \tag{10}$$

where, $\widehat{m}$ represents number of alternatives indicating experimental runs (17) and n depicts number of criteria indicating output responses (4) like MRR, SR, KW and OC. An assumption of decision group of k members is considered for the rating of assignment to the criteria and alternatives. Here, $k = 4$, is assumed where each DM is chosen from four (4) decision makers. The fuzzy rating of kth DM about the alternative A_i is designated as $x_{ij}^k = (l_{ij}^k, m_{ij}^k, u_{ij}^k)$ and the weight is indicated by $w_j^k = (w_{j1}^k, w_{j2}^k, w_{j3}^k)$, w.r.t. to criterion C_j.

Step 2: Calculation of aggregated fuzzy ratings of alternatives and criteria weights using Eq. (11) and Eq. (12): The aggregated fuzzy rating of $x_{ij}^k = (l_{ij}^k, m_{ij}^k, u_{ij}^k)$ of ith alternative w.r.t. j^{th} criterion is given below in Eq. (11):

$$l_{ij} = \min_k \{l_{ij}^k\}, m_{ij} = \frac{1}{K} \sum_{k=1}^{K} m_{ij}^k, u_{ij} = \max_k \{u_{ij}^k\} \tag{11}$$

The aggregated fuzzy weight is shown in the Eq. (12):

$$w_{j1} = \min_k \{w_{j1}^k\}, w_{j2} = \frac{1}{K} \sum_{k=1}^{K} w_{j2}^k, w_{j3} = \max_k \{w_{j3}^k\} \tag{12}$$

By incorporating fuzzy scale as shown in table 4.5, rates individual criterion with apposite linguistic expressions depending on importance of machining responses as shown in table 4.6. The combined DM matrix is hence calculated and shown in table 4.7.

Table 4.5. Fuzzy scale of responses

Importance	Fuzzy numbers
Lowest (L1)	(0, 0, 0.1)
Lower (L2)	(0, 0.1, 0.3)
Low (L3)	(0.1, 0.3, 0.5)
Medium (M)	(0.3, 0.5, 0.7)
High (H3)	(0.5, 0.7, 0.9)
Higher (H2)	(0.7, 0.9, 1)
Highest (H1)	(0.9, 1, 1)

Table 4.6. Importance by DM

Response	DM1	DM2	DM3	DM4
MRR	H1	H2	H1	H3
SR	H2	H1	H3	H2
KW	H3	M	M	L3
OC	M	M	L3	M

Table 4.7. Combined decision makers' matrix

Criteria	Response	Combined Decision makers' matrix		
B	MRR	0.5	0.9	1
NB	SR	0.5	0.875	1
NB	KW	0.1	0.5	0.9
NB	OC	0.1	0.45	0.7

Step 3: Normalization of decision matrix using Eq. (13):

$$r_{ij} = \frac{x_{ij}}{\sqrt{\sum_{i=1}^{\bar{m}} x_{ij}^{2}}} \tag{13}$$

where, r_{ij} represents normalized decision matrix. By the support of fuzzy scale as depicted in table 4.5, individual DM rates individual criterion with the help of appropriate linguistic terminologies depending on the importance of performance measures as revealed in table 4.6 and the aggregated fuzzy weights are considered using FAHP method [61, 62] as illustrated in table 4.7. The mean of the fuzzy weights are calculated using centre of area (COA) method which is computed from fuzzy geometric mean value. As the summation of COA is larger than 1 hence normalized weight $\breve{w}_{j}$ of each response is calculated whose summation must be equal to 1 for obtaining accurate outcomes.

The vector normalization [62] of the decision matrix is given by Eq. (14) for beneficial criteria (B) and Eq. (15) for non-beneficial criteria (NB) or cost criteria. Vector normalization is employed in FTOPSIS approach because in numerous different realistic circumstances, preference model of an individual is inexact and DM is inept to place crisp numbers for contrasting the judgments, inferring the system to be inexact, therefore fuzzy environment is considered using TFN for more accuracy and precision for higher production at minimum cost.

$$\tilde{r}_{ij} = \left(\frac{l_{ij}}{u_j^*}, \frac{m_{ij}}{u_j^*}, \frac{u_{ij}}{u_j^*} \right) \text{ and } u_j^* = \max_i \{ u_{ij} \} \quad (B) \tag{14}$$

$$\tilde{r}_{ij} = \left(\frac{l_j^-}{u_{ij}}, \frac{l_j^-}{m_{ij}}, \frac{l_j^-}{l_{ij}} \right) \text{ and } l_j^- = \min_i \{ l_{ij} \} \quad (NB) \tag{15}$$

Fuzzy scale of criteria weights for FAHP is depicted in table 4.8 and the relative importance matrix (4x4) for the output responses are computed as depicted by table 4.9.

Table 4.8. Fuzzy scale of criteria weights for FAHP

Fuzzy Number	Linguistic importance	Triangular Fuzzy weights
1	Equal	(1, 1, 1)
2	Weak	(1, 2, 3)
3	Not Bad	(2, 3, 4)
4	Preferable	(3, 4, 5)
5	Good	(4, 5, 6)
6	Fairly Good	(5, 6, 7)
7	Very Good	(6, 7, 8)
8	Absolute	(7, 8, 9)
9	Perfect	(8, 9, 10)

Table 4.9. Relative importance matrix (4x4) for the output responses

Response	MRR	SR	KW	OC
MRR	(1, 1, 1)	(1.0491, 1.5280, 2.0891)	(1.2841, 1.6723, 2.1853)	(0.9246, 1.2160, 1.6548)
SR	(0.4787, 0.6544, 0.9532)	(1, 1, 1)	(1.3761, 1.9029, 2.5212)	(0.9030, 1.2524, 1.6841)
KW	(0.4576, 0.5980, 0.7787)	(0.3966, 0.5255, 0.7267)	(1, 1, 1)	(0.9448, 1.3392, 1.8135)
OC	(0.6043, 0.8224, 1.0815)	(0.5938, 0.7984, 1.1074)	(0.5514, 0.7467, 1.0584)	(1, 1, 1)

After the pair-wise comparison of the fuzzy matrices, the fuzzy weight $\tilde{w}_j$ is determined by Eq. (16):

$$\tilde{w}_j = \tilde{r}_j \times \left(\tilde{r}_1 + \tilde{r}_2 + \ldots + \tilde{r}_n \right)^{-1}; \text{ where } \tilde{r}_j = \left[\tilde{a}_{j1} \times \tilde{a}_{j1} \times \ldots \times \tilde{a}_{jn} \right]^{\frac{1}{n}} \tag{16}$$

The aggregated fuzzy weights are computed by FAHP [61, 62] as depicted in table 4.10.

Table 4.10. Fuzzy weight calculation using FAHP

Response	Fuzzy Sum of Each Row			Fuzzy Synthetic Extent			Degree of Possibility (Mi > Mj)				Degree of Possibility (Mi)	Normalized weights
MRR	4.2579	5.4163	6.9292	0.1966	0.3176	0.5108	■	1	1	1	1.0000	0.346
SR	3.7578	4.8098	6.1585	0.1735	0.2820	0.4540	0.8786	■	1	1	0.8786	0.304
KW	2.7991	3.4627	4.3189	0.1293	0.2030	0.3184	0.5153	0.6472	■	1	0.5153	0.179
OC	2.7495	3.3675	4.2473	0.1270	0.1974	0.3131	0.4923	0.6227	0.9705	■	0.4923	0.171
Sum	13.5643	17.0563	21.6539	Consistency Ratio (CR) = 0.0368 Consistency Index (CI) = 0.03312						Sum	2.8863	1.000

According to extent analysis method [62] as proposed by Chang, all items are considered and extent analysis is presented on each goal $g_{\tilde{i}}$. Hence, $\tilde{m}$ values of extent analysis are attained by Eq. (17):

$$M_{g\tilde{i}}^1, M_{g\tilde{i}}^2, \ldots, M_{g\tilde{i}}^{\tilde{m}} \quad (\tilde{i} = 1, 2, \ldots, \tilde{n}) \tag{17}$$

where; $M_{g\tilde{i}}^{\tilde{j}} \quad (\tilde{j} = 1, 2, \ldots, \tilde{m})$ are TFNs.

The steps are:

(i) Synthetic extent value w.r.t its object is defined by Eq. (18), obtained from Eq. (19) and Eq. (20), and shown in table 4.10:

$$S_{\tilde{i}} = \sum_{\tilde{j}=1}^{\tilde{m}} M_{g\tilde{i}}^{\tilde{j}} \otimes \left[\sum_{\tilde{i}=1}^{\tilde{n}} \sum_{\tilde{j}=1}^{\tilde{m}} M_{g\tilde{i}}^{\tilde{j}} \right]^{-1} \tag{18}$$

where; $\sum_{\tilde{j}=1}^{\tilde{m}} M_{g\tilde{i}}^{\tilde{j}} = \left(\sum_{\tilde{j}=1}^{\tilde{m}} l_{\tilde{j}}, \sum_{\tilde{j}=1}^{\tilde{m}} m_{\tilde{j}}, \sum_{\tilde{j}=1}^{\tilde{m}} u_{\tilde{j}} \right) \tag{19}$$

and; $\sum_{\tilde{i}=1}^{\tilde{n}} \sum_{\tilde{j}=1}^{\tilde{m}} M_{g\tilde{i}}^{\tilde{j}} = \left(\sum_{\tilde{i}=1}^{\tilde{n}} l_{\tilde{i}}, \sum_{\tilde{i}=1}^{\tilde{n}} m_{\tilde{i}}, \sum_{\tilde{i}=1}^{\tilde{n}} u_{\tilde{i}} \right) \tag{20}$$

and the inverse vector is computed using Eq. (21):

$$\left[\sum_{\tilde{i}=1}^{\tilde{n}}\sum_{\tilde{j}=1}^{\tilde{m}}M_{g\tilde{i}}^{\tilde{j}}\right]^{-1}=\left(\frac{1}{\sum_{\tilde{i}=1}^{\tilde{n}}u_{\tilde{i}}},\frac{1}{\sum_{\tilde{i}=1}^{\tilde{n}}m_{\tilde{i}}},\frac{1}{\sum_{\tilde{i}=1}^{\tilde{n}}l_{\tilde{i}}}\right) \tag{21}$$

(ii) The degree of possibility as shown in table 4.10, of $M_2=\left(l_2,m_2,u_2\right)\geq M_1=\left(l_1,m_1,u_1\right)$ is defined by Eq. (22):

$$V\left(M_2\geq M_1\right)=\sup\left[\min\left(\mu_{M_1}\left(x\right),\mu_{M_2}\left(y\right)\right)\right] \tag{22}$$

or can be also equivalently expressed as in Eq. (23):

$$V\left(M_2\geq M_1\right)=highest\left(M_1\bigcap M_2\right)=\mu_{M_2}\left(d\right) \tag{23}$$

where; d signifies the ordinate of the highest intersection point.

(iii) The degree of possibility of a convex fuzzy number if found to be greater than $\tilde{k}$ convex fuzzy numbers $M_{\tilde{i}}$ $(\tilde{i}=1,2,....,\tilde{k})$ can be defined by Eq. (24):

$$\begin{aligned}V\left(M\geq M_1,M_2,...,M_{\tilde{k}}\right)&=V\left[\left(M\geq M_1\right)and\left(M\geq M_2\right).....and\left(M\geq M_{\tilde{k}}\right)\right]\\&=\min V\left(M\geq M_{\tilde{i}}\right);\ (\tilde{i}=1,2,...,\tilde{k})\end{aligned} \tag{24}$$

An assumption is taken as per Eq. (25): $d'\left(A_{\tilde{i}}\right)=\min V\left(S_{\tilde{i}}\geq S_{\tilde{k}}\right)$ (25)

for $\tilde{k}=1,2,....,\tilde{n};\tilde{k}\neq\tilde{i}$. Then the weight vector is calculated by Eq. (26):

$$\tilde{w}=(d'\left(A_1\right),d'\left(A_2\right),.....,d'\left(A_{\tilde{n}}\right)^T \tag{26}$$

where; $A_{\tilde{i}}$ $(\tilde{i}=1,2,....,\tilde{n})$ are of $\tilde{n}$ elements.

(iv) Then the normalized weights are calculated by Eq. (27):

$$w_j = \left(d\left(A_1 \right), d\left(A_2 \right), ..., d\left(A_{\tilde{n}} \right) \right)^T \tag{27}$$

The normalized weightage summation is equal to 1 showing the consistency which provides the main concern of solitary alternative compared to the others.

(v) Furthermore, *Saaty* introduced the consistency index (CI) and consistency ratio (CR) for the measurement of deviation level from consistency by Eq. (28):

$$CI = \frac{\lambda_m - n}{n-1}, \quad CR = \frac{CI}{RI} \tag{28}$$

where; λ_m is the maximum eigen-value and n is the order of pair-wise comparison matrices. *RI* is the random index which is considered to be 0.9 [39] of $n=4$ order. In this research, CI obtained is 0.03312 and CR as 0.0368. CR obtained is less than 0.10 which proves the consistency of the matrix [39]. The values are incorporated in the table 4.10.

Step 4: Multiplication of normalized decision matrix with criteria weights or normalized weights as obtained from step 2, to determine the weighted normalized fuzzy decision matrix, V as depicted in Eq. (29):

$$V = \left[v_{ij} \right]_{mxn} = r_{ij} . w_j \tag{29}$$

Step 5: Computation of FPIS and FNIS:

$$FPIS = (v_1^+, v_2^+, ..., v_n^+) = \left\{ \left(Max_i v_{ij} \| j \in K \right), \left(Min_i v_{ij} \| j \in K' \right) \| i = 1, 2, ..., m \right\} \tag{30}$$

$$FNIS = (v_1^-, v_2^-, \ldots, v_n^-) = \left\{ \left(Min_i v_{ij} \parallel j \in K \right), \left(Max_i v_{ij} \parallel j \in K^{'} \right) \parallel i = 1, 2, \ldots, m \right\} \tag{31}$$

where, K fits in superior the improved criterion and $K^{'}$ fits in inferior the improved criterion. In this present research, MRR is considered to be beneficial criteria (higher the improved type) whereas SR, KW and OC are considered to be non-beneficial criteria (inferior the improved kind).

Step 6: Computation of the distances of every alternative from FPIS and FNIS:

$$D_i^+ = \sum_{j=1}^{n} d\left(v_{ij}, v_j^+\right); \quad j = 1 \, to \, n; \quad i = 1 \, to \, m \tag{32}$$

$$D_i^- = \sum_{j=1}^{n} d\left(v_{ij}, v_j^-\right); \quad j = 1 \, to \, n; \quad i = 1 \, to \, m \tag{33}$$

FPIS and FNIS are then computed for the accuracy estimation of experimented results using Eq. (30) and Eq. (31). Therefore, intervals between FPIS and FNIS are determined using Eq. (32) and Eq. (33). Eq. (9) is used to compute intervals of two TFN and the propinquity of entity experimental run to the superlative solution is determined by Eq. (22).

Step 7: To find the closeness co-efficient CC illustrated as in Eq. (34):

$$CC_i = \frac{D_i^-}{D_i^+ + D_i^-}; \quad i = 1 \, to \, m; \quad 0 \leq CC \leq 1 \tag{34}$$

Higher the closeness co-efficient, better ranking is obtained. Table 4.11 depicts the ranking of DGRA and FTOPSIS on performance measures where rank 1 is run 2 of DGRG 0.7233 in DGRA; whereas, run 5 of CC 0.7286 is considered to be rank 1 in case of FTOPSIS. Table 4.12 depicts the response of these advanced MCDM approaches for the means of DGRG and

FTOPSIS where it is clearly identified that peak current provides maximum main effect in both the approaches designated to be rank 1.

Table 4.11. DGRA and FTOPSIS ranking on performance measures

Machining Parameters				Performance Measures			
Run	P (W) : A	Toff (µs) : B	IP (A) : C	CC_i	δ_i	RANK (FTOPSIS)	RANK (DGRA)
1	7	30	5	0.523314	0.5520243	10	15
2	6	25	10	0.339028	**0.7233158**	16	**1**
3	8	20	8	0.495486	0.5685061	12	13
4	7	25	8	0.591262	0.6391668	3	3
5	6	20	8	**0.728564**	0.6333009	**1**	4
6	7	25	8	0.552917	0.6024239	5	7
7	7	20	5	0.667441	0.5930627	2	10
8	7	25	8	0.524247	0.5965464	9	9
9	7	25	8	0.533045	0.598332	7	8
10	7	20	10	0.395223	0.5814148	14	11
11	7	30	10	0.360584	0.6474989	15	2
12	7	25	8	0.552344	0.602861	6	6
13	6	25	5	0.582395	0.5547221	4	14
14	8	25	10	0.263495	0.5093703	17	17
15	6	30	8	0.428801	0.5208223	13	16
16	8	30	8	0.532356	0.6184054	8	5
17	8	25	5	0.512737	0.5795287	11	12
Mean of CC_i = 0.5048964				**Mean of δ_i = 0.5953707**			

Table 4.12. Response table for the means of DGRG and FTOPSIS

Symbol	Machining Parameters	MCDM	Level 1	Level 2	Level 3	Main effect (max-min)	RANK (FTOPSIS)	RANK (DGRA)
A	Power (W)	FTOPSIS	0.519697	0.522264	0.451018471	0.071245575	3	
		DGRG	0.60804	0.6014812	0.568952624	0.039087641		2
B	Time off (µs)	FTOPSIS	0.571678	0.4946078	0.461263856	0.110414558	2	
		DGRG	0.594071	0.6006963	0.584687716	0.016008611		3
C	Peak Current (A)	FTOPSIS	0.571472	0.5487801	0.339582462	0.231889492	1	
		DGRG	0.569834	0.5978183	0.615399963	0.045565527		1

It is inferred that different rankings are obtained by DGRA and FTOPSIS because of consideration of various and unique decision makers on all 4 responses. Novel DGRA is a

simpler form of MOO where responses are analyzed on 17 experimental and predicted values, however in FTOPSIS relative normalized decision matrix is computed on all the 17 experimental runs along with criteria weights in FAHP method which is much more complex. It is also observed that Mean of Closeness Co-efficient of FTOPSIS is 0.5048964 and Mean of Desirable Grey Relational Grade is 0.5953707, inferring 17.924% improvement with DGRA method.

CHAPTER 5

5. Results and discussions

5.1. *Measurement of performance measures of composite development*

The experimental runs are obtained by varying foremost input laser process parameters as obtained by RSM-BBD like laser power (P) allocated by "A" at 150-400 W, scan speed (V) allocated by "B" at 10-15 mm/s and energy input/area (E) allocated by "C" at 20-80 J/mm^2 calculated from Eq. (1). Hardness measurement (average of 10 measurements) is computed using Vicker's microhardness (load of 500 g for 10 s). Table 5.1 represents the particulars of 12 experimental run-orders of performance measures of composite development. It is pragmatic that elevated cooling rates are engendered at squat energy input/area because of the increment in thermal gradients in close proximity to the vicinity of melt pool. Likewise, with the enhancement of the energy input/area there is a decrement in the thermal gradients owing to the decrement in cooling rate also.

Table 5.1. Performance measures of composite development

Exp. No.	Laser power: P (W)	Scan speed: V (mm/s)	Energy input/area: E (J/mm^2)	Melting Temperature: Tm (K)	Temperature variation during cooling (K)	Cooling Rate (K/s)	Hardness (HV)
	P	V	E	Tm	dT	dT/dt	H
1	150	10	30	1732	1434	-5859635.4	392
2	150	15	20	1734	1436	-8813987.5	391
3	200	10	40	1738	1440	-4431579.4	394
4	200	15	26.67	1741	1443	-6675095.4	393
5	250	10	50	1744	1446	-3574869	392
6	250	15	33.33	1750	1452	-5406896.2	393
7	300	10	60	1753	1455	-3016256.6	395
8	300	15	40	1759	1461	-4561776.3	395
9	**350**	**10**	**70**	1763	1465	**-2621022.5**	**396**
10	350	15	46.67	1768	1470	-3958416	396

11	400	10	80	1772	1474	-2321659.5	395
12	400	15	53.33	1780	1482	-3520393.6	393

The cooling rate ($\dfrac{dT}{dt}$) [11] in K/s can be calculated by Eq. (35):

$$\frac{dT}{dt} = -2\pi k \left(\frac{V}{P} \right) \Delta T^2 \qquad (35)$$

where; melting temperature is Tm in K, ambient temperature is Ta in K (298 K), thermal conductivity is k (6.8 W/mK), laser power (P), scan speed (V) and temperature variation during cooling (K) which is $\Delta T = Tm - Ta$.

From Eq. (35), it is inferred that cooling rate augments with the enhancement in scan speed and dwindles with the augmentation of laser power. At 150 W laser power low melting is observed and maximum cooling rate of -8813987.5 K/s is observed at 15 mm/s scan speed. Here, minimum hardness of 391 HV is obtained which is enhanced by the increment of laser power and scan speed. The optimum cooling rate (-2621022.531 K/s) and enhanced hardness of 396 HV are obtained 350/10 laser process parameter which is the best case amongst all the laser process parameters. During processing below 40 J/mm^2 energy input/area low melting of the mixture powder occurs resulting non-uniform distribution with irregularities with weak interfacial bonding of Ti matrix. With the increment in energy input/area between 50 to 70 J/mm^2 good melting occurs with uniform deposits. Optimum condition is achieved at 70 J/mm^2 with optimum cooling rate and enhanced hardness at experimental run number 9. With further increment to 80 J/mm^2 energy input/area overheating followed by rapid cooling occurs leading to significant internal stresses generation at experimental run number 11. Here, although minimum

cooling rate (-2321659.5 K/s) and greater amount of harness (395 HV) occurs, there is an occurrence of overheating caused by severe burns where unstable deposits are formed with cracking. Enhanced heat is developed resulting in overlapping layer-by-layer deposition and formation of thick deep cracks. This illuminates that with the enhancement of energy input/area there is a decrement in cooling rate during LENS processing.

5.2. Microstructure and characterization

SEM is used for determining the microstructure and characterization. Fig. 5.1 establishes the development of microstructure by LENS on TMC at an unchanging scan speed of 10 mm/s. Fig. 5.1(a) identifies a capricious distribution of TiB_2 discrepancy region within the dispersal of Ti-matrix at 200 W laser power which implies a non-uniform distribution with TiB_2 deficient zone within the Ti-matrix. However, good melting with an uncouth microstructure at 250 W laser power is depicted in Fig. 5.1(b). However fine but partial bonding between Ti and TiB_2 particles are formed when it is increased to 300 W as depicted in Fig. 5.1(c) corresponding to good melting with fine but partial bonding sandwiched between Ti and TiB_2 elements. On further increment of laser power to 350 W, more formations of white layers occur signifying fine dispersion of TiB_2 particles owing to fully 3d quasi-continuous networking inferring enhanced tribo-mechanical properties and excellent interfacial bonding which infers copious 3d pseudo-continuous arrangement owing to excellent interfacial bonding as designated by Fig. 5.1(d). Table 5.2 represents the detailed observations from the characterization of SEM microstructure. At 150 W laser power low melting is observed with some irregularities and crack formations. Complete melting only occurs at 350 W, but further increment of laser power to 400 W causes over heating which leads to crack formation.
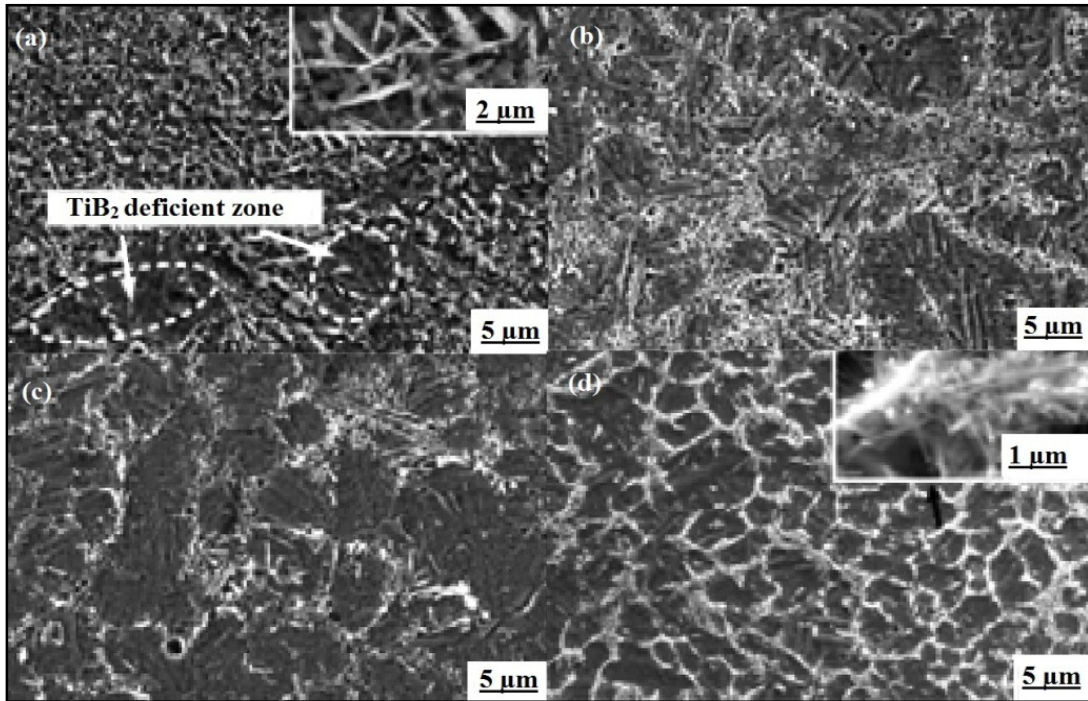
Fig. 5.1. SEM images at scan speed: 10 mm/s: **(a)** 200 W, **(b)** 250 W, **(c)** 300 W, and **(d)** 350 W, respectively
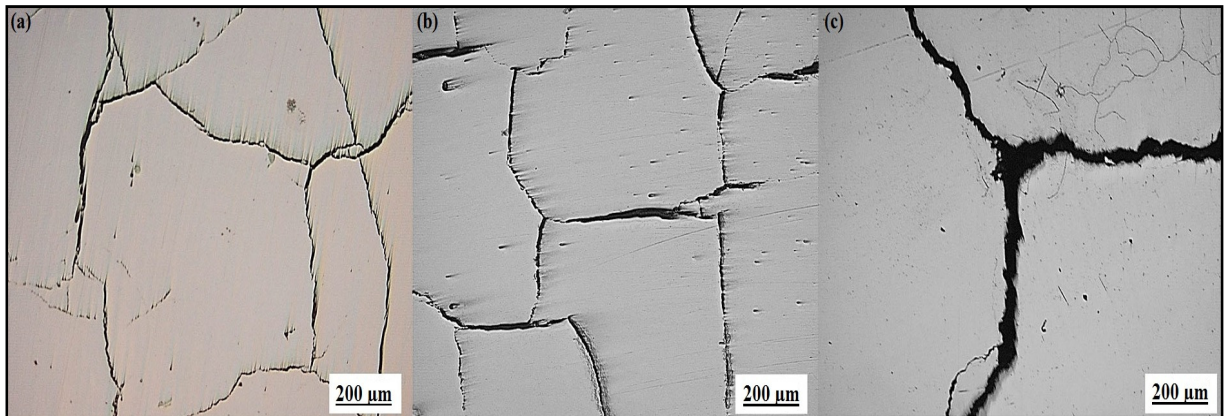
Fig. 5.2. Crack formations at diverse laser power/ scan speed: **(a)** 350/15, **(b)** 400/10, and **(c)** 400/15, respectively

SEM images of crack formations at different laser power/ scan speed are represented in Fig. 5.2. Fig. 5.2(a) represents good melting with tiny surface cracks at 350/15. Fig. 5.2(b) depicts minimum cooling rate at 400/10 causing overheating by severe burns owing to unstable deposits with cracking, and in Fig. 5.2(c) overheating owing to unstable deposits arises which results in

deep thick crack formation during post-processing at 400/15. Overall, defective deposits occur resulting in meager melting with huge amount of porosity resulting in large crack formation by the combination of laser power and scan speed.

Table 5.2. Observations from SEM microstructure

Exp. No.	Observations
1	Low melting with some irregularities are formed
2	Maximum cooling rate with crack formations occurs
3	Capricious distribution of TiB_2 discrepancy region within the dispersal of Ti-matrix occurs
4	Partial melting of powder and excessive porosity occurs
5	Good melting occurs with coarse microstructure
6	Melting is improved with visible cracks and surface porosity
7	Good melting occurs with fine but partial bonding. Cracks are formed after polishing
8	Good melting occurs with uniform deposits when white layers start occurring
9	Optimum cooling rate is obtained. Proper melting with uniform deposit. No visible defects. More white layers are appeared signifying excellent spreading of TiB_2 particles which infers copious 3d pseudo-continuous arrangement owing to excellent interfacial bonding
10	Good melting occurs with tiny surface cracks
11	Minimum cooling rate occurs. Overheating causing by severe burns where unstable deposits are formed with cracking
12	Overheating owing to unstable deposits occurs which cracked during post-processing

5.3. ANOVA and Multi-objective optimization of composite development

In 1918, Ronald Fisher discovered a statistical tool named as ANOVA for analysis of statistical problems which splits a hardnosed group of inconsistency acquired from information set into methodical arbitrary factors, where statistical influence is obtained by the systematic factors whereas random factors do not influence the data sets. ANOVA test is carried to determine the contribution and influence of independent variables and their quadratic and interactive effects in a regression analysis. Advantages of ANOVA over other existing methods are: its robust design and enhancement of statistical power. The two-way ANOVA reduces the randomness and provides the interactive effects of the process variables, which is highly accurate for determining

MOO problems. Here, ANOVA is used for determining the optimal solution for machining TMC using maximum signal to minimum noise ratio technique. Here, statistical sway is attained by organized factors while there are no influences of random factors on the information sets. Regression analysis is conceded for ANOVA test to ascertain the contribution and persuade of linear, quadratic and interactive effects on different variables. The foremost advantages of ANOVA when contrasted to additional accessible techniques are robustness and statistical power augmentation. The two-way ANOVA decreases the unpredictability and offers major contribution of the input process variables on the interactive effects that is extremely precise for formative MOO problems. Table 5.3 depicts the abridged ANOVA table. The "significant" criterion is reliant on "P>F" which must be less than 0.05. Apart from C, which is energy input/area and AC, BC under CR, everyone is significant. For CR, quadratic mathematical objective function is the best fitted. The "Lack of Fit F-value" of CR is 0.0864 indicates "not significant" which can be inferred that the mathematical model is outstanding for fitting. "Pred R²" of CR is 0.9981 is in realistic harmony with "Adj R²" of CR of 0.9997. R^2 of CR is 0.9999 that infers excellent result as it is in close proximity to 1 making an allowance for a good signal. Adeq Prec. of CR is 232.8724 in lieu of a copious signal computing signal-to-noise ratio. Acceptable exactness ought to be superior than 4. "F-value" of CR is 4792.7 and H is 147.27. For H, linear mathematical objective function is the best fitted. Except C, each and every one is significant. The "Lack of Fit F-value" of H is 0.6105 necessitates not significant criteria. "Pred R²" of H is 0.9535 is near proximity with "Adj R²" of H of 0.9669. Adeq Prec. is 34.4674 signifying an ample signal. This model also navigates in the design space for it excellent fitting with observed values.

Table 5.3. Abridged ANOVA table

Source	CR		H	
	F-value	p-value	F-value	p-value
Model	4792.7	< 0.0001	147.27	< 0.0001
A-Laser Power	31424.02	< 0.0001	427.64	< 0.0001
B-Scan Speed	6904.13	< 0.0001	13.64	0.0031
C-Energy input/area	0.291	0.609*	0.5455	0.4744*
AB	701.72	< 0.0001	-	-
AC	0.0098	0.9243*	-	-
BC	1.79	0.2296*	-	-
A^2	4025.19	< 0.0001	-	-
B^2	33.4	0.0012	-	-
C^2	43.74	0.0006	-	-
Lack of Fit	6.07	0.0864*	0.8889	0.6105*
R^2 (CR) = 0.9999	Adj R^2 (CR) = 0.9997	Pred R^2 (CR) = 0.9981	Adeq Prec (CR) = 232.8724	
R^2 (H) = 0.9736	Adj R^2 (H) = 0.9669	Pred R^2 (H) = 0.9535	Adeq Prec (H) = 34.4674	* not significant

Fig. 5.3 reveals surface plot of P and V on CR demonstrating the involvement of the major input laser process parameters on CR. CR augments with the enhancement in V but diminishes with the enhancement in P. This is due to the fact of increment in number of deposition in the net-shaping layers from LENS process because of the enhancement of V. Larger the V, more the deposited layers, and enhanced is the heat transfer rate. Now, when P increases, the temperature of the preceding deposit enhances leading to decrement in temperature gradients in close proximity to melt pool of the liquid and as a result CR decreases. Fig. 5.4 portrays 3-d surface plot of P and E on CR. It is pragmatic that elevated CR is engendered at low E because of the increment in thermal gradients near the vicinity of melt pool. Likewise, with the enhancement of E there is a decrement in the thermal gradients owing to the decrement in CR also. Fig. 5.5 elucidates 3-d surface plot of V and E on CR which resemblances almost linear plot. This can be

explained as CR increases with the increment in V, but decreases almost linearly with the increment in E. This illuminates that mounting E diminishes CR during LENS processing. Fig. 5.6 portrays the enhancement of H with amplification of P and V. Fig. 5.7, it is pragmatic that H also boosts with the augmentation of P and E. Fig. 5.8 elucidates 3-d surface plot of V and E on H which clarifies stable optimum characteristics with the enhancement of V and E as E does little contribution to H which can be validated from table 5.3. It is perceptible that because of the enhancement of P and V, there is also an improvement in H due to complete melting and cooling with uniform deposits with the formation of more white layers. There is an occurrence of fine dispersion of reinforcement particles to Ti-matrix resulting in fully 3d quasi-continuous networking owing to excellent interfacial bonding and superior hardness. The objective functions for CR and H are given by Eq. (36) and Eq. (37), respectively:

$$CR = -4.112E+06 +2.201E+06A -1.032E+06B -6698.12C +4.652E+05AB \\ +1739.10AC +23483.90BC -1.114E+06A^2 +1.015E+05B^2 +1.161E+05C^2 \tag{36}$$

$$H = +393.00 +3.50A +0.6250B -0.1250C \tag{37}$$

Fig. 5.3. Surface graph (P vs. V) on CR

Fig. 5.4. Surface graph (P vs. E) on CR

70

-8.85085E+06 ▊▊▊▊▊ -2.32796E+06

X1 = B: Scan Speed
X2 = C: Energy input/area

Actual Factor
A: Laser Power = 350.956
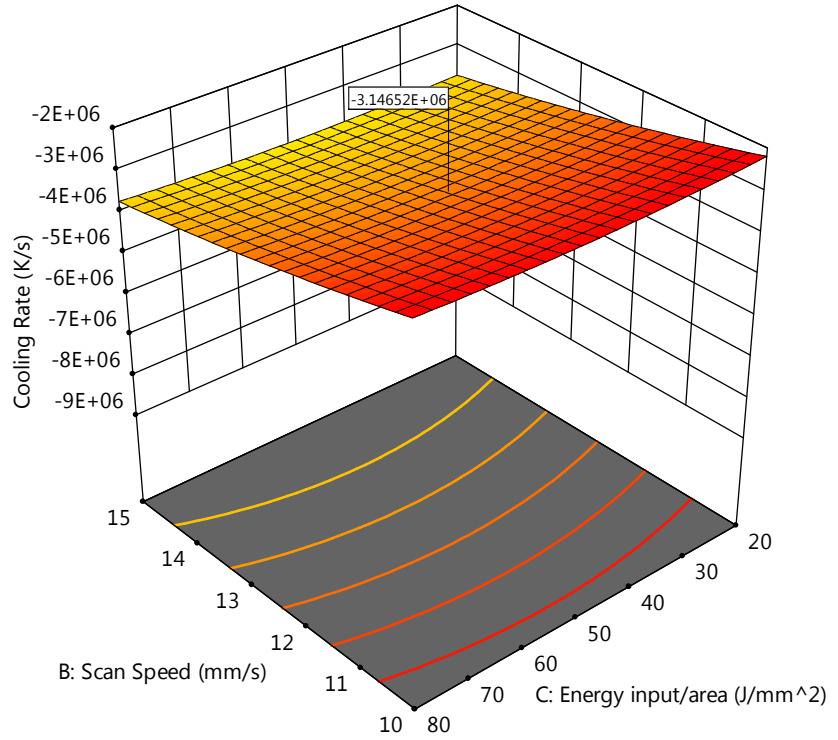
Fig. 5.5. Surface graph (V vs. E) on CR

Hardness (HV)

389 ▊▊▊▊▊ 397

X1 = A: Laser Power
X2 = B: Scan Speed

Actual Factor
C: Energy input/area = 49.4753
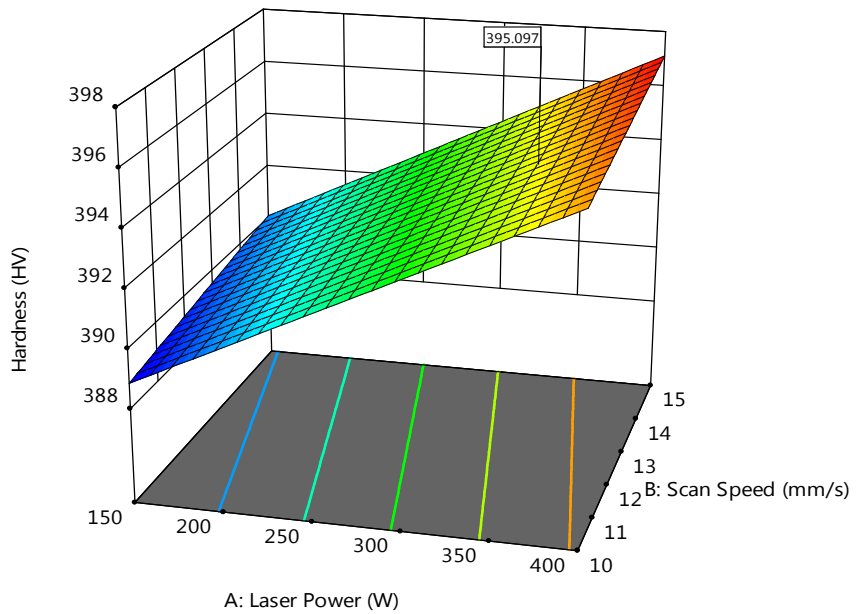
Fig. 5.6. Surface graph (P vs. V) on H

71
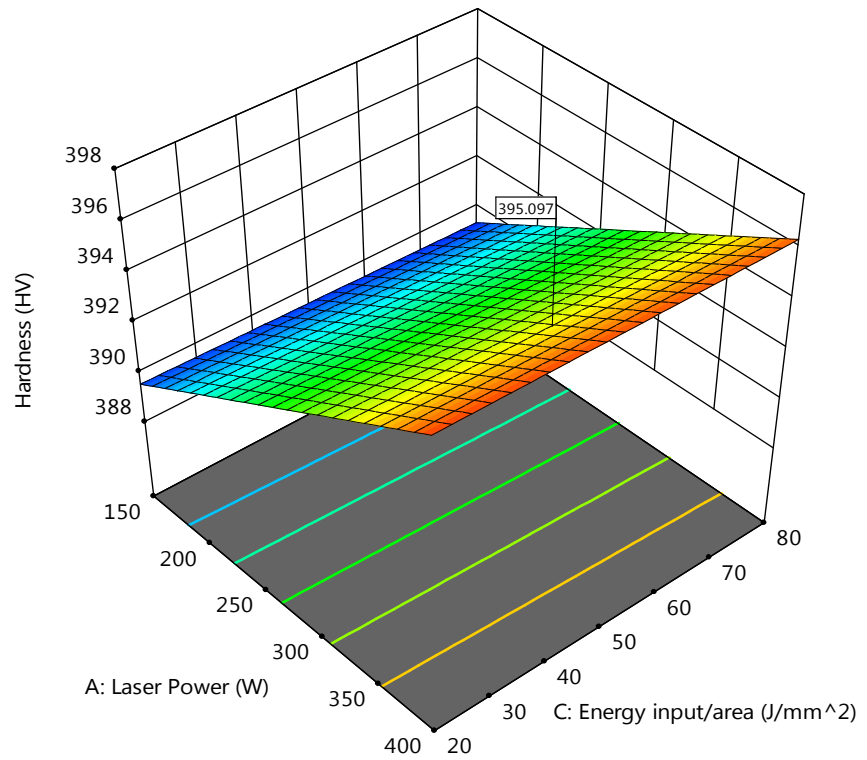
Fig. 5.7. Surface graph (P vs. E) on H
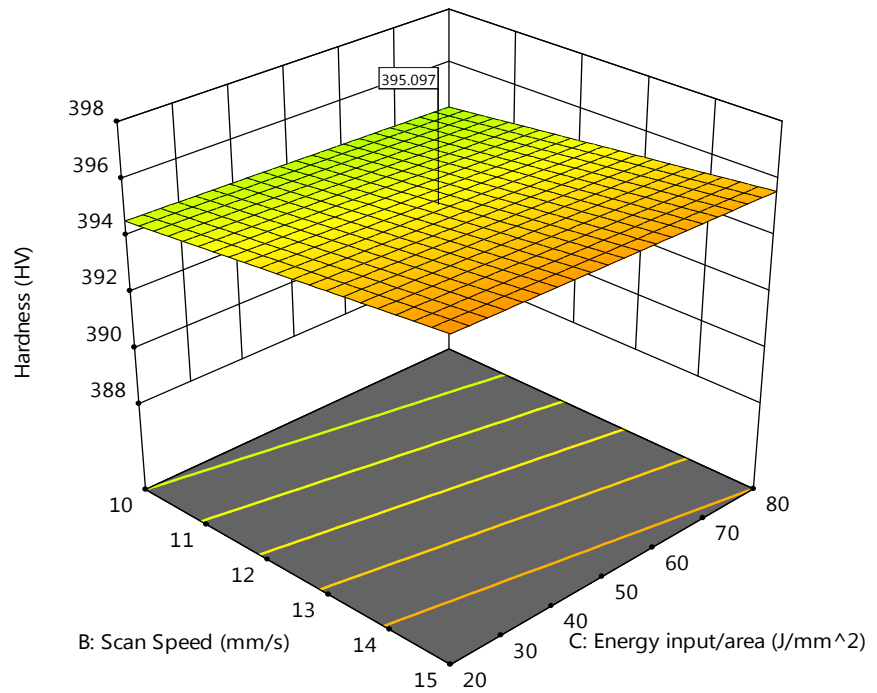
Fig. 5.8. Surface graph (V vs. E) on H

72

Fig. 5.9 represents the desirability of individual laser process parameters, performance measures and combined desirability. MOO solution is accomplished after DGA whilst P is 350.956 W, V is 12.371 mm/s, E is 49.475 J/mm^2, CR is -3146515.795 K/s and H is 395.097 HV, and combined desirability is 0.838. The individual desirability of the three major laser parameters are 1, CR as 0.874511 and H as 0.762088, and overall combined desirability is 0.837584.
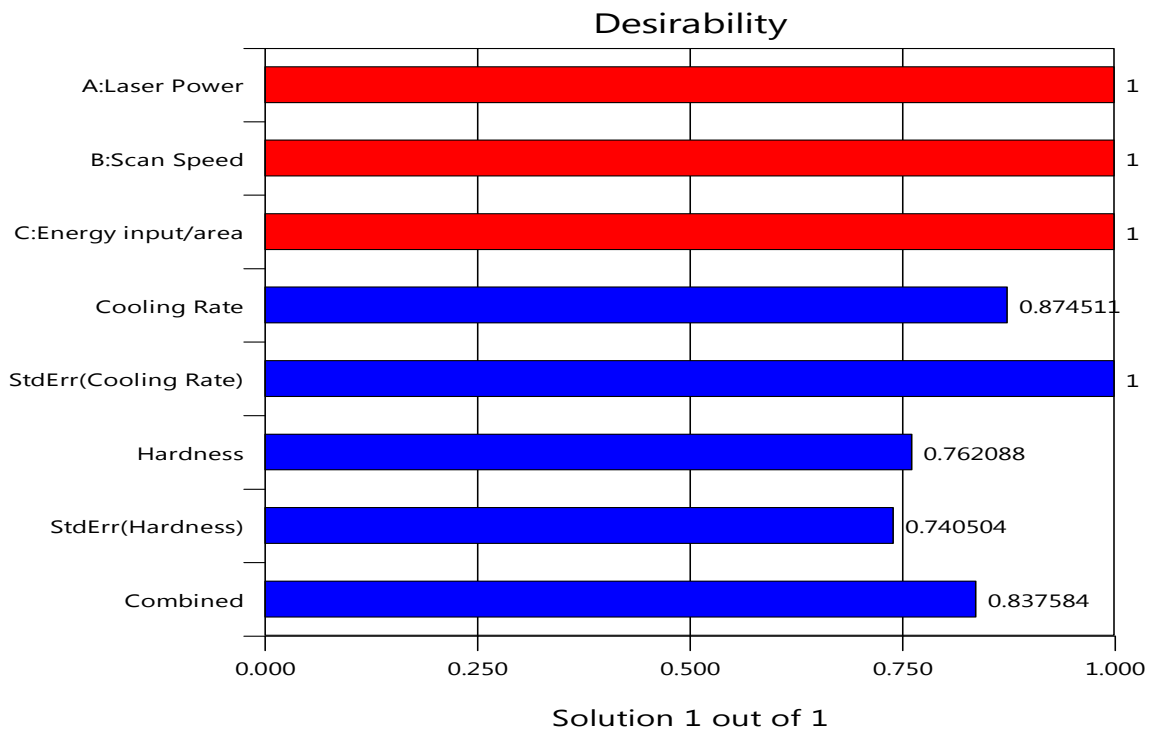
Fig. 5.9. Desirability of individual laser process parameters, performance measures and combined desirability

Eq. (36) and Eq. (37) are now further incorporated in GA in MATLAB R2018a, obtained after desirability function, where the predicted responses are also considered along with the experimental responses. Main advantage of incorporating this novel DGA technique is more accuracy and robustness. Both the responses are in close agreement with each others. This novel DGA has additional ascendancy in accomplishing the MOO solution. The lower and upper bounds of the laser process parameters are incorporated by Eq. (38-40) below:

$$150 \ <= \ A \ <= \ 400 \tag{38}$$

$$10 \ <= \ B \ <= \ 15 \tag{39}$$

$$20 \ <= \ C \ <= \ 80 \tag{40}$$

A thorough investigation has been carried and optimum criteria have been selected. The optimal setting of the genetic contrivance decides the selection to be remainder and cross-over fraction to be 0.8. Cross-over is heuristic with a ratio of 1.4. Mutation is uniform with a ratio of 0.2. Migration is forward. Population is considered to be 100 initially.
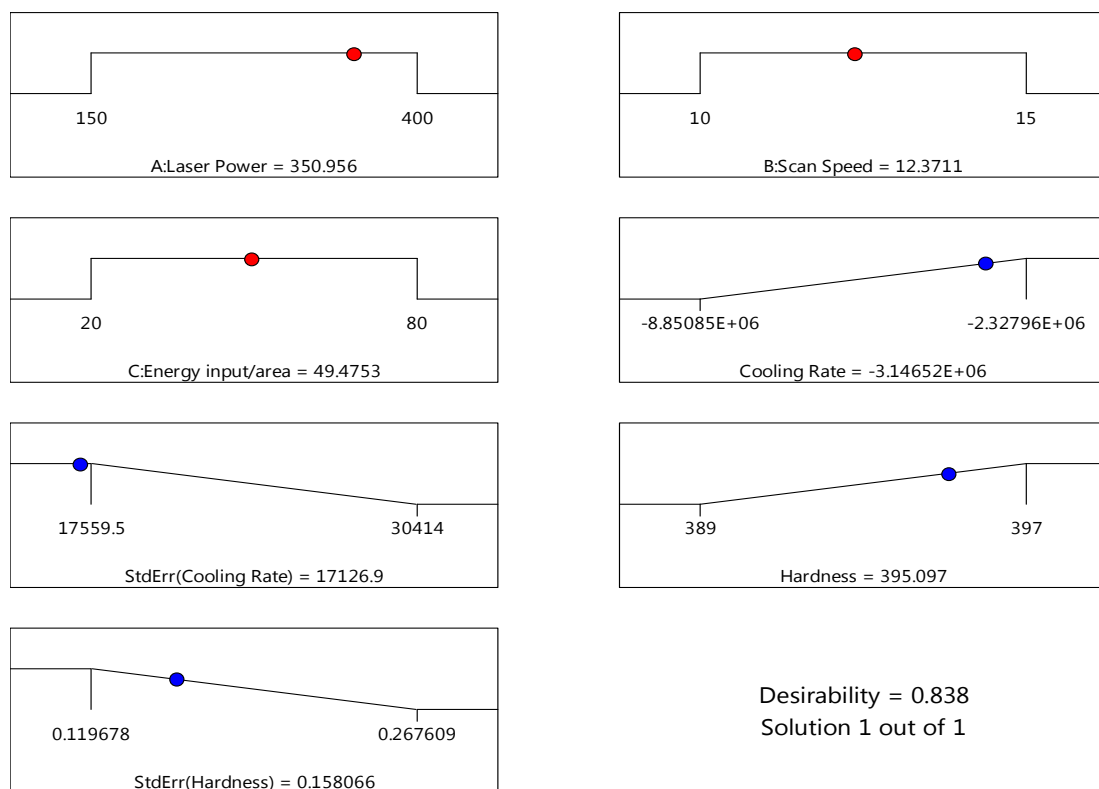
Fig. 5.10. Multi-objective optimized solution using DGA

Fig. 5.10 depicts multi-objective optimized solution where the ramp diagram indicates the improved optimal solution by DGA method. Fig. 5.11 portrays the fitness and generation plot

after application of DGA when Fig. 5.11(a) resemblances the fitness value for CR and Fig. 5.11(b) portrays the fitness value for H. The best fitness and mean fitness of both the performance measures of CR and H are in close proximity with each other. It is pragmatic that there is a decrement of the mean fitness with the increment in iteration numbers. In case of CR, function tolerance is obtained after 68 iteration number and in case of H, it is 60.

(a)   **Fitness value for CR**   **(b)**   **Fitness value for H**
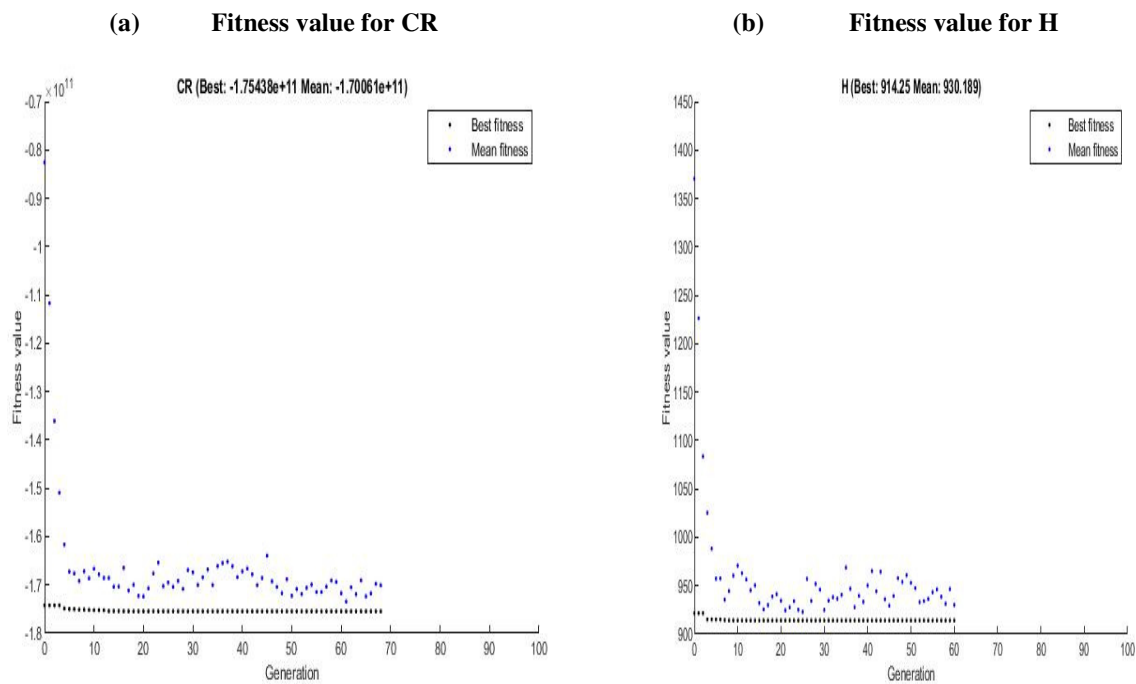
Fig. 5.11. Fitness vs. Generation plot after DGA: (a) Fitness value for CR, (b) Fitness value for H

The ranges of these iterations with generations are provided in Fig. 5.12 which corresponds to scores and generation plot after DGA where Fig. 5.12(a) represents scores for CR and Fig. 5.12(b) indicates scores for H, where the best, worst and mean scores are highlighted. Optimization is further improved by 20.049% of CR and 0.229% of H when evaluated with DGA as depicted in table 5.4 which illustrates the analysis of sensitivity of the parametric MOO for DGA method where excellent %improvement has been obtained.

75
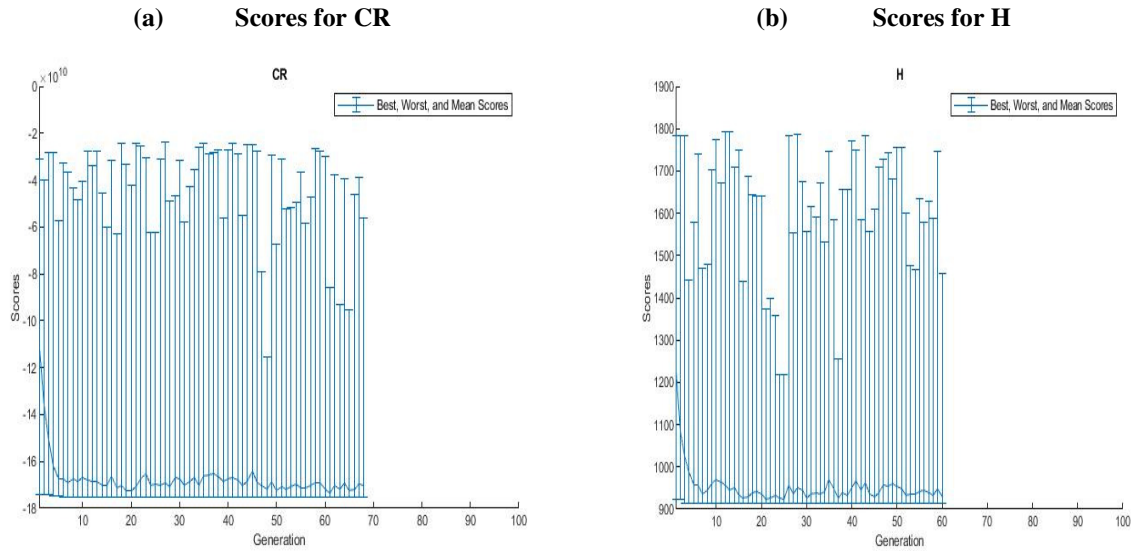
Fig. 5.12. Scores vs. Generation plot after DGA: (a) Scores for CR, (b) Scores for H

Table 5.4. %improvement in MOO using DGA

Laser Process Parameters			Laser Performance Measures				
Laser power: P (W)	Scan speed: V (mm/s)	Energy input/area: E (J/mm^2)	Output Responses	Combined desirability after DGA	Cooling Rate (K/s)	Hardness (HV)	% improvement (%)
350	10	70	Measured		-2621022.531	396	20.049 (CR)
350.956	12.371	49.475	Predicted by DGA	0.838	-3146515.795	395.097	0.229 (H)

5.4. Machining of the sample by WEDM

The experimental runs are conceded in a CNC WEDM (model number: AF 35/ONA; capacity of: 1060mmX750mmX400mm and UV axes: 120X120 with 1500 kg; accuracy: +- 0.005) which is portrayed in Fig. 5.13. The constant parameters are: wire diameter (0.25 mm) of diffused zinc coated brass, medium of dielectric is deionized water (conductivity 20 mho), servo voltage is maintained at 52 V, open arc voltage is kept at 80 V, wire tension at 18 kgf, wire feed at 10 mm/min dielectric flush at 25 kg/cm^2, polarity at 2 and finish at 0. Dimension of the developed cylindrical sample used for the WEDM is of diameter 11 mm and height 16 mm. Power (P)

factor A (6W, 7W, 8W), Time off (Toff) factor B (20µs, 25µs, 30µs) and Peak Current (IP) factor C (5A, 8A, 10A), by low, medium and high levels, as designated by RSM in Design Expert 11 software, are considered to be the most influencing parameters, keeping the other parameters constant.

Fig. 5.13. Experimental setup of WEDM

The details of the mechanical properties of the developed TMC are depicted in table 3.1. An enhanced heat conductivity of the wire with proper wire tension and wire feed is necessary to avoid sharp temperature gradient leading to high stress and recast layers. Table 4.2 depicts the detailed design matrix of RSM where various output responses like material removal rate (MRR), surface roughness (SR), kerf width (KW) and over cut (OC) are measured and their effects are investigated. The parameters and their levels are determined by the specification of the CNC WEDM machine of machining titanium based alloys and composite materials. The

process parametric selections with their criteria levels are found to influence the MRR, SR, KW and OC.

5.5. *Measurement of MRR, KW and OC*

MRR is the quantity of material eliminated from the sample per unit machining time when the electrical discharge transpires in the dielectric of WEDM machine. As the wire advances towards the workpiece, a gap is created resulting in high voltage generation thus disintegrating the dielectric. Electrical discharge initiates a spark between the wire-workpiece interfaces creating plasma bubble which then collapses eroding the machined material to disperse into the dielectric. Hence material removal takes place in this electro-thermal mechanism. Higher MRR results in advanced productivity of the manufacturing arena. Therefore, increment in power and peak current leads to high current density resulting in high discharge and improved MRR. MRR and OC are computed with the help of Eq. (41) and Eq. (42) below. Cutting speed (Vc) is one of the machining criteria which is directly recorded from the monitor of WEDM machine, KW is recorded from the profile projector and OC is calculated according to the Eq. (42). After the stabilization of Vc, values are measured after 2 mm (t) machining from the commencement of the cut. Proper stabilization of Vc is essential for accuracy. First cut first pass is incorporated for 2 mm (t) machining.

$$\text{MRR} = \text{Vc} * \text{KW} * \text{t} \left(\text{mm}^3 / \min \right) \tag{41}$$

$$\text{OC} = \text{KW} - \text{d} \left(\text{mm} \right) \tag{42}$$

(where 'd' is the wire diameter which is 0.25 mm)

5.6. Measurement of SR

SR is another important response which is deliberated by the divergences from the standard surface. Larger the deviations, rough will be the surface conditions. Rough surface conditions will be exhibited with greater deviations. For the measurement of SR, Mitutoyo SJ-210 portable surface roughness tester is used where a mean of five measurements of Ra value are considered to eliminate variations for each machining condition.

5.7 ANOVA for MRR

ANOVA is again used to acquire the optimal solution by using maximum signal to minimum noise ratio method. ANOVA implies "F-value" of the MRR model used in this research is 92.21 depicting the significance of the model with a 0.01% chance for the generation of noise. The "significant" criteria about the model terms is when "P>F" is less than 0.05. Here, A, B, C, BC, A², B², C² are significant. When the values of "P>F" is greater than 0.1, then they are rendered as "not significant". AB and AC may be considered as not significant as their values are higher than 0.05 but less than 0.1 and may be eliminated. The "Lack of Fit F-value" of 0.27 entails the "Lack of Fit" is not significant when contrasted with the "pure error". Only a chance of 84.68% is there for a "Lack of Fit F-value", that may occur due to noise. If it is not significant then the response of the model is excellent for fitting. "Pred R²" of 0.9657 value is in pragmatic conformity with the "Adj R²" of 0.9809 and it is in close conformity as the difference is less than 0.2. R^2 is 0.9916 which is excellent as it close to 1 and PRESS is 0.0437 which is very less considering a good signal. Adeq Precision is 27.730 representing an adequate signal measuring the signal to noise ratio. Enough accuracy ought to be larger than 4. Therefore, this model is accomplished to steer in design domain. Table 5.5 signifies ANOVA on MRR where it is clear that this developed

model is extremely fitted with the observed values. Fig. 5.14 provides an apparent understanding about the residuals which are located near the vicinity of the straight line demonstrating the normal distribution of the errors. Fig. 5.15 represents the random scattering of the residuals causing it structure less. Fig. 5.16 portrays the perturbation plot designating the contribution of all input process parameters to MRR. Fig. 5.17 illustrates the Box-Cox plot for transformation of power on MRR signifying the best lambda (1.22) and current lambda (1.0) where the CI value for the lambda is (-3.14, 5.01) and the current lambda is in the design space. Fig. 5.18 infers the close agreement of actual and predicted responses of MRR.

Table 5.5. ANOVA on MRR for WEDM machining of TMC

Source	Sum of Squares	df	Mean Square	F-value	p-value	
Model	1.26	9	0.1404	92.21	< 0.0001	significant
A-Power	0.9110	1	0.9110	598.48	< 0.0001	*
B-Time Off	0.0354	1	0.0354	23.28	0.0019	*
C-Peak Current	0.0273	1	0.0273	17.94	0.0039	*
AB	0.0060	1	0.0060	3.94	0.0877	
AC	0.0072	1	0.0072	4.76	0.0654	
BC	0.0573	1	0.0573	37.68	0.0005	*
A²	0.0345	1	0.0345	22.68	0.0021	*
B²	0.1656	1	0.1656	108.77	< 0.0001	*
C²	0.0107	1	0.0107	7.04	0.0328	*
Residual	0.0107	7	0.0015			
Lack of Fit	0.0018	3	0.0006	0.2668	0.8468	not significant
Pure Error	0.0089	4	0.0022			
Cor Total	1.27	16				

R² = 0.9916   **Adj R² = 0.9809**   **Pred R² =** 0.9657 **Adeq Precision =** 27.7302 **PRESS =** 0.0437   * significant
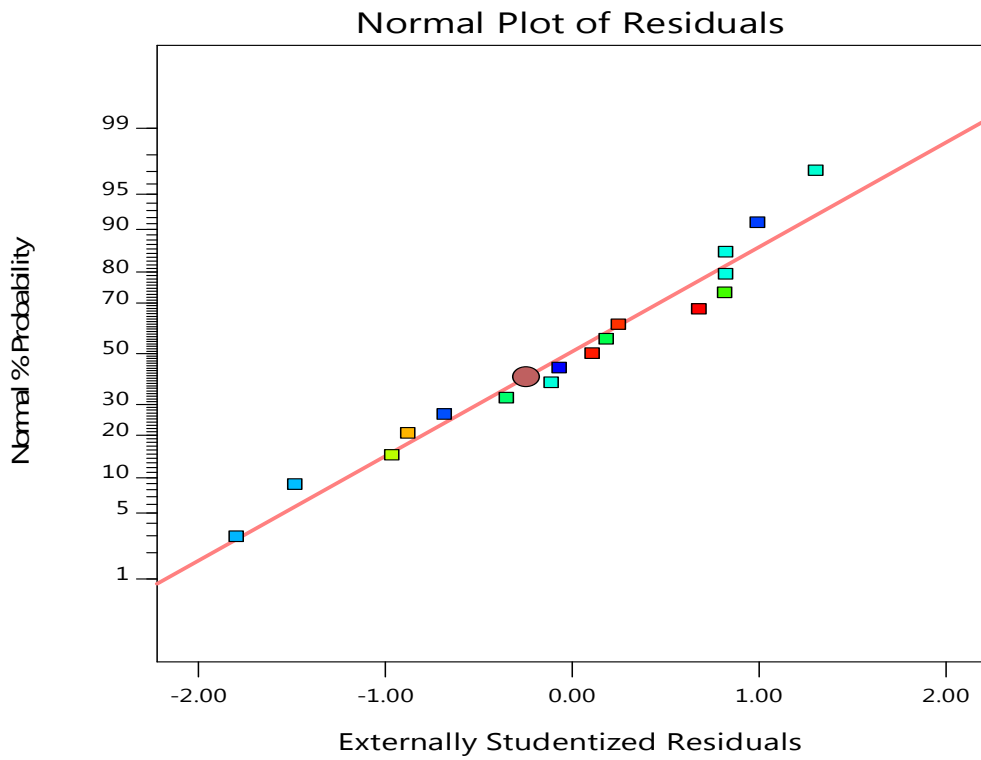
Fig. 5.14. Normal plot of residuals related to MRR
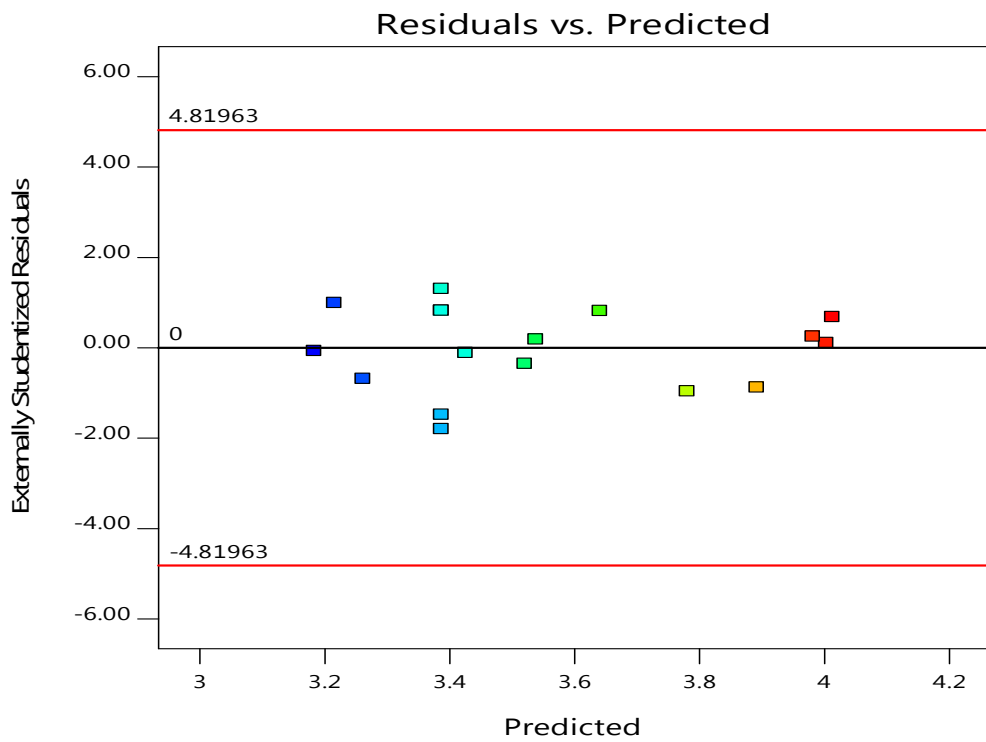
Fig. 5.15. Residuals and Predicted plots on MRR

81
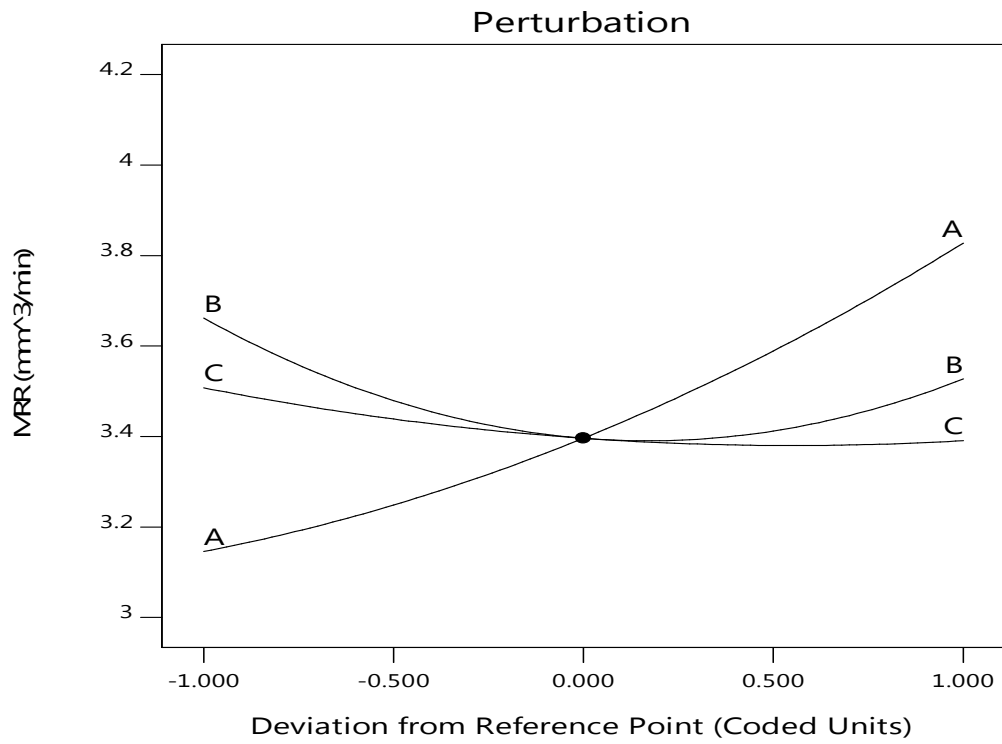
Fig. 5.16. Perturbation plot of MRR
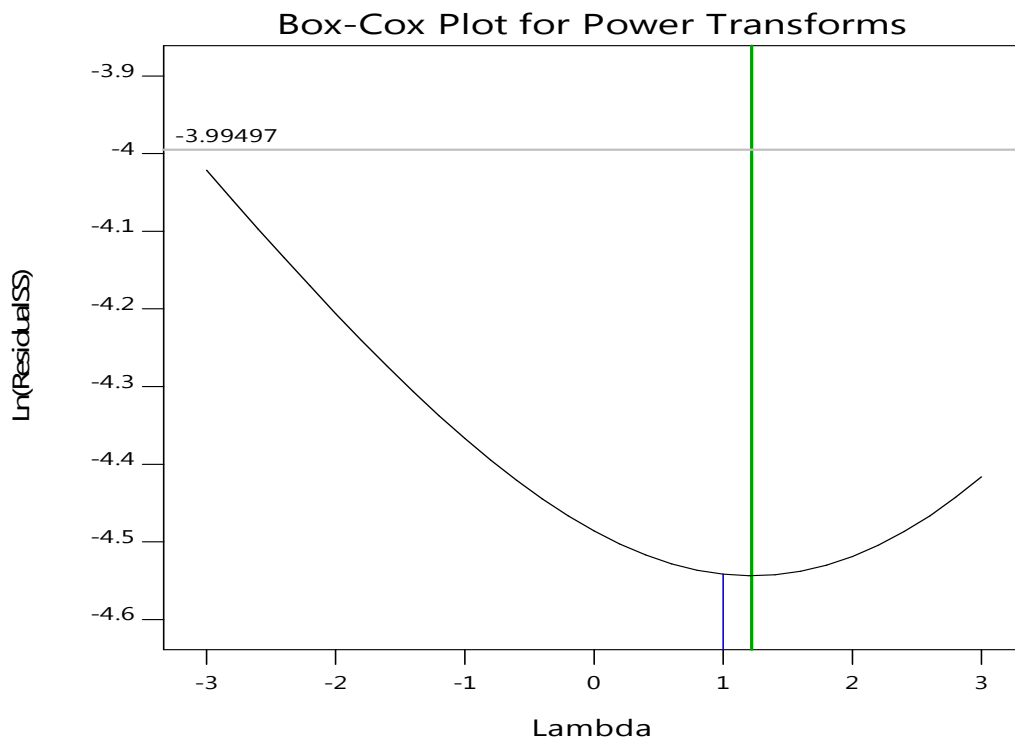
Fig. 5.17. Box-Cox plot on MRR

82
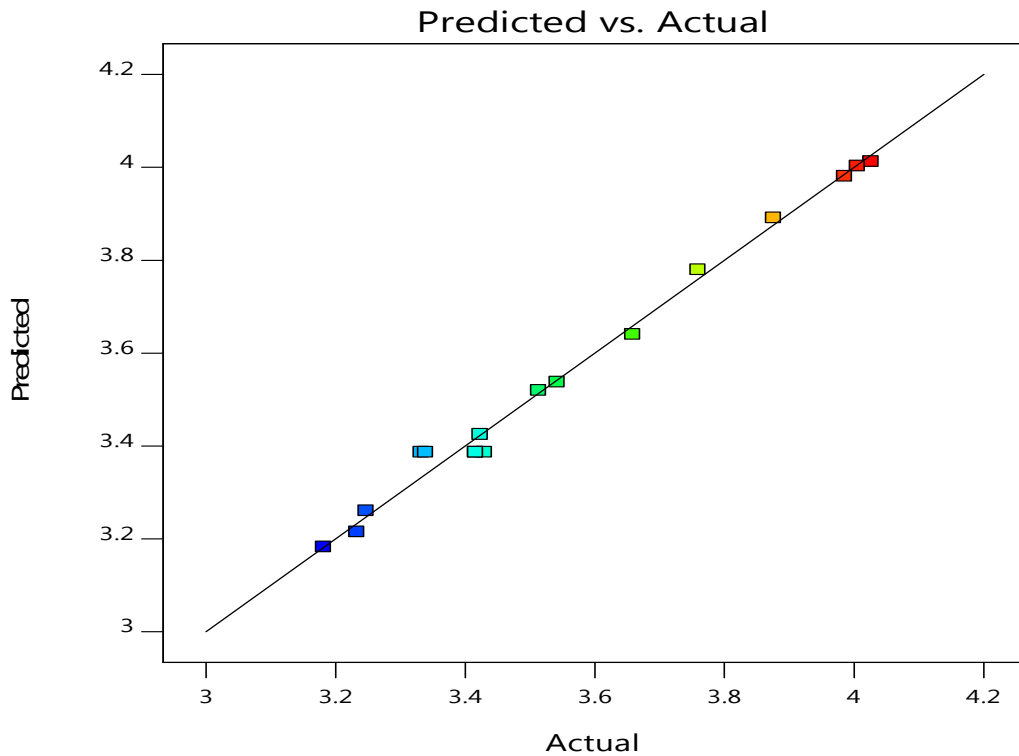
Fig. 5.18. Predicted and Actual responses of MRR

Hence, the mathematical model's equation for MRR is revealed in Eq. (43):

$$\text{MRR} = +3.40 + 0.3407A - 0.0672B - 0.0584C + 0.0387AB - 0.0422AC$$
$$+ 0.1186BC + 0.0905A^2 + 0.1983B^2 + 0.0531C^2 \tag{43}$$

From ANOVA result, the two-sided 95% confidence significant process parameters are P, Toff and IP. From Fig. 5.19, it is realistic that MRR augments with the enhancement in P but decreases with the augmentation of Toff. The shared response graph from Fig. 5.20 recognizes that MRR augments with the enhancement in P and IP. Fig. 5.21 clarifies that MRR augments with the augmentation in P and IP, but augments with the diminution in Toff. The optimal zone is obtained in between 25-28 µs of Toff, as MRR diminishes here and increases further with the decrease in Toff. MRR is highly dependent on the electrical conductivity and thermal conductivity. With the increment in P and IP, it is apparent that MRR also improves due to the

83

amplification of heat energy. MRR reduces with the augmentation in Toff because of the generation of lesser amount of discharges for an explicit time. Consequently, higher Toff outcomes in lesser melting in the gap and improper flushing of the ejected material occur with the dielectric flow. Therefore, minimum Toff is requisite for sustaining an effective machining condition for higher MRR.
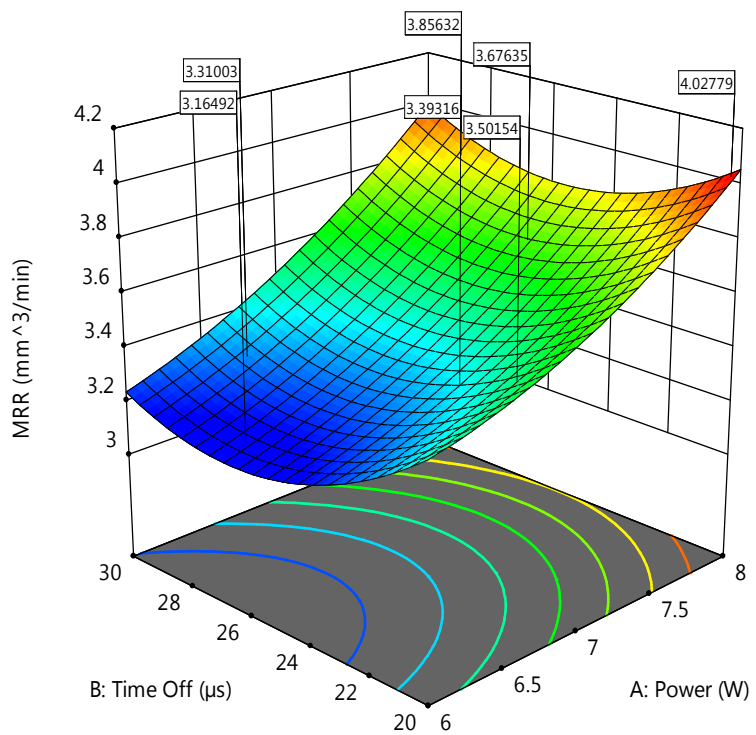
Fig. 5.19. Surface plot (P with Toff) on MRR

Fig. 5.20. Surface plot (P with IP) on MRR

Fig. 5.21. Surface plot (Toff with IP) on MRR

85

5.8. ANOVA for SR

To obtain the significance of the process parameters with maximum signal to minimum noise ratio is very exigent task for the machining of TMC. Inverse square-root transformation on the SR is implemented as required by the Box-Cox plot as shown Fig. 5.25 and ANOVA is performed. "P>F" lesser than 0.05 are significant. ANOVA implies SR model's "F-value" (121.83) which infers about its significance with a 0.01% chance for the noise. Here, A, B, C, AB, AC, C² are significant and the rest BC, A², B² are not significant and can be eliminated. The "Lack of Fit F-value" of 0.33 entails the "Lack of Fit" is not significant. Only 80.65% chance is there for a "Lack of Fit F-value" this big may occur due to the noise. If it is not significant then the response of the model is excellent for fitting. The "Pred R²" of 0.9706 is in pragmatic harmony with the "Adj R²" of 0.9855 with close compliance as the difference is less than 0.2. R^2 value is 0.9937 which is excellent as it tends to 1 and PRESS is 0.0065 which is very less considering a good signal. Adeq Precision is 37.0949 representing a sufficient signal. Table 5.6 represents ANOVA on SR for machining TMC where it is very much clear that the model which is developed is highly fitted with the observed values.

Table 5.6. ANOVA on SR for WEDM machining of TMC

Source	Sum of Squares	df	Mean Square	F-value	p-value	
Model	0.2210	9	0.0246	121.83	< 0.0001	significant
A-Power	0.0218	1	0.0218	108.28	< 0.0001	*
B-Time Off	0.0167	1	0.0167	82.76	< 0.0001	*
C-Peak Current	0.1309	1	0.1309	649.63	< 0.0001	*
AB	0.0044	1	0.0044	21.83	0.0023	*
AC	0.0017	1	0.0017	8.68	0.0215	*
BC	0.0002	1	0.0002	0.9782	0.3556	
A²	0.0004	1	0.0004	1.81	0.2199	
B²	0.0005	1	0.0005	2.33	0.1711	
C²	0.0682	1	0.0682	338.17	< 0.0001	*

Residual	0.0014	7	0.0002			
Lack of Fit	0.0003	3	0.0001	0.3282	0.8065	not significant
Pure Error	0.0011	4	0.0003			
Cor Total	0.2224	16				

R^2 = 0.9937 **Adj R^2** = 0.9855   **Pred R^2** = 0.9706 **Adeq Precision** = 37.0949 **PRESS** = 0.0065 * significant

Fig. 5.22 also bestows about the residuals which are located near the vicinity of the straight line demonstrating the normal distribution of the errors. Fig. 5.23 represents the random scattering of the externally studentized residuals causing it structure less and inside the design boundary. Fig. 5.24 portrays the perturbation plot on SR representing the contribution of all the input process parameters to SR, and peak current (factor C) contributes highest impact on SR. Fig. 5.25 elucidates the Box-Cox plot for power transforms on SR signifying the best lambda (-0.51) while the current lambda (-0.5) exactly coincides inferring excellent results. CI for the lambda is (-1.67, 0.46) and the current lambda is in the design space. Fig. 5.26 infers a very close conformity with the actual and predicted SR responses.
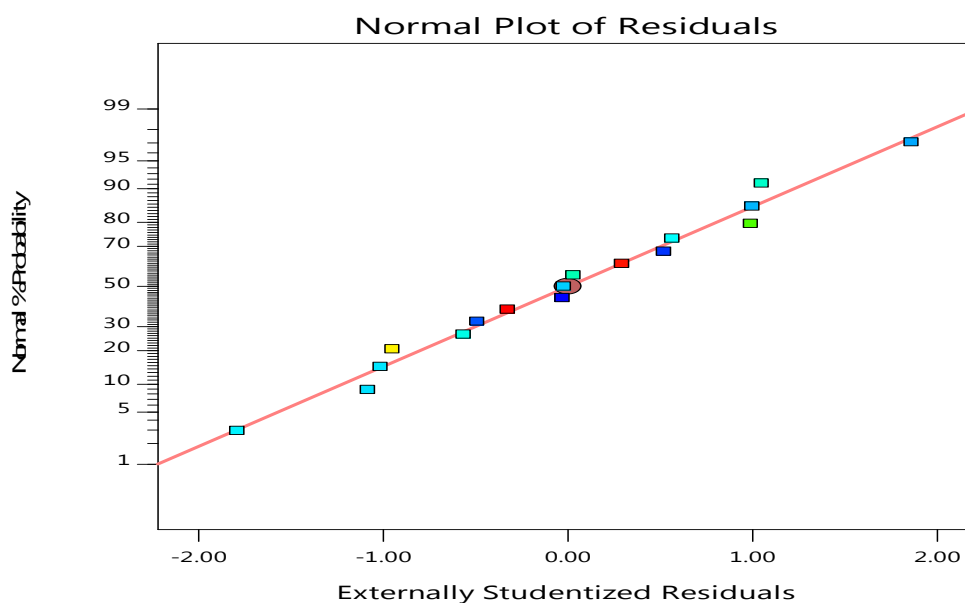
Fig. 5.22. Normal plot of residuals related to SR
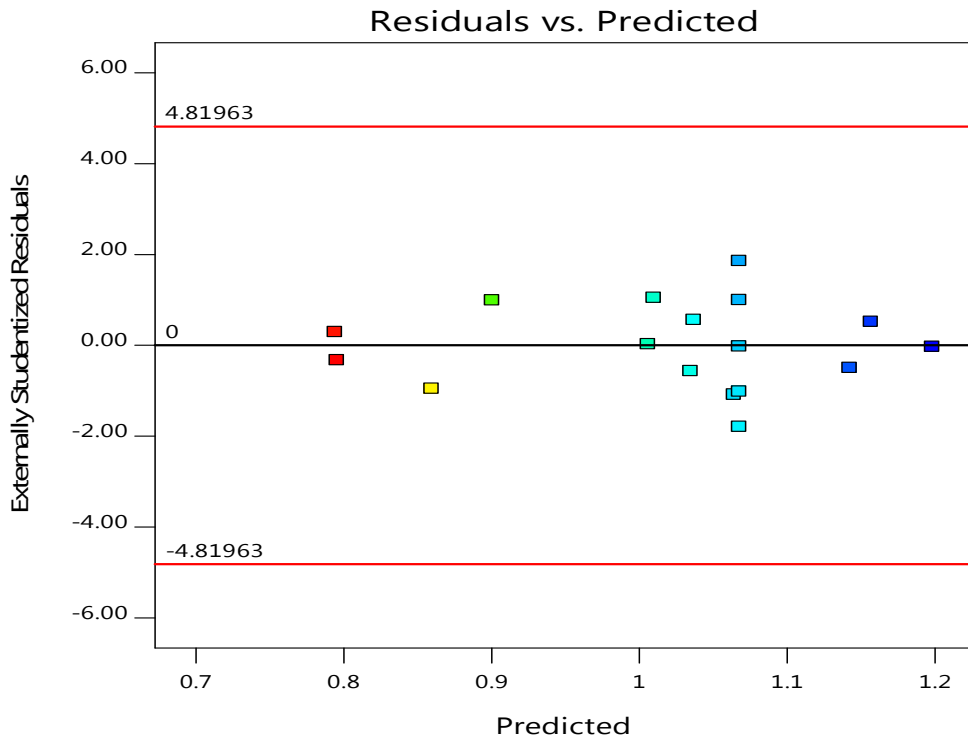
Fig. 5.23. Residuals and Predicted plots on SR
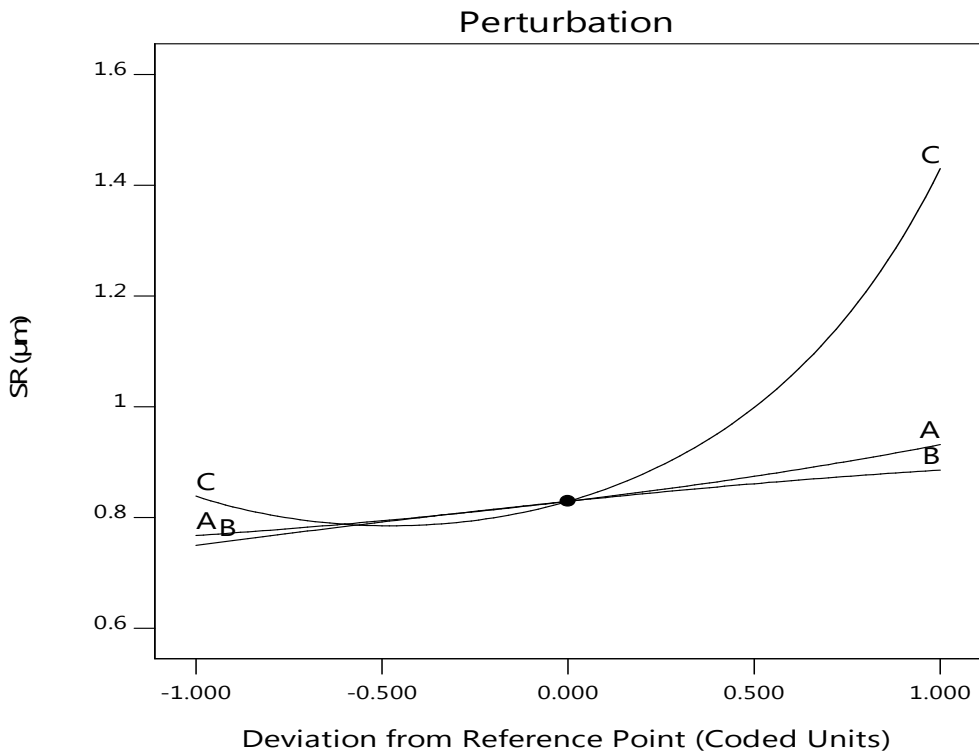
Fig. 5.24. Perturbation plot of SR

88
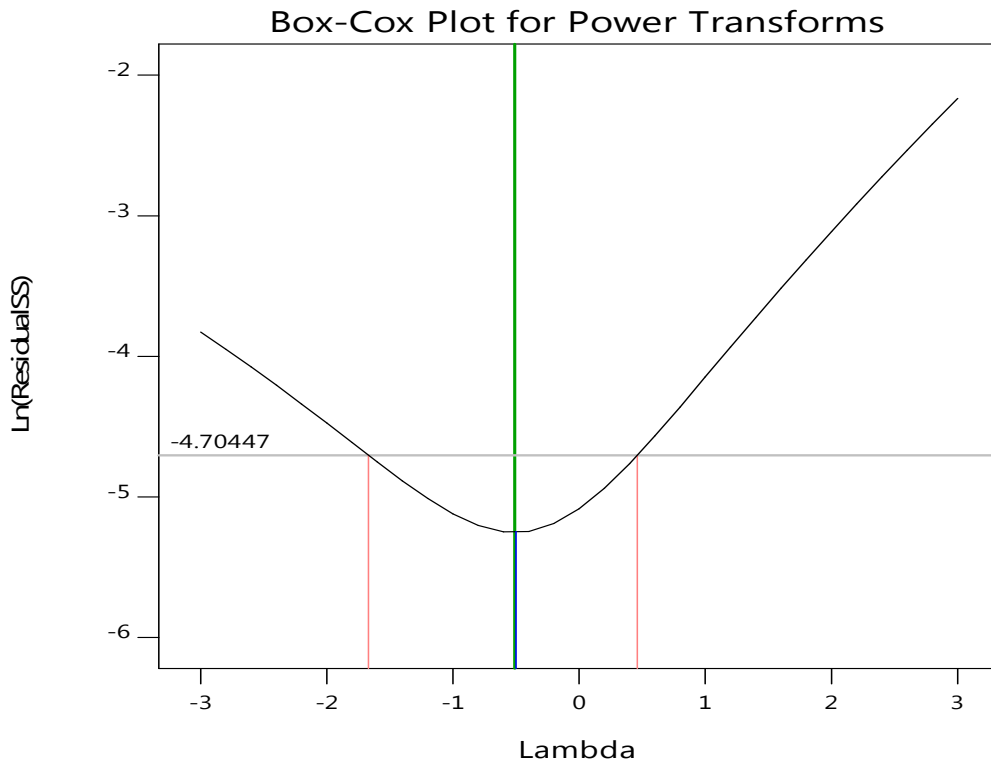
Fig. 5.25. Box-Cox plot on SR
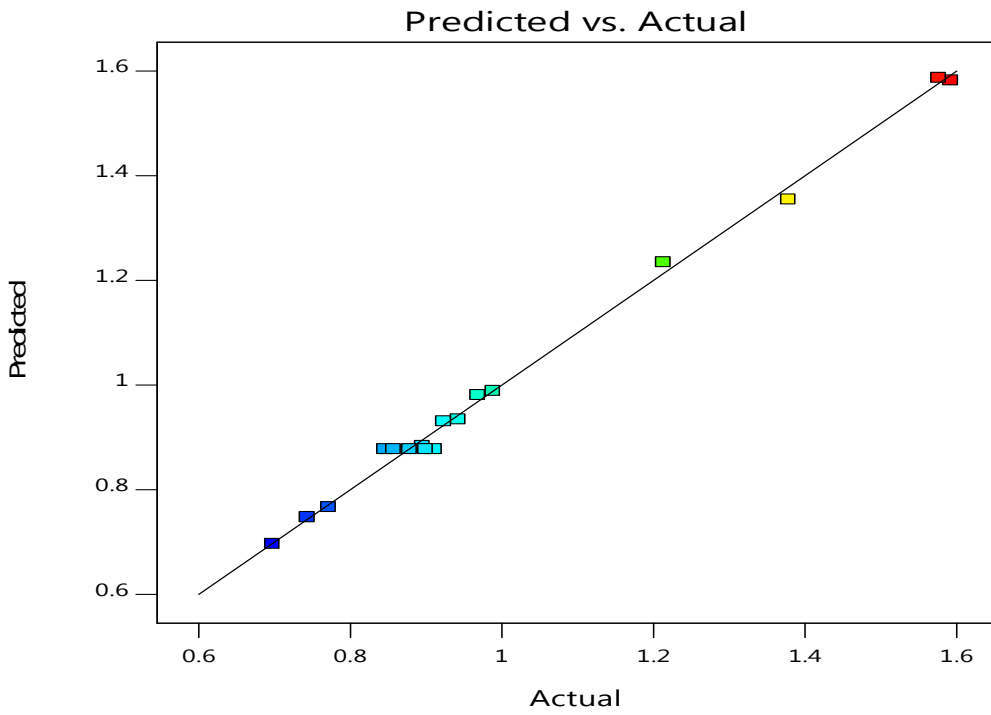
**Fig. 5.26.** Predicted and Actual responses of SR

Hence, the mathematical model for SR is provided in Eq. (44):

$$1/\text{Sqrt}(\text{SR}) = +1.10 - 0.0527A - 0.0461B - 0.1279C + 0.0332AB + 0.0207AC - 0.0070BC - 0.0093A^2 + 0.0105B^2 - 0.1339C^2$$

(44)

While machining TMC the ANOVA result signifies that the two-sided 95% confidence significant process parameters are P, Toff and IP. From the Fig. 5.27, SR augments with the enhancement of P and Toff, but the variation is very less. Fig. 5.28 portrays the enhancement of SR with the enhancement of P and IP. Fig. 5.29 clarifies that SR improves with the augmentation in IP and diminishes with the augmentation in Toff.
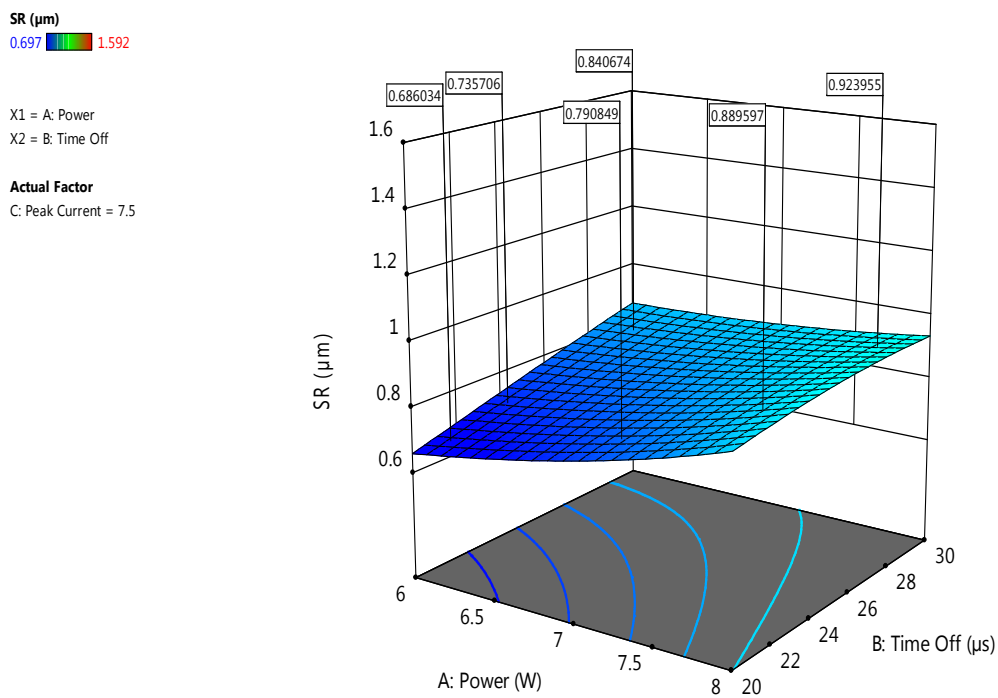
Fig. 5.27. Surface plot (P with Toff) on SR

90
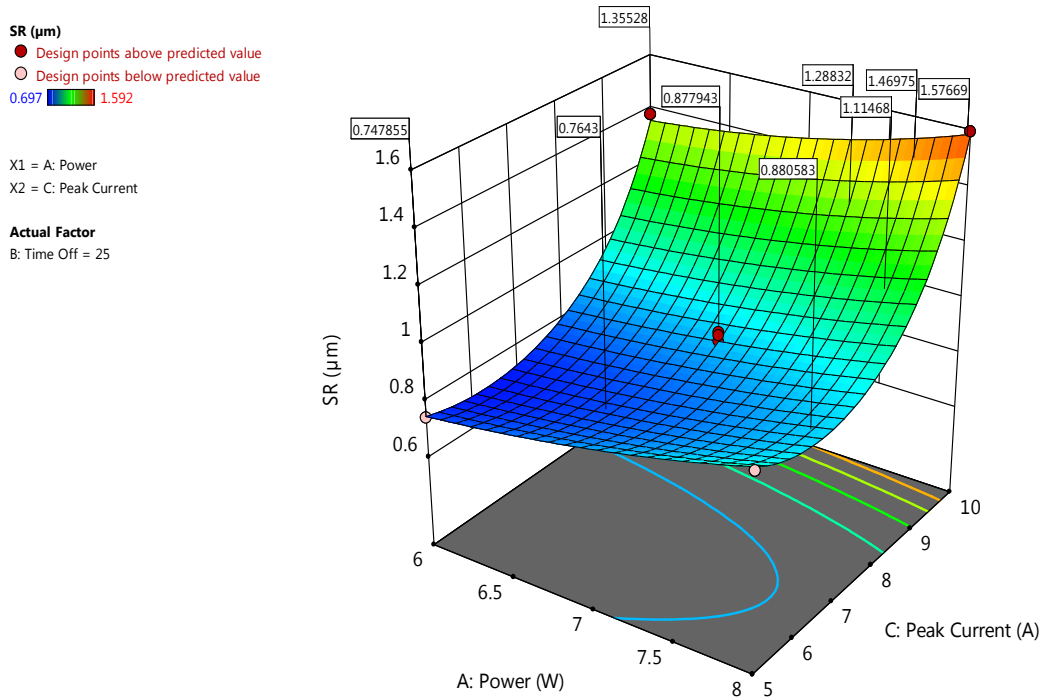
Fig. 5.28. Surface plot (P with IP) on SR
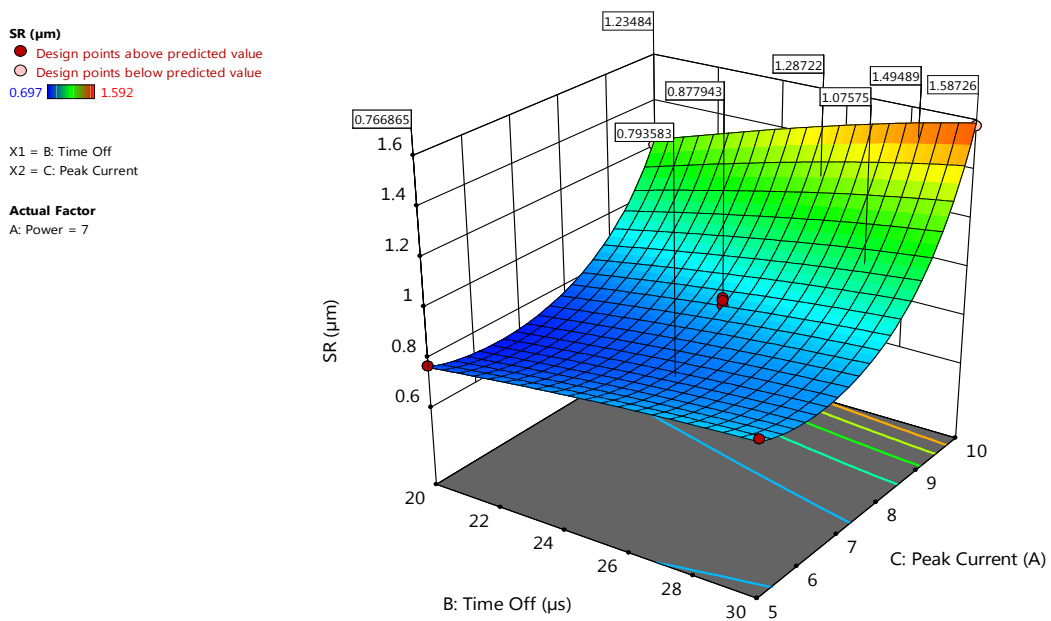
Fig. 5.29. Surface plot (Toff with IP) on SR

The enhancement of SR related to the above factors is due to longer duration of spark ensuing in additional discharge energy per spark. Only a very small amount of the workpiece is melted for

this reason. Improper flushing results in deeper and wider crater generation producing a rough surface. Therefore P and IP should be kept very less for smooth surface generation. It is also evident that if there is an augmentation in Toff then there is a reduction of SR due to the occurrence of fewer discharges for a meticulous period ensuing in less amount of crater formation resulting in lesser micro-damage. For acquiring excellent surface finish Toff should be higher.

5.9. ANOVA for KW and OC

Fig. 5.30 explains the Box-Cox plot on KW signifying the best lambda (1.6) while the current lambda (1.0) exactly coinciding providing excellent results. CI value for the lambda is (-3.16, 5.25) and the current lambda is in the design space. Hence, the developed second-order equation for KW is portrayed in Eq. (45):

$$KW = +0.3507 + 0.0185A - 0.0065B - 0.0125C - 0.0100AB + 0.0027AC + 0.0027BC + 0.0160A^2 + 0.0110B^2 - 0.0042C^2 \tag{45}$$
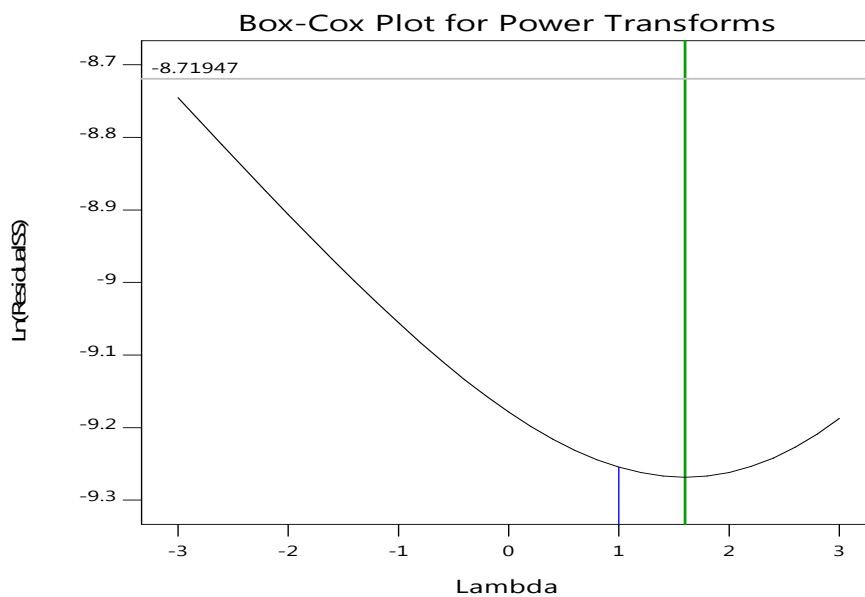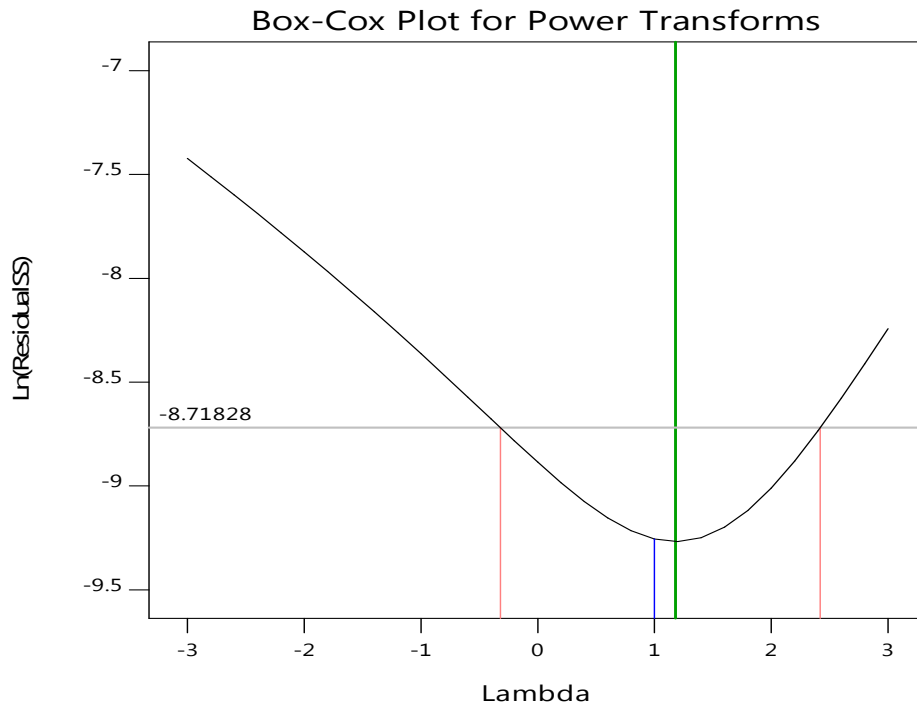

Fig. 5.30. Box-Cox plot on KW

92

Table 5.7 indicates the abridged ANOVA table for performance measures of WEDM machining of TMC which clearly contrasts between the characteristics of all the output responses.

Table 5.7. Abridged ANOVA table for WEDM machining of TMC

Source	MRR		SR		KW		OC	
	F-value	p-value	F-value	p-value	F-value	p-value	F-value	p-value
Model	92.21	< 0.0001	121.83	< 0.0001	52.87	< 0.0001	52.87	< 0.0001
A-Power	598.48	< 0.0001	108.28	< 0.0001	196.03	< 0.0001	196.03	< 0.0001
B-Time Off	23.28	0.0019	82.76	< 0.0001	24.4	0.0017	24.4	0.0017
C-Peak Current	17.94	0.0039	649.63	< 0.0001	91.44	< 0.0001	91.44	< 0.0001
AB	3.94	0.0877*	21.83	0.0023	29.26	0.001	29.26	0.001
AC	4.76	0.0654*	8.68	0.0215	2.17	0.1843*	2.17	0.1843*
BC	37.68	0.0005	0.9782	0.3556*	2.17	0.1843*	2.17	0.1843*
A²	22.68	0.0021	1.81	0.2199*	78.85	< 0.0001	78.85	< 0.0001
B²	108.77	< 0.0001	2.33	0.1711*	37.27	0.0005	37.27	0.0005
C²	7.04	0.0328	338.17	< 0.0001	4.83	0.064*	4.83	0.064*
Lack of Fit	0.2668	0.8468*	0.3282	0.8065*	0.2614	0.8504*	0.2614	0.8504*
R² (MRR) = 0.9916	Adj R² (MRR) = 0.9809	Pred R² (MRR) = 0.9657	Adeq Prec (MRR) = 27.7302	PRESS (MRR) = 0.0437	Pure Error (MRR) = 0.0089			
R² (SR) = 0.9937	Adj R² (SR) = 0.9855	Pred R² (SR) = 0.9706	Adeq Prec (SR) = 37.0949	PRESS (SR) = 0.0065	Pure Error (SR) = 0.0011			
R² (KW) = 0.9855	Adj R² (KW) = 0.9669	Pred R² (KW) = 0.9434	Adeq Prec (KW) = 28.6272	PRESS (KW) = 0.0004	Pure Error (KW) = 0.0001			
R² (OC) = 0.9855	Adj R² (OC) = 0.9669	Pred R² (OC) = 0.9434	Adeq Prec (OC) = 28.6272	PRESS (OC) = 0.0004	Pure Error (OC) = 0.0001		* not significant	

Fig. 5.31 explains the Box-Cox plot on OC signifying the best lambda (1.18) while the current lambda (1.0) exactly coinciding providing excellent results. CI value for the lambda is (-0.32, 2.42) and the current lambda is in the design space. The equation for OC is provided in Eq. (46):

$$OC = +0.1007 + 0.0185A - 0.0065B - 0.0125C - 0.0100AB + 0.0027AC$$
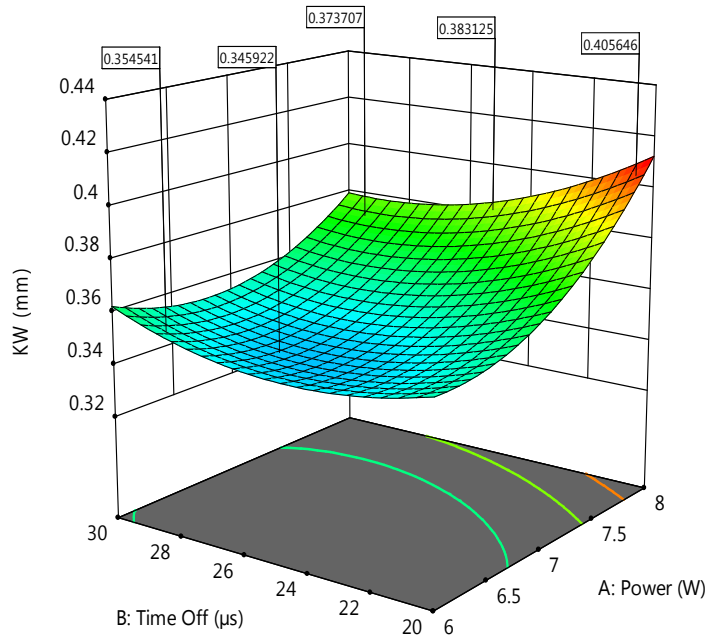$$+0.0027BC + 0.0160A^2 + 0.0110B^2 - 0.0042C^2$$

(46)

Fig. 5.31. Box-Cox plot on OC

While machining TMC the ANOVA result signifies that the two-sided 95% confidence significant process parameters are P, Toff and IP. From the Fig. 5.32, KW augments with the enhancement of P and Toff. Fig. 5.33 portrays the enhancement of KW with the enhancement of P and IP. Fig. 5.34 clarifies that KW also increases with the augmentation in IP and Toff. The enhancement of KW is due to longer spark duration resulting in greater heat and thermal energy resulting in improper melting and improper flushing ensuing blow holes, crater formation and generation of residual stresses. Therefore P and IP must be low for lower KW. It is also evident that if there is an increment in Toff then there is an increment of KW due to high discharges and irregular plasma channels.

Fig. 5.32. Surface plot (P with Toff) on KW
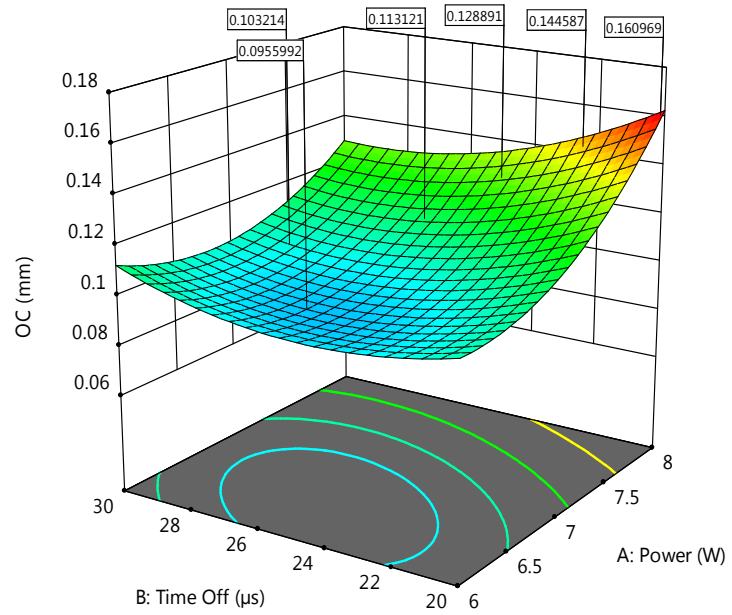

Fig. 5.33. Surface plot (P with IP) on KW
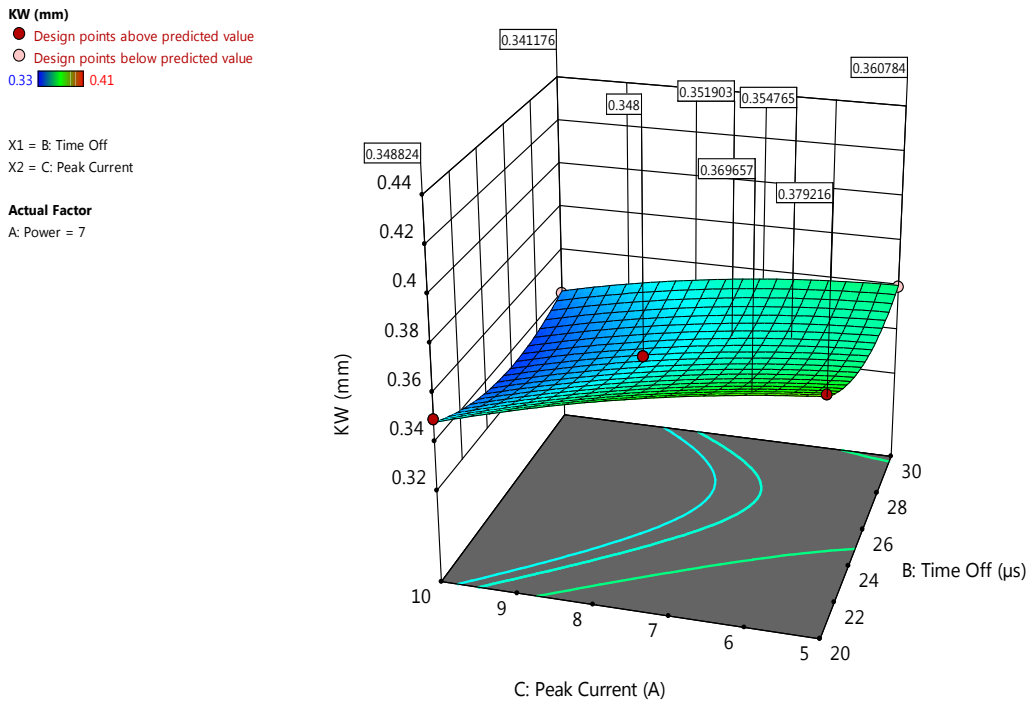
Fig. 5.34. Surface plot (Toff with IP) on KW

From the Fig. 5.35, OC augments with the enhancement of P and Toff. Fig. 5.36 portrays the enhancement of OC with the enhancement of P and IP. Fig. 5.37 clarifies that OC also increases with the augmentation in IP and Toff. As OC is directly proportional to KW therefore all the reasons are exactly the same for increment of KW and OC due to the raise of P, Toff and IP.

OC (mm)

0.08 ▮▮▮ 0.16

X1 = A: Power
X2 = B: Time Off

Actual Factor
C: Peak Current = 7.5

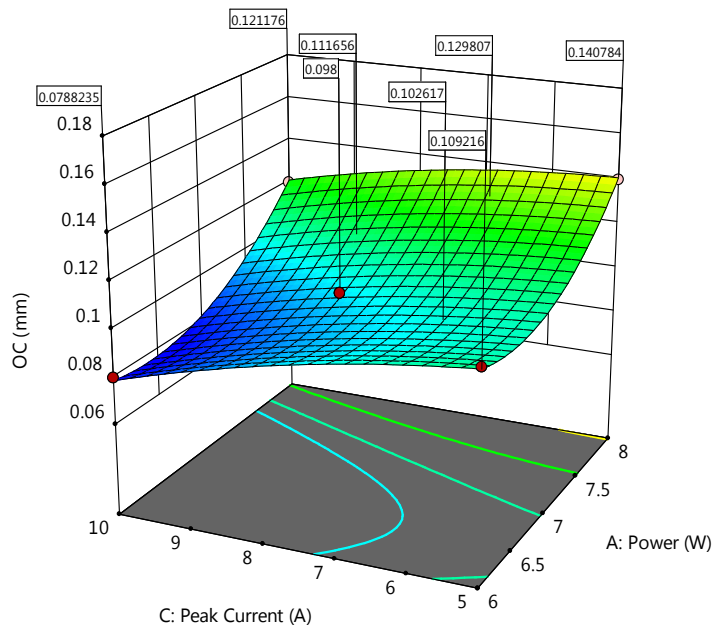0.103214   0.113121   0.128891   0.144587   0.160969
0.0955992

Fig. 5.35. Surface plot (P with Toff) on OC

OC (mm)
● Design points above predicted value
○ Design points below predicted value

0.08 ▮▮▮ 0.16

X1 = A: Power
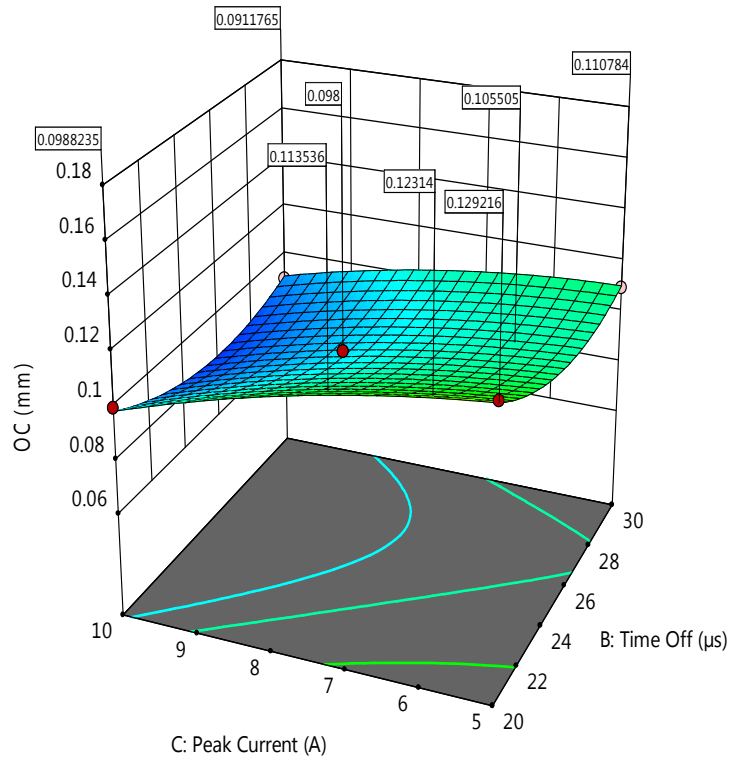X2 = C: Peak Current

Actual Factor
B: Time Off = 25

0.121176   0.111656   0.129807   0.140784
0.0788235   0.098   0.102617
0.109216

Fig. 5.36. Surface plot (P with IP) on OC

97

Fig. 5.37. Surface plot (Toff with IP) on OC

98
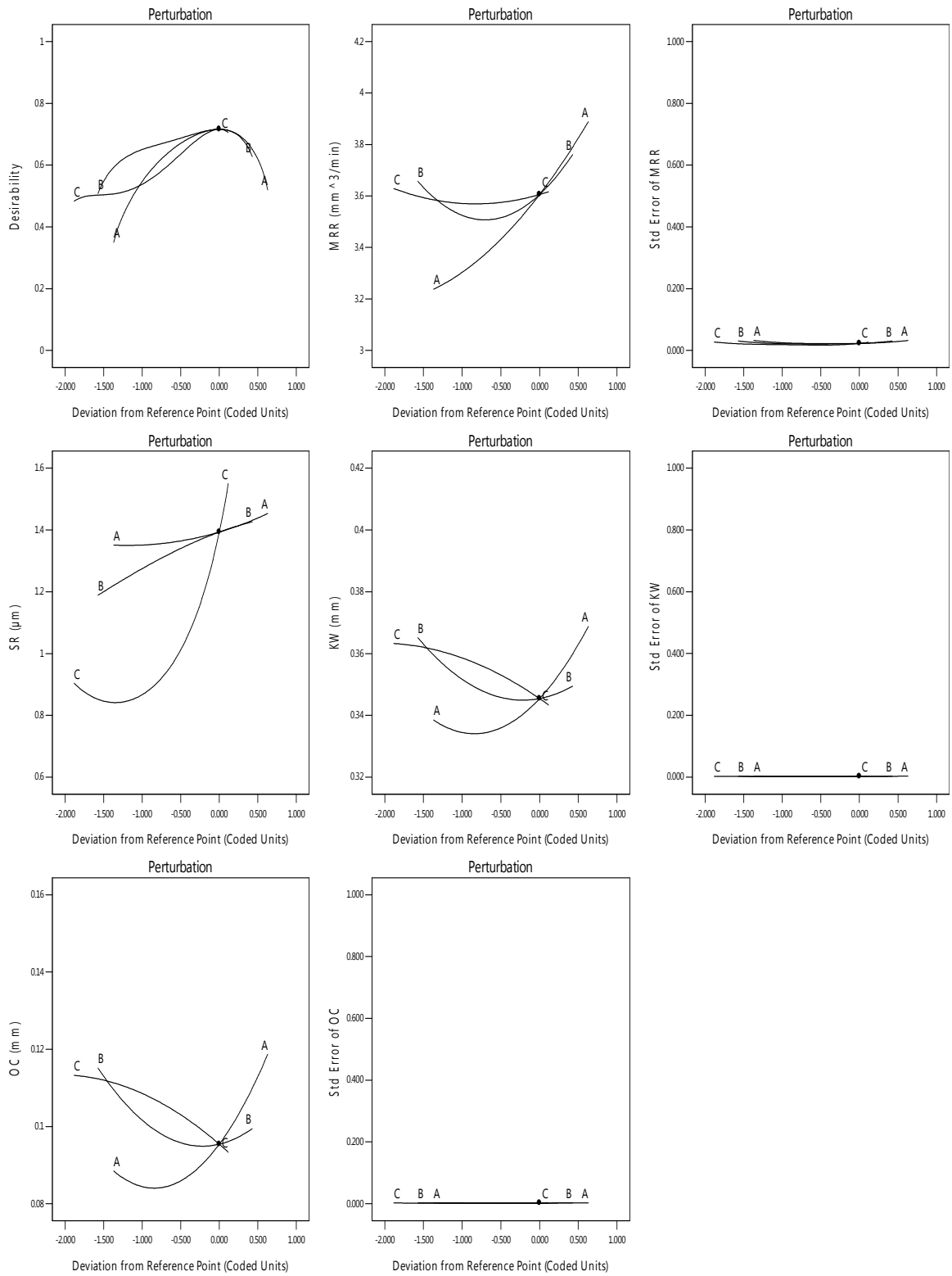
Fig. 5.38. Combined perturbation plot on performance measures

99

Fig. 5.38 portrays the combined perturbation plot on the output responses indicating the contribution of all the three input process parameters to all the output responses. There is a random scattering of the residuals resulting in structure-less within the design boundary and close agreement with the experimental and predicted results. All these values coincide with each other providing excellent results depicting its navigation in design space.

5.10. Multi-objective optimization of WEDM parameters and responses

Fig. 5.39 corresponds to the multi-objective optimized solution of WEDM on Ti-TiB$_2$ hybrid composite depending on the above D-optimality technique. The graphical and numerical optimizations are applied and the results are validated. From the graph, it is pragmatic that the main objective of optimization is improving as the slope of MRR is upwards which concludes higher the MRR, better is the productivity. The responses of KW and OC are in decreasing slope resembling lower the better condition. Since, the domain of SR is transposed; therefore its upward slope actually signifies lower the better criteria. The optimized solution is attained when P is 7.3704 W, Toff is 27.8665 µs, IP is 9.70767 A, MRR is 3.60565 mm^3/min, SR is 1.39197 µm, KW is 0.34542 mm, OC is 0.09542204 mm, StdErr(MRR) is 0.0227795, StdErr(SR) is 0.00828911, StdErr(KW) is 0.0021587, StdErr(OC) is 0.0021587 and combined desirability is 0.716. From Fig. 5.40, the individual desirability of all the input process parameters is obtained as 1, signifying 100% desirability, and MRR as 0.50231, SR as 0.864192, KW as 0.807245, OC as 0.807245, StdErr(MRR) as 0.69311, StdErr(1/Sqrt(SR)) as 0.69311, StdErr(KW) as 0.69311, StdErr(OC) as 0.69311 and overall combined desirability is 0.715931 (considered as 0.716). This graph infers the individual desirability of the parameters and combined desirability of the parameters and responses signifying multi-objective optimized value. All the individual and overall desirability is greater than 0.5 (50%) signifying excellent results. It also represents the

100

overall interaction of performance and process parameters of the optimized solution where the optimal solution of all the individual responses is highlighted along the graphs of the process parameters. Fig. 5.41 represents overall interactions of performance and process parameters of the optimized solution.
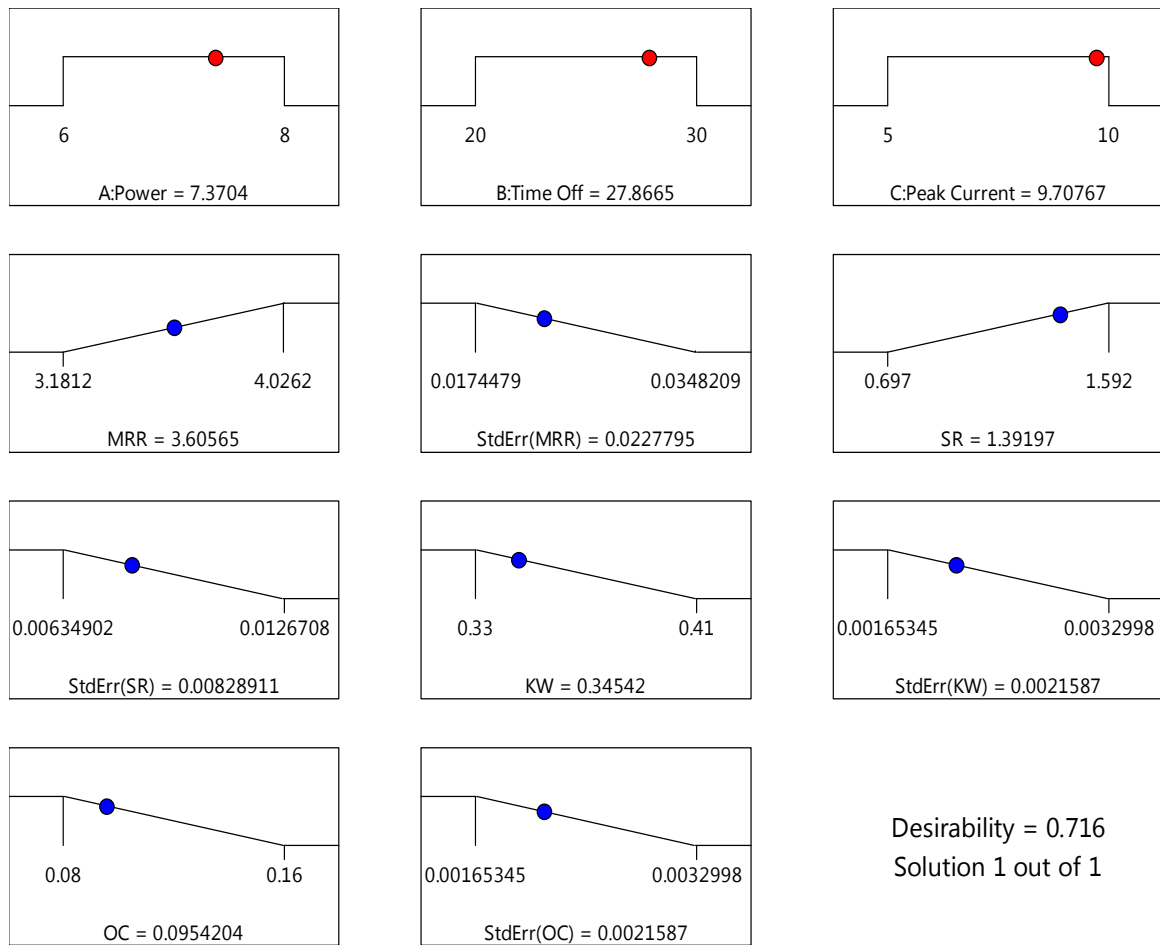
Fig. 5.39. Multi-objective optimized solution of WEDM
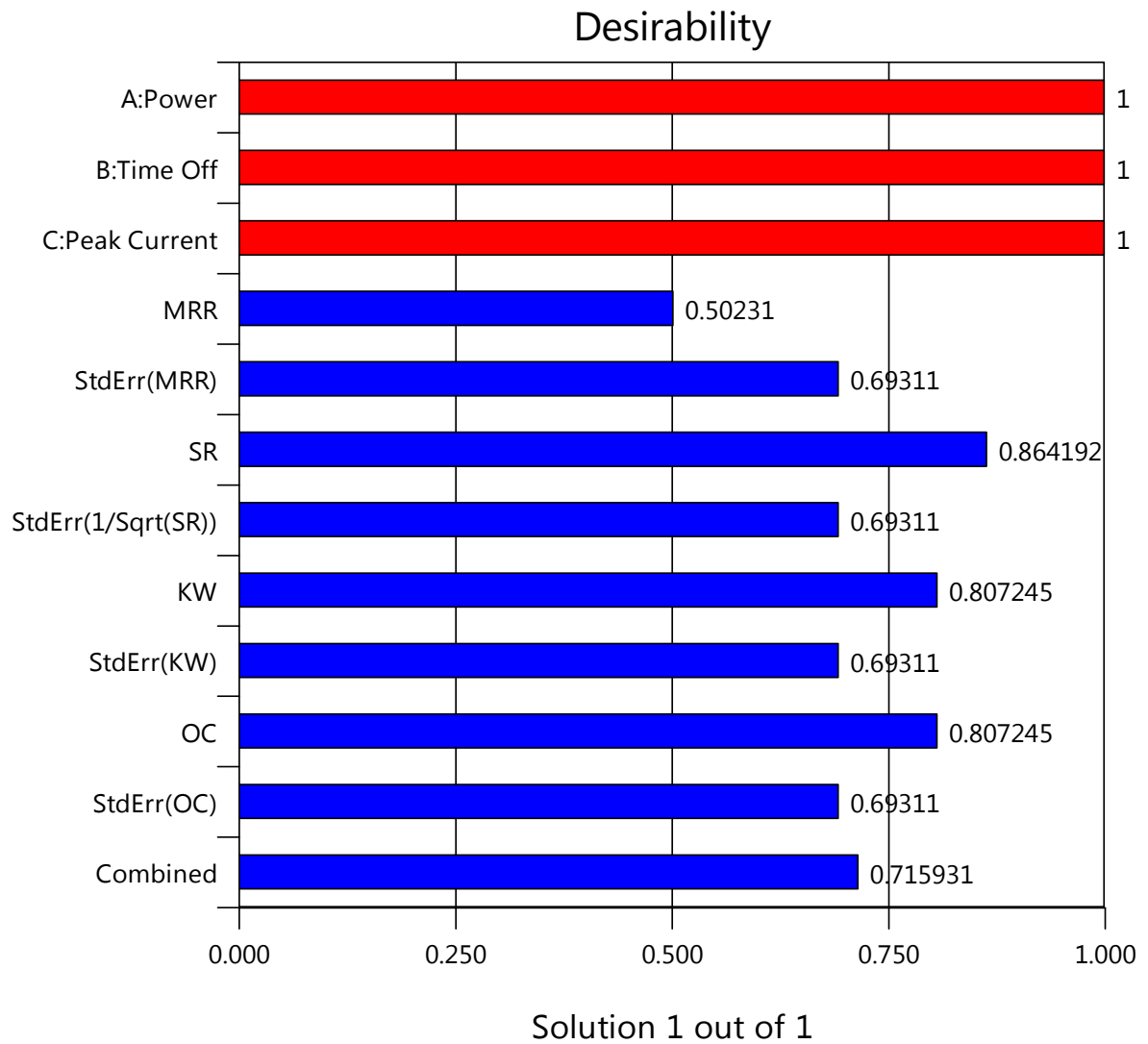
**Fig. 5.40.** Desirability of input process parameters and output responses
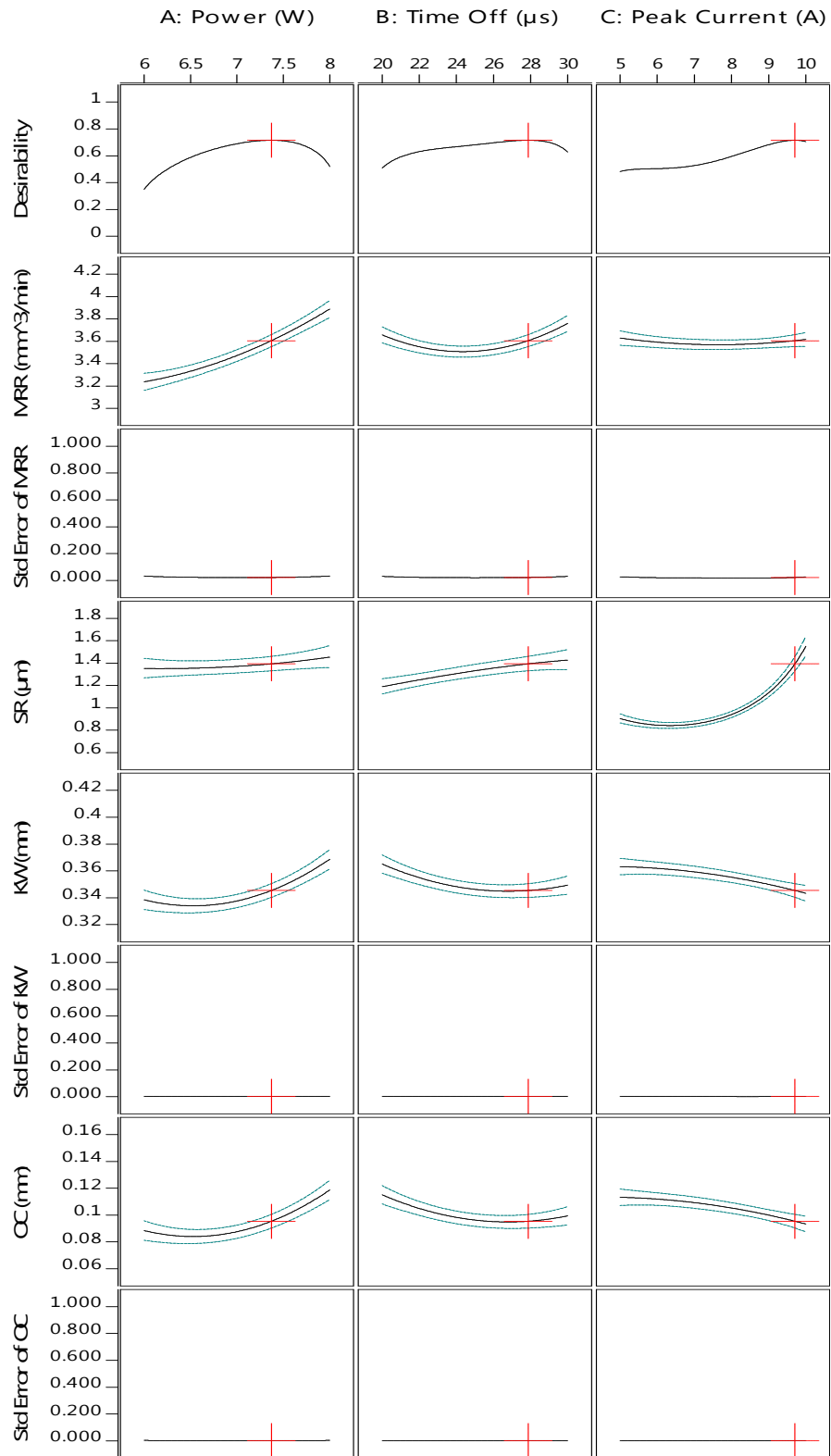
Fig. 5.41. Overall interactions of performance and process parameters of the optimized solution

Fig. 5.42 portrays the variation of 2-d contour plots of different performance measures where a relationship can be built between two process parameters while keeping the other parameter at medium level. MRR is an extensive performance response which vastly impacts productivity and cost. Therefore, much preference is to be given for superior MRR in machining for improvement in production minimizing the overall cost. From table 5.7, it is pragmatic that power is the most significant process variable which influences greater in MRR, while peak current is the most significant process variable in case of SR. There is an augmentation of MRR with the enhancement of P but a subsequent reduction occurs with the augmentation in Toff as depicted by Fig. 5.42(a). Fig. 5.42(b) portrays a large amplification of MRR with the enhancement of P and IP, as there is an amplification of heat energy which increases the plasma energy and MRR is unwaveringly proportional to plasma. Fig. 5.42(c) illustrates the enrichment of MRR with the rise in IP and P, but intensifies with the decrement in Toff due to the occurrence of insufficient amount of discharges of plasma. From the Fig. 5.42(d), it is apparent about the augmentation of SR as P and Toff augments. From Fig. 5.42(e), it is obvious that SR gets increased with the augmentation in P and IP. Fig. 5.42(f) conjectures about the augmentation of SR, when IP augments but further decreases when Toff lessens, due to the occurrence of extended spark duration ensuing in additional discharge energy per spark. Therefore, it is pragmatic that with the increment in Toff, SR gets abridged due to the formation of squat discharges for a precise period ensuing in small crater formation. Thus, Toff should be higher for smooth surface finish. Similar results are obtained in Fig. 5.42(g-i) in determining the KW responses with the process parameters. With the increase in P and IP, KW and OC increases but with the increment in Toff both decreases; which hence designates that with the adherence of molten metal there is a formation of micro voids. This is due to weak interaction of plasma jet to the sample at superior

104

cutting speed. With the increment of the discharge the cutting speed increases resulting in elevated concentration of plasma energy leading to swift melting and hence the molten metal vaporizes increasing the MRR. Fig. 5.42(j-l) represents the same for OC response. It is pragmatic that since OC is directly proportional to KW therefore the dependency of these parameters exhibit similar results for both the performance measures KW and OC. In all these figures minimum zone symbolizes in blue and maximum zone symbolizes in red contours.
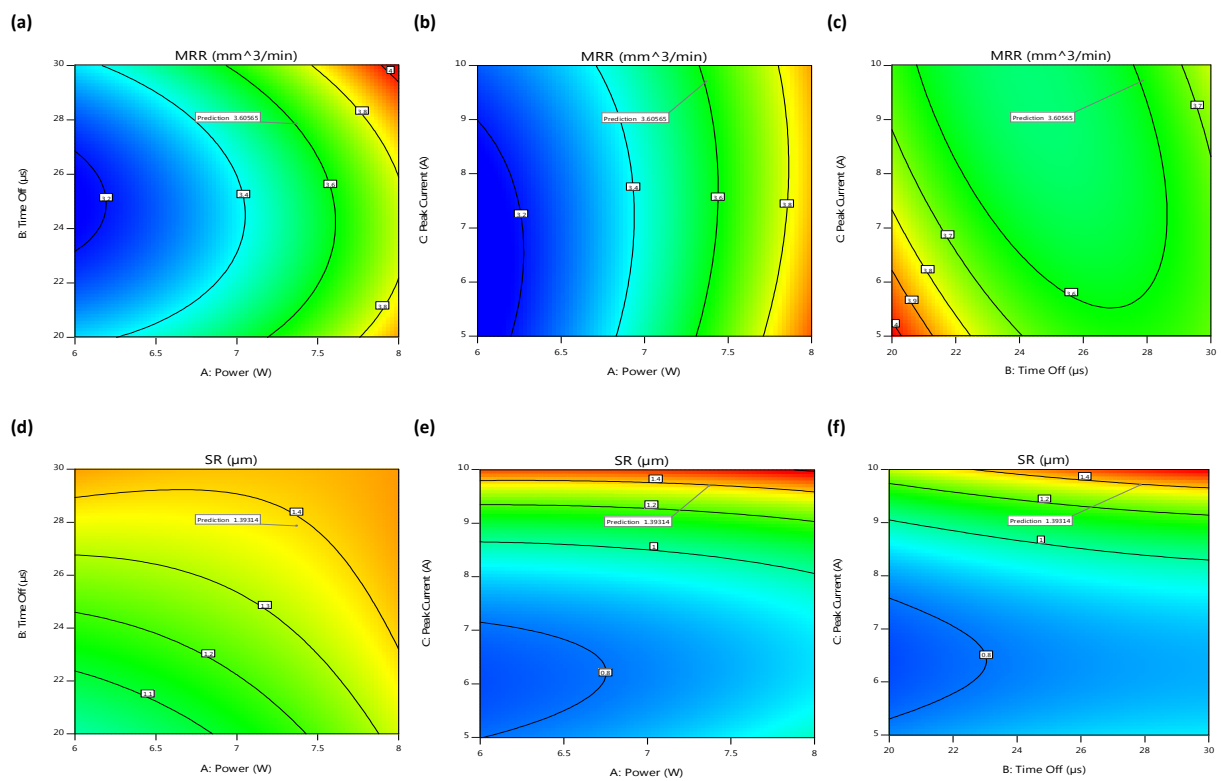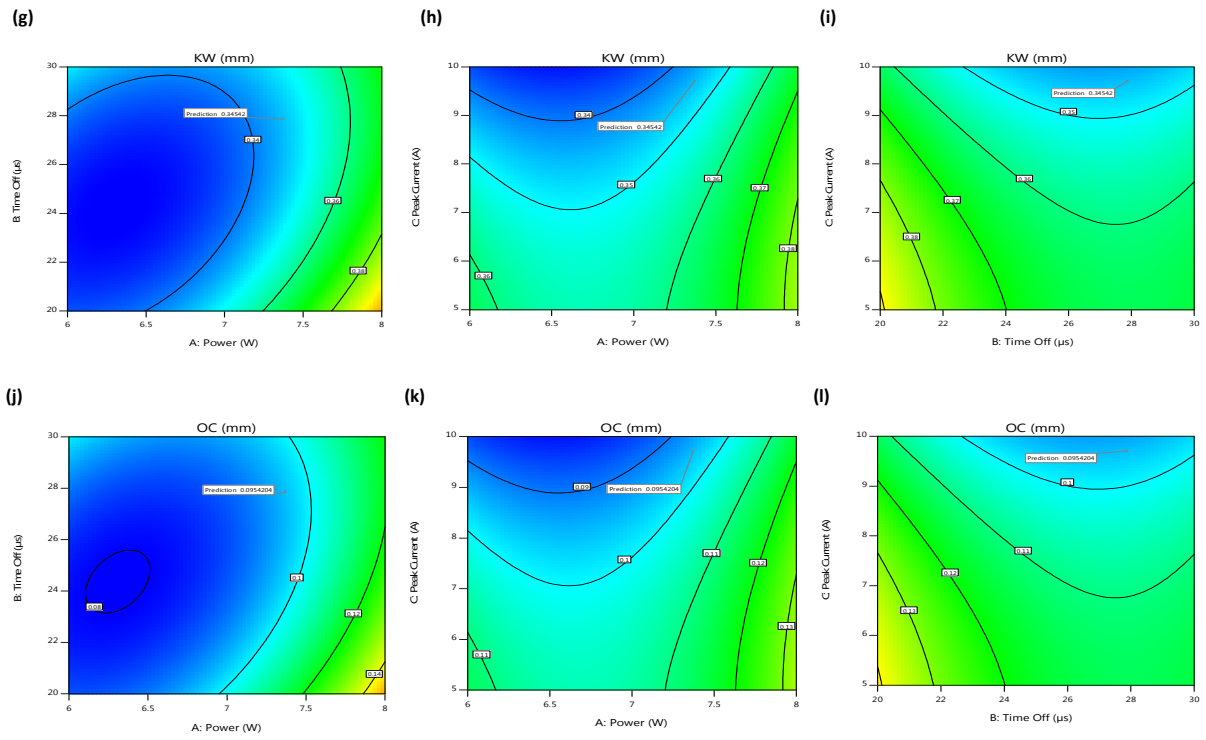
Fig. 5.42. Contour plots of performance measures: (a) P vs. Toff on MRR, (b) P vs. IP on MRR, (c) Toff vs. IP on MRR, (d) P vs. Toff on SR, (e) P vs. IP on SR, (f) Toff vs. IP on SR, (g) P vs. Toff on KW, (h) P vs. IP on KW, (i) Toff vs. IP on KW, (j) P vs. Toff on OC, (k) P vs. IP on OC, (l) Toff vs. IP on OC

Fig. 5.43 represents the surface plot of overall desirability considering the P and Toff parameters keeping IP as medium value and constant. It is pragmatic that desirability enhances with the combining effect of increment in P and decrement in Toff. Similarly, both P and IP show an augment in the desirability with their enhancement, keeping Toff to be invariant and in medium level, as evident from Fig. 5.44. But from Fig. 5.45, it is clear that the overall desirability can be improved in higher IP but lower Toff, when P is kept constant and in medium level. Hence, an optimum point is essential for MOO analysis.
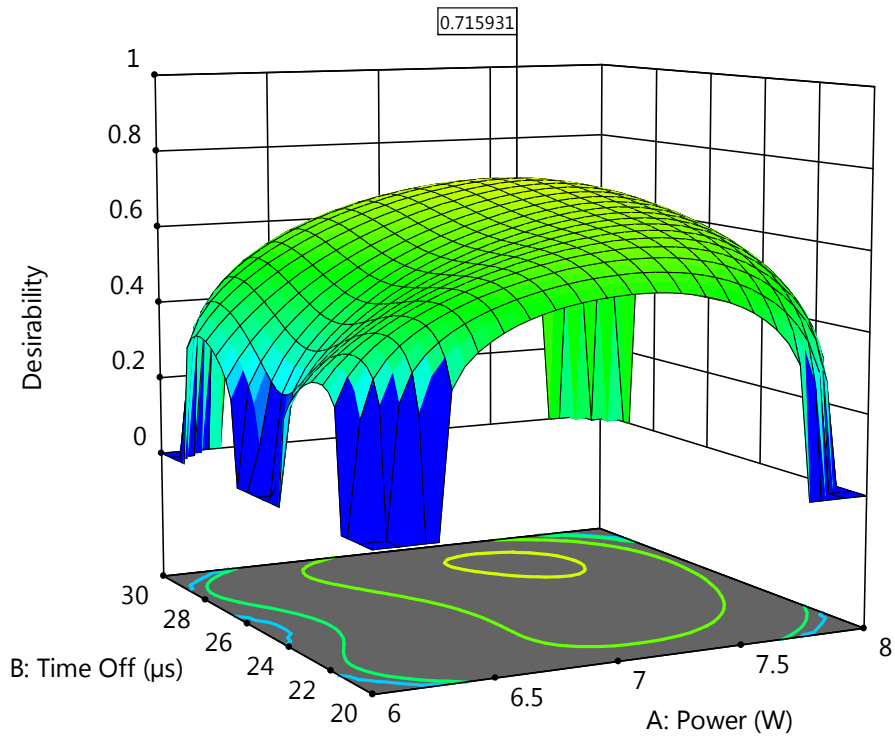
Fig. 5.43. Desirability graph of P vs. Toff
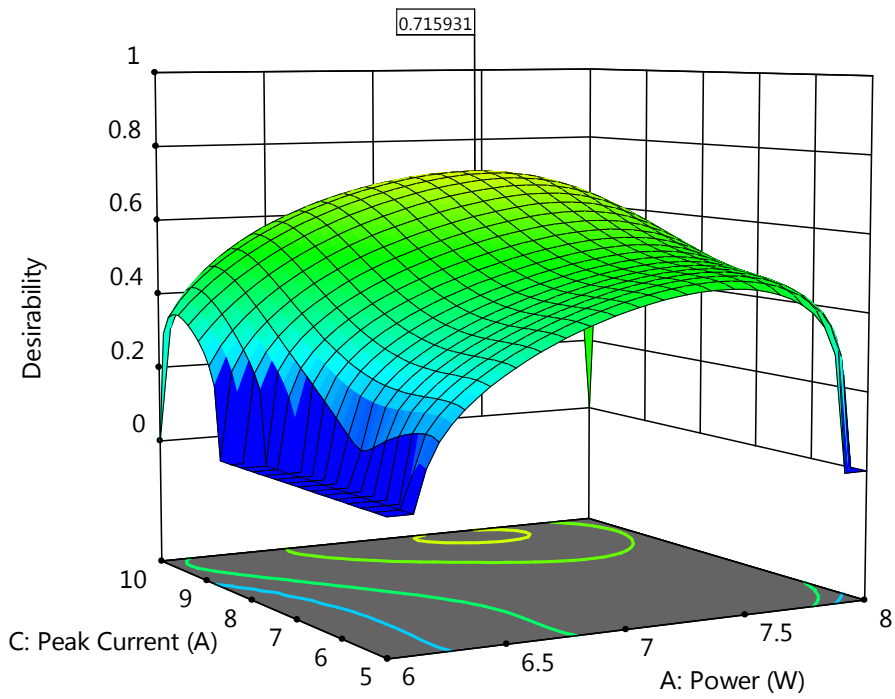
Fig. 5.44. Desirability graph of P vs. IP

107
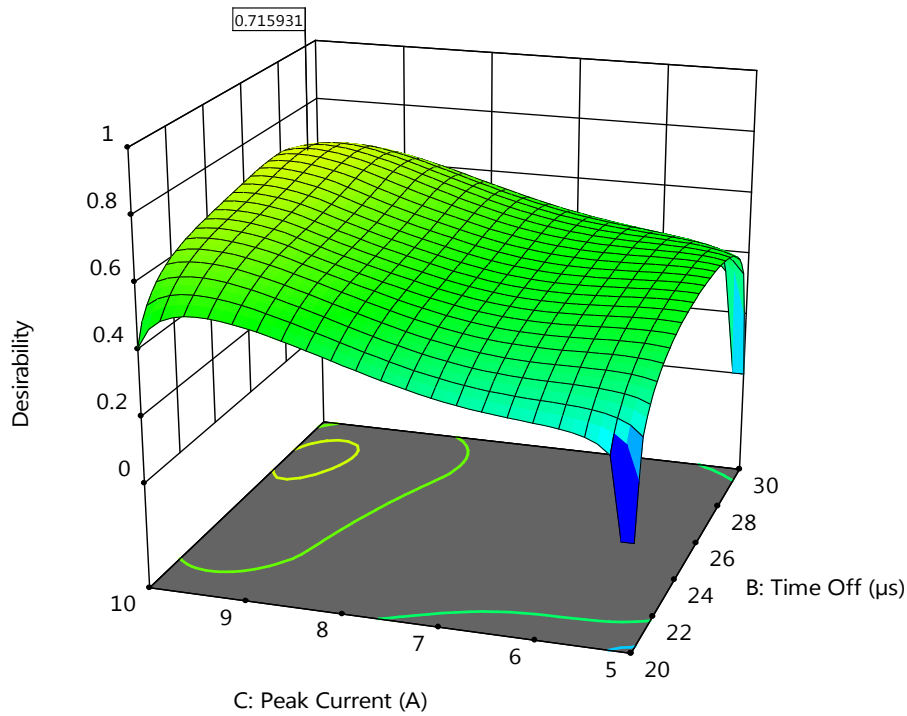
Fig. 5.45. Desirability graph of Toff vs. IP

From table 4.11, it is clear that rank 1 is obtained in experimental run number 2 comprising of machining parameters of factors A at 6 W, B at 25 µs, C at 10 A, with DGRG of 0.7233158. This optimized value has improved result when compared with the desirability approach (0.715931). The means of DGRG (DGRG$_m$) is 0.5953707 which is in close proximity of the rank 17 of run 14 (0.5093703). The difference of the DGRG values between two successive rankers is very nominal inferring superior results in MOO problems. By considering the overall effects in DGRA, IP is inferred to be rank 1, P to be rank 2 and Toff to be rank 3. Ranking signifies the contribution of each process parameters to all the four performance measures. Fig. 5.46 portrays % improvement and comparative study between DGRA, desirability and *Kumar et al.* [4]. It is pragmatic that by incorporating DGRA, maximum % error has been reduced and there is an improvement in the manufacturing and machining processes. Again considering run number 12, % improvement in DGRA is obtained to be 4.163% whereas for desirability it is 1.868%, and

when compared with *Kumar et al.* [4] the % improvement is 2.3%. From the graph it is evident that in every experimental runs DGRA and desirability is superior to *Kumar et al.* [4]. However, much exploration in comparison with DGRA to GA and ANN in future has to be endeavored for better optimal results.
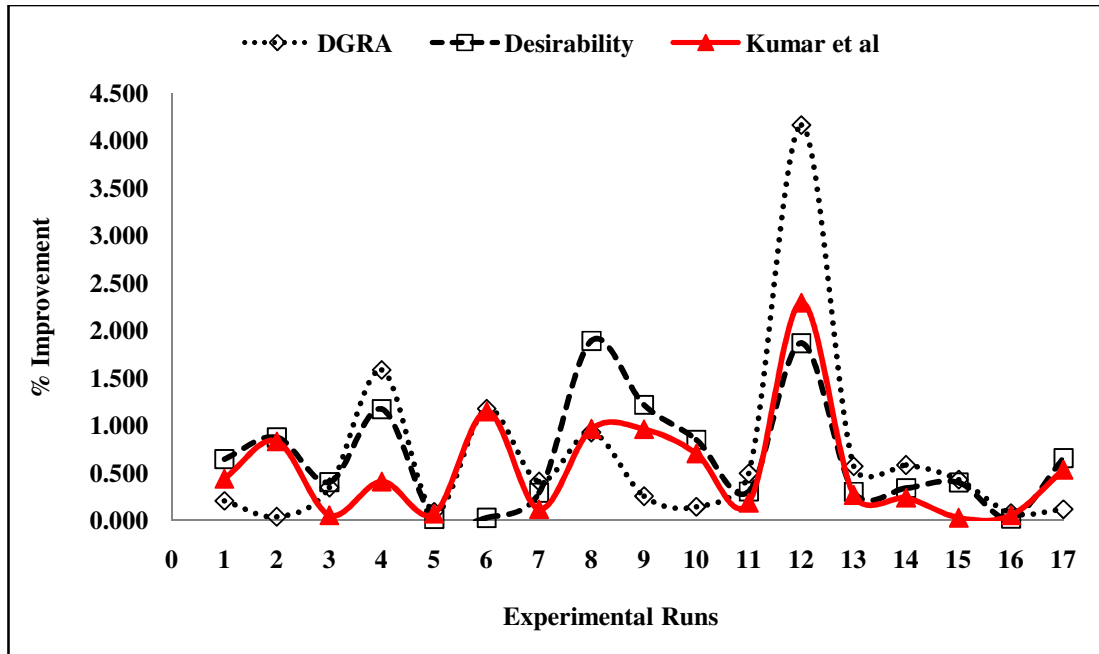
Fig. 5.46. % improvement and comparative study

5.11. Confirmation tests with validation

After successful optimization, the optimized result is validated using confirmatory tests. % error is represented by Fig. 5.47 that communicates palpably delegating a nominal divergence involving the actual and results. The %error of both the performance measures is below 1.4% which infers excellent result and robustness. Fig. 5.48 and Fig. 5.49 signify confirmation graphs between the predicted and experimental performance measures following outstanding concurrence and close proximity with one other. The data mean lies in the existence inside the province of 95% PI low and 95% PI high which infers the validation of test results.
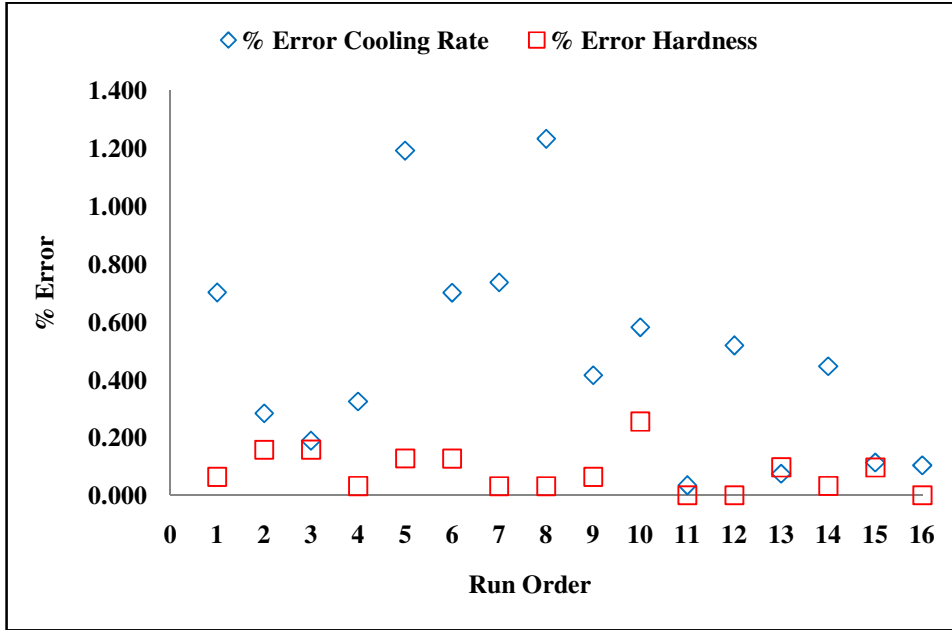
Fig. 5.47. % Error computation of performance measures of composite development
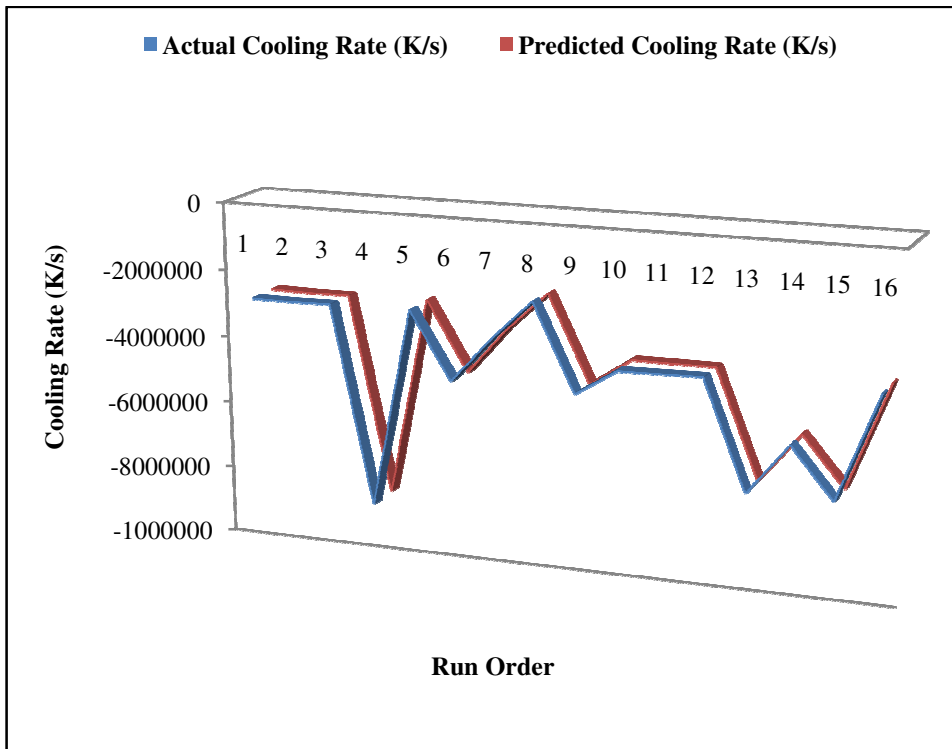
Fig. 5.48. Confirmatory graph on Cooling Rate
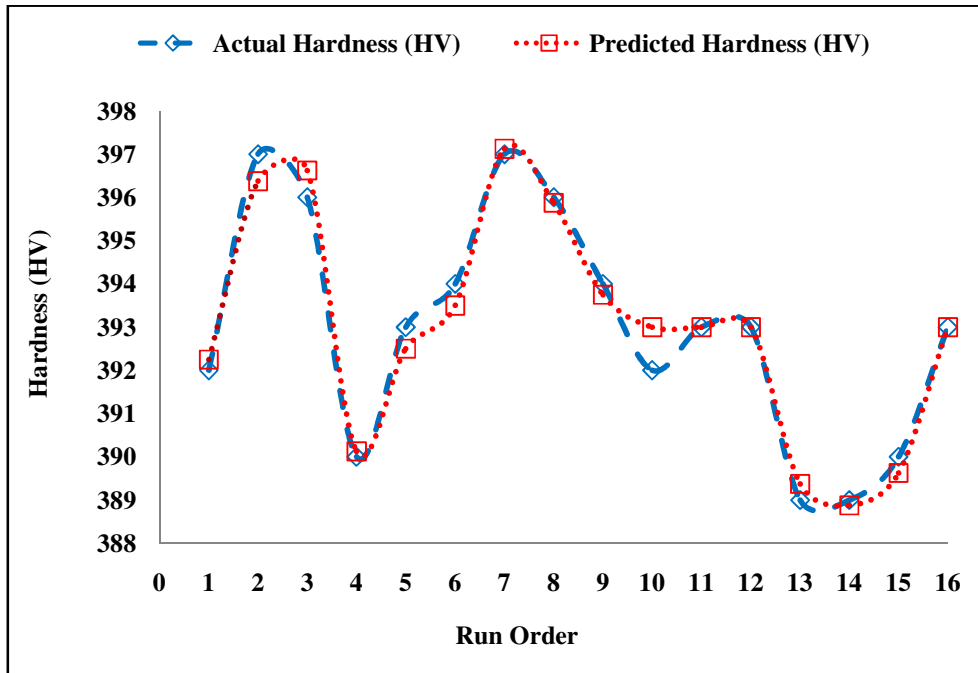
Fig. 5.49. Confirmatory graph on Hardness

Table 4.1 depicts the RSM-BBD design of experiments of composite development and table 4.2 provides all the details of the experimental runs of the WEDM of the developed Ti-TiB$_2$ hybrid composite as obtained by the RSM-BBD model, where the actual and predicted values of RSM-BBD output responses MRR, SR, KW and OC are mentioned and are in close conformity. Fig. 5.50 represents % error which clearly indicates that the deviation of actual from predicted is very nominal giving excellent results. % error of all output responses of experimental runs are below 2% except for the KW (2.35 %) and OC (8.89 %) of run 4 which has to be minimized by taking new experimental reading in same input condition. Fig. 5.51-5.54 represents confirmatory graphs of actual and predicted output responses with respect to experimental runs which represent excellent agreement of test results. From table 5.8, results are validated using confirmatory tests where the data mean is within the domain space. Table 5.9 portrays validation test where the optimal solution is further enhanced by 1.75% when contrasted with desirability to FTOPSIS,

0.73% when evaluated with FTOPSIS to DGRA and 1.02% when evaluated with desirability to DGRA. The output responses are improved to a greater extent when compared with the experimental and the predicted optimized results. MRR is improved by 1.463%, SR by 13.221%, KW by 1.594% and OC by 6.024%. The confirmation graphs between the predicted and experimental performance measures following outstanding concurrence and close proximity with one other. All the performance measures are enhanced to a superior extent when evaluated with the experimental and the predicted optimized results. From the above figures it is evident that nominal deviations are there which can be due to machine chatter; unstable vibration and improper dielectric flush which can again be controlled at optimum conditions.
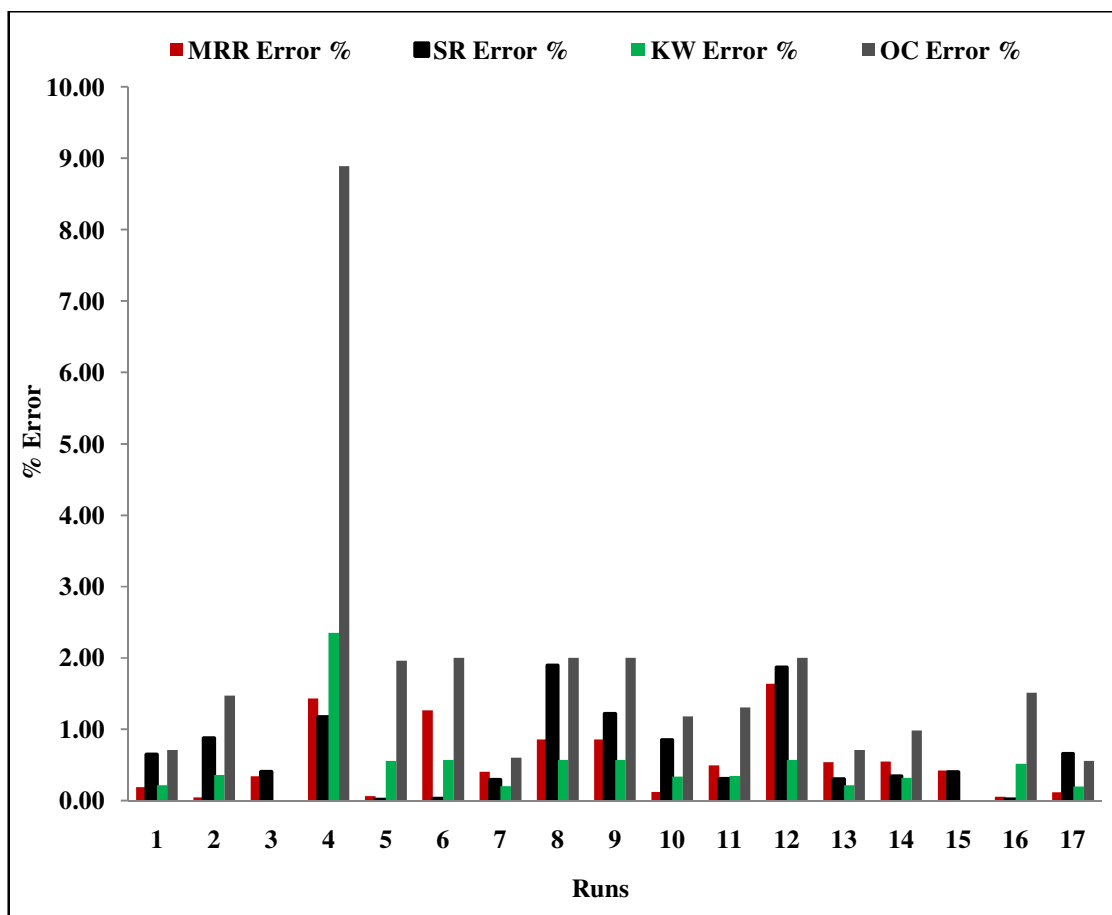
Fig. 5.50. % Error calculation of performance measures after WEDM
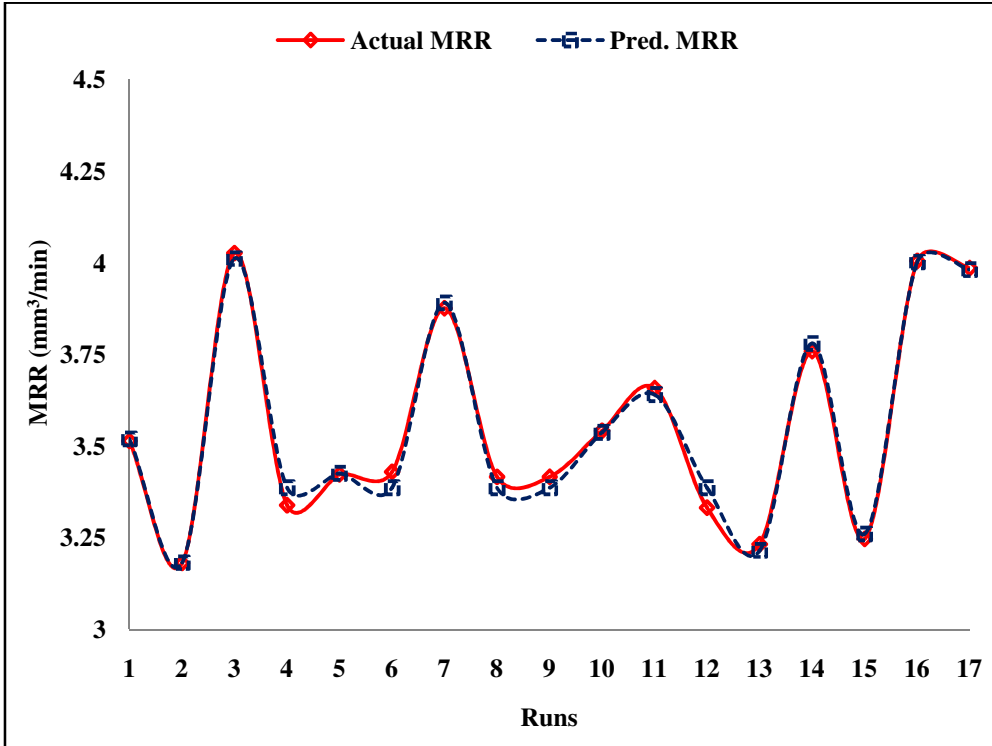
Fig. 5.51. Confirmatory graph on MRR responses
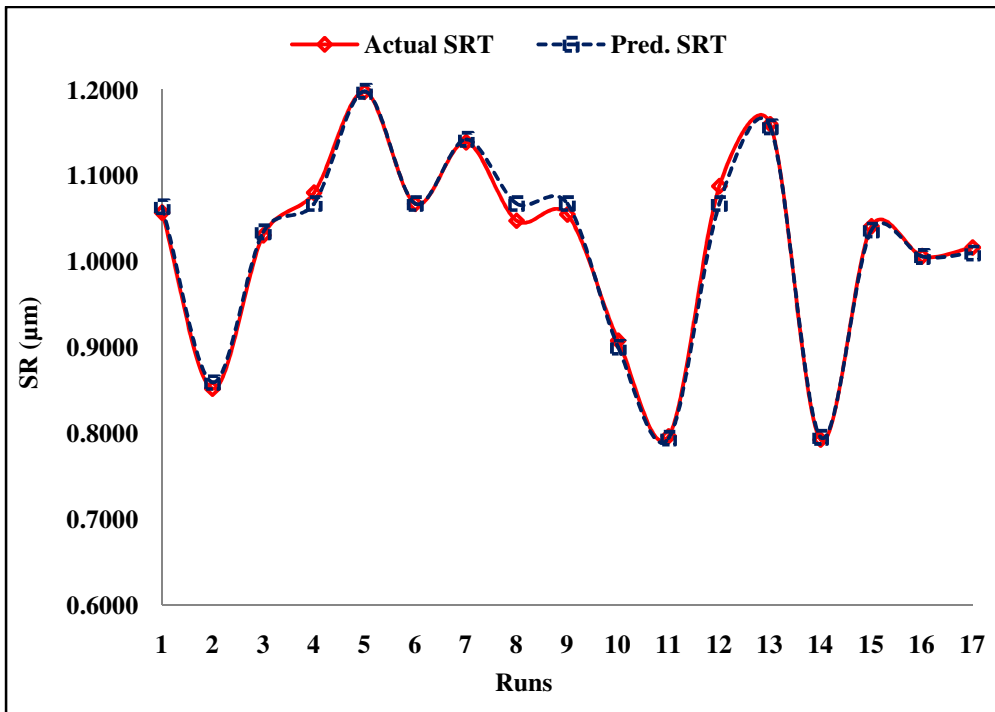
Fig. 5.52. Confirmatory graph on SR responses
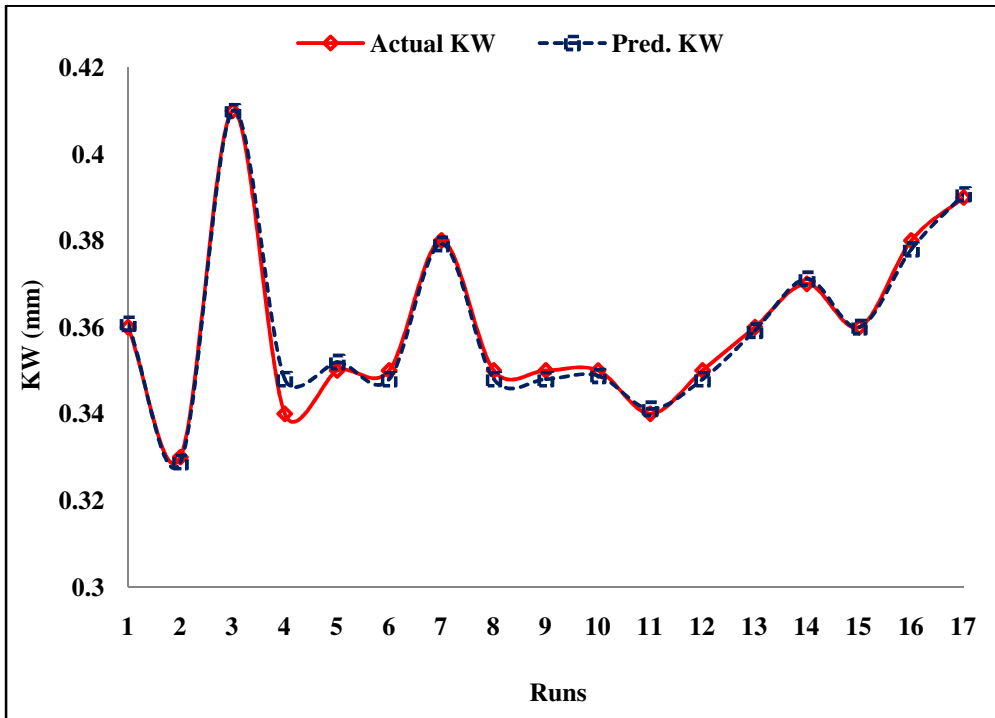
Fig. 5.53. Confirmatory graph on KW responses
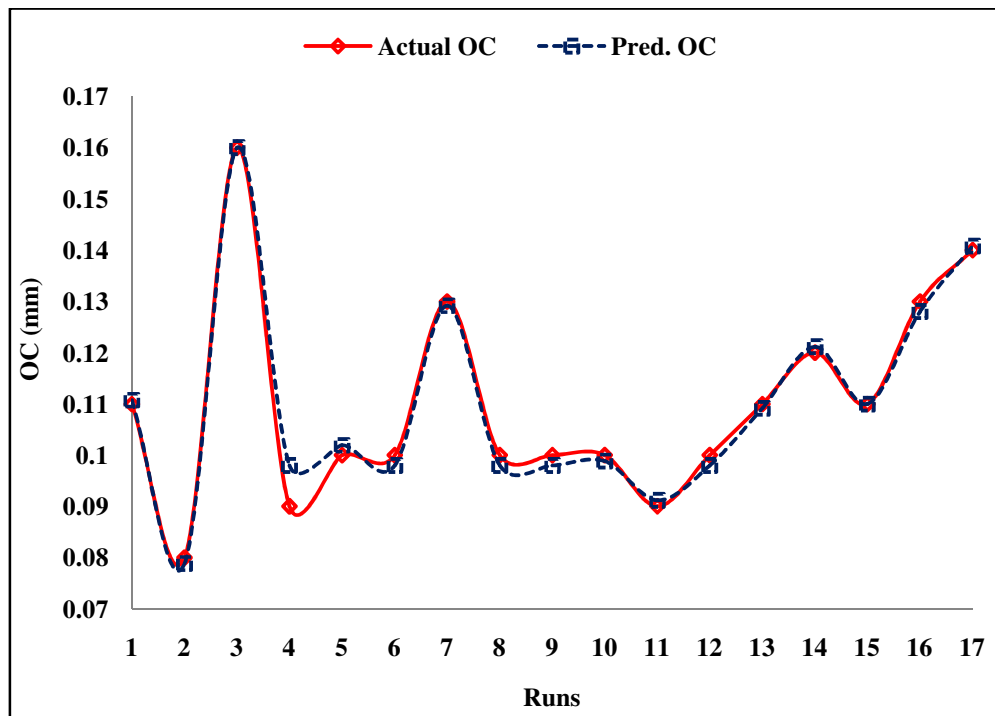
Fig. 5.54. Confirmatory graph on OC responses

114

Table 5.8. Results of confirmatory test after WEDM

Response Solution	Predicted Mean	Predicted Median	95% PI low	Data Mean	95% PI high
MRR	3.60565	3.60565	3.53474	3.5352	3.67657
SR	1.39314	1.39197	1.31093	1.42659	1.48076
KW	0.34542	0.34542	0.3387	0.3475	0.352141
OC	0.0954204	0.0954204	0.0887	0.0975	0.102141

Table 5.9. Validation test and %improvement in MOO using DGRA in WEDM

Machining Parameters			WEDM Performance Measures						
Power (W)	Time Off (µs)	Peak Current (A)	Responses	Optimized value	% improvement (%)	MRR (mm^3/min)	SR (µm)	KW (mm)	OC(mm)
7	30	10	Measured			3.6584	1.576	0.34	0.09
7.3704	27.8665	9.70767	Predicted by Desirability	0.716	1.75	3.60565	1.39197	0.34542	0.09542204
6	20	8	Predicted by FTOPSIS	0.7285637	0.73	**% improvement (%)**			
6	25	10	Predicted by DGRA	0.7233158	1.02	1.462981709	13.2208	1.594118	6.02448889

CHAPTER 6

6. Conclusions

6.1. Conclusions

This present investigation infers the development of a novel TMC by LENS process, microstructural characterization, and optimization of performance measures of composite development and machining by WEDM. The optimal solution of laser performance measures is determined using a novel MOO called DGA and WEDM performance measures by a new MOO named DGRA. The experimental results are further compared with advanced MCDM methods like FTOPSIS for % improvement analysis. The chief concluding points from this present investigation are:

1. CR is inversely proportional to energy input/area. Enhanced CR stimulates stumpy energy input/area because of the increment in thermal gradients near the vicinity of the melt pool and vice-versa. CR also augments with the enhancement in V and diminishes with the enhancement in P.

2. H augments with the increment in the combining effect of P and V and the merging effect of P and E; but remains invariable in the combination of V and E. Optimum results are obtained at an elevated hardness of 396 HV and cooling rate of -2621022.531 K/s at 350/10 laser process parameter.

3. The developed novel TMC possesses superior tribo-mechanical properties when fabricated after the LENS process. SEM images infer the optimum and best condition of laser parameters at 350 W laser power and 10 mm/s scan speed. More formation of white layers is evident portentous excellent dispersal of TiB_2 particles owing to proper interfacial bonding. Complete melting only occurs when the laser power is 350 W, but

additional augmentation in laser power to 400 W causes overheating owing to thick crack formation.

4. The optimized solution is attained after the desirable genetic algorithm when P is 350.956 W, V is 12.371 mm/s, E is 49.475 J/mm^2, CR is -3146515.795 K/s, and H is 395.097 HV, and combined desirability is 0.838. Optimization is additionally enhanced by 20.049% of CR when evaluated with DGA.

5. MRR and SR enhance with an increment of P and IP. MRR also amplifies with a reduction in Toff. SR enhances with an increment in IP and decreases with an increment in Toff. KW and OC are directly proportional to P, IP, and Toff. Therefore, minimum values of these performance measures are mandatory for better results and productivity.

6. It is pragmatic that MRR is highly dependent on electrical and thermal conductivity. When P and IP increase, it is evident that MRR also improves for the high amplification of heat energy resulting in a high discharge current. MRR reduces with the enhancement of Toff due to low discharge current. Therefore, higher Toff results in lesser melting in the gap. Also, higher Toff results in improper dielectric flushing of removed material.

7. The augmentation of SR with the enhancement of IP and diminishes with the enhancement in Toff is due to longer spark duration, ensuing in more discharge energy per spark. It is also perceptible that due to enhancement in Toff, there is a reduction in SR due to low discharges for a conscientious period ensuing in minor crater formation with a negligible micro-damage.

8. The developed novel TMC fabricated by the LENS process possesses improved tribo-mechanical properties like Young's modulus (550 GPa), coefficient of thermal expansion (8.6x10^{-6} /K), Hardness (396 HV), Yield strength in compression (945-1020 MPa),

Ultimate compressive strength (1020-1096 MPa) and Elongation (25-32.5%), and the microstructure depicts an excellent interfacial bonding of TiB_2 with Ti.

9. The WEDM process parameters at the optimized solution are P, 7.3704 W, Toff, 27.8665 µs, IP, 9.70767 A, and performance measures are MRR, 3.60565 mm^3/min, SR, 1.39197 µm, KW, 0.34542 mm, and OC, 0.09542204 mm. The desirability of all the input process parameters is 1, MRR is 0.5023, SR is 0.8642, KW is 0.8072, OC is 0.8072, and combined desirability is 0.716.

10. The variation in the ranking of performance measures in both the MCDM methods is because in FTOPSIS (coupled with FAHP), equivalent normalized weights are considered in the weightage matrix of DM. This weightage matrix is dependent on the COA criteria. But in DGRA, no such criteria weights are considered. FTOPSIS deals with only the experimental output responses but DGRA considers both the experimental and predicted responses. DGRG mean value (0.5953707) is higher than that of the closeness coefficient mean value of FTOPSIS (0.5048964) owing to better results in optimization under DGRA. The mean values of CC_i is 0.5049 and of δ_i is 0.5954, indicate better-optimized results in the proposed algorithm DGRA with an improvement of 17.924 %.

11. Sensitivity analysis has been conceded for robustness and sensitivity of four decision makers' preference on the optimality of the performance measures for the DGRG means, and FTOPSIS means where it is pragmatic that peak current contributes the maximum main effect in both the MCDM methods, thereby being designated as rank 1.

12. The graph between actual and predicted output responses depicts excellent conformity, which convinces this research to be on the correct path. The confirmatory tests infer the

validated results where the data mean is within the domain space of 95% PI low and 95% PI high.

13. Optimization is further improved by 1.75%, 0.73%, and 1.02% when contrasted with desirability to FTOPSIS, FTOPSIS to DGRA, and desirability to DGRA. MRR is improved by 1.463%, SR by 13.221%, KW by 1.594%, and OC by 6.024%.

Results infer that this novel DGA technique has more ascendancy in accomplishing the optimal solution in MOO problems. Also, the TMC is favorable for machining with the most efficient non-traditional machining process WEDM. Results infer that the approach of DGRA has superiority in obtaining the optimal solution rather than the desirability function in multi-objective optimization problems. Results conclude that the DGRA technique has more dominance in achieving the optimal solution over the desirability function in MOO problems.

6.2. Achievements

The achievements of the work lie in the characterization and microstructural analysis of the experimental run-orders of LENS developed novel TMC. Major input laser process parameters are varied and optimal solutions for performance measures are identified. Furthermore, the experimental results are compared with novel MOO called DGA and improved results are obtained by % improvement. The chief contributions of this present investigation are:

1. The prime novelty of this research lies in the proposed algorithm of the optimization technique called desirable genetic algorithm which is a combination of desirability function and genetic algorithm where a new titanium composite material is developed by LENS, which minimizes the error and validates the experimental results.

2. Further, another novel optimization algorithm is developed known as desirable grey relational analysis which is a combination of desirability function and grey relational analysis where machining is carried on the developed TMC and an optimal solution is identified. Improved tribo-mechanical properties are developed and the microstructure depicts an excellent interfacial bonding of TiB_2 with Ti.

3. The experimental and the predicted results are then compared with the multi-criteria decision-making (MCDM) method like FTOPSIS coupled with FAHP for criteria weights and improved statistical results are obtained. The investigation is done on the response surface methodology on performance measures like MRR, SR, KW, and OC.

4. An optimal solution is identified and authenticated after the confirmatory tests, where the experimental and predicted results provide excellent conformity and close agreement with each other.

5. This research work provides the contemporary state-of-the-art of enhancement of tribo-mechanical properties like corrosion, wear, fatigue resistant and biocompatible properties, when compared to pure titanium and other titanium alloys, to make complex shapes for various industrial applications, and other biomedical applications specifically in bones, hips, dental problems, knee replacement enucleation and have an assortment of various other surgical instruments.

6.3. Scope for Future Works

➤ The presented work relates to the development of novel TMC by LENS process and machining by WEDM, which can be additionally deployed for advanced hybrid composite materials reinforcing with Ti-6Al-4V, IN625, and IN718 by varying the % composition of mass or volume. Proper distribution of powder stream can be obtained by

incorporating powder transport and functional grading. The varying proportion of distribution of powder flux which designates the mass flow rate can be further studied in deposition modeling.

➢ This model can be further improved with the optimality test of combination of powder flow over melt pool, for the study of multi-track and multi-layer deposition. Complete analysis of thermal responses can be performed for diverse scanning techniques and assortment of strategies of depositions.

➢ A promising area can be the investigation of deposition directions on quality and accuracy, adaptive process control, and deposition strategy to manifest the anisotropy of the fabrication process.

➢ In the future, more advanced MOO techniques like ANN and PSO may be incorporated with the desirability function to maximize production at minimum cost in the smallest amount of machining time for sustainable manufacturing.

➢ Also, other process parameters like wire tension and wire feed can be varied along with the existing process parameters used in this research to obtain the effects on other performance measures like specific cutting edge and wire wear rate along with the existing output responses and combined desirability can be obtained for maximum and cost-effective products in least machining time for sustainable manufacturing.

➢ More tribo-mechanical and metallurgical properties can be determined. TEM and XRD can be incorporated in the future. CCD can be implemented and compared with the existing RSM-BBD model which may be much more economic and efficient for machining complicated complex silhouettes. Better alternatives of dielectrics and recycling of wire electrodes can be implemented in the future for better results.

REFERENCES

[1] Gu L, Li L, Zhao W, et al. Electrical Discharge Machining of Ti6Al4V with a Bundled Electrode. *Int J Mach Tool Manu*. 2012; 53: 100-106.

[2] Elias CN, Lima JHC, Valiev R, et al. Biomedical Applications of Titanium and its Alloys. *Bio Mater Sci*. 2008; 60: 46-49.

[3] Younas M, Jaffery SHI, Khan M, et al. Multi-objective optimization for sustainable turning Ti6Al4V alloy using grey relational analysis (GRA) based on analytic hierarchy process (AHP). *Int J Adv Manuf Technol*. 2019; 105: 1175–1188.

[4] Kumar A, Kumar V and Kumar J. Multi-response optimization of process parameters based on response surface methodology for pure titanium using WEDM process. *Int J Adv Manuf Technol*. 2013; 68: 2645–2668. https://doi.org/10.1007/s00170-013-4861-9

[5] Kumar A, Kumar V and Kumar J. Surface integrity and material transfer investigation of pure titanium for rough cut surface after wire electro discharge machining. *Proc. IMechE Part B: J. Eng. Manuf*. 2014; 228: 880–901.

[6] Kumar A, Kumar V and Kumar J. Investigation of machining parameters and surface integrity in wire electric discharge machining of pure titanium. *Proc. IMechE Part B: J. Eng. Manuf*. 2013; 227: 972–992.

[7] Kumar A, Kumar V and Kumar J. Surface crack density and recast layer thickness analysis in WEDM process through response surface methodology. *Mach. Sci. Technol. Int. J*. 2016; 20: 201–230. https://doi.org/10.1080/10910344.2016.1165835

[8] Saji VS, Jeong YH, Yu JW, et al. Corrosion Behavior of Ti-13Nb-13Zr and Ti-6Al-4V Alloys for Biomaterial Application. *Corros Sci Technol*. 2010; 9: 12-15.

[9] Fleck C and Eifler D. Corrosion, Fatigue and Corrosion Fatigue Behavior of Metal Implant

Materials, Especially Titanium Alloys. *Int J Fatigue*. 2010; 32: 929-935.

[10] Niu HZ, Xiao SL, Kong FT, Zhang CJ, Chen YY. Microstructure characterization and mechanical properties of TiB$_2$/TiAl in situ composite by induction skull melting process. *Mater. Sci. Eng. A*. 2012; 532: 522–527. https://doi.org/10.1016/j.msea.2011.11.017

[11] Attar H, Ehtemam-Haghighi S, Kent D, Wu X, Dargusch MS. Comparative study of commercially pure titanium produced by laser engineered net shaping, selective laser melting and casting processes. *Mater. Sci. Eng. A*. 2017; 705: 385–393. https://doi.org/10.1016/j.msea.2017.08.103

[12] Hu Y, Ning F, Wang H, Cong W, Zhao B. Laser engineered net shaping of quasi continuous network microstructural TiB reinforced titanium matrix bulk composites: microstructure and wear performance. *Optics Laser. Technol*. 2018; 99: 174–183. https://doi.org/10.1016/j.optlastec.2017.08.032

[13] Hu Y, Cong W, Wang X, Li Y, Ning F, Wang H. Laser deposition-additive manufacturing of TiB-Ti composites with novel three-dimensional quasi-continuous network microstructure: effects on strengthening and toughening. *Compos. B Eng*. 2018; 133: 91–100. https://doi.org/10.1016/j.compositesb.2017.09.019

[14] Attar H, Bönisch M, Calin M, Zhang LC, Zhuravleva K, Funk A, Scudino S, Yang C, Eckert J. Comparative study of microstructures and mechanical properties of in situ Ti–TiB composites produced by selective laser melting, powder metallurgy, and casting technologies. *J. Mater. Res*. 2014; 29(17): 1941–1950. https://doi.org/10.1557/jmr.2014.122

[15] Khan MA, Jaffery SHI, Khan M, et al. Multi-objective optimization of turning titanium-based alloy Ti-6Al-4V under dry, wet, and cryogenic conditions using gray relational analysis (GRA). *Int J Adv Manuf Technol*. 2020; 106: 3897–3911.

[16] Lin H C, Lin K M and Chen Y C 2000 A study on the machining characteristics of TiNi shape memory alloys. *J. Mater. Process. Technol*. 105: 327-332

[17] Chen S L, Yan B H and Huang F Y 1999 Influence of kerosene and distilled water as dielectrics on the electric discharge machining characteristics of Ti–6A1–4V. *J. Mater. Process. Technol*. 87: 107-111

[18] Alias A, Abdullah B and Abbas N M 2012 Influence of Machine Feed Rate in WEDM of Titanium Ti-6Al-4V with constant Current (6A) using brass wire. *Procedia Eng*. 41: 1806 – 1811

[19] Yadav RN. A hybrid approach of Taguchi-Response Surface Methodology for modeling and optimization of Duplex Turning process. *Measurement*. 2017; 100: 131-138. https://doi.org/10.1016/j.measurement.2016.12.060

[20] Ananthakumar K, Rajamani D, Balasubramanian E, Paulo Davim J. Measurement and optimization of multi-response characteristics in plasma arc cutting of Monel 400™ using RSM and TOPSIS. *Measurement*. 2019; 135: 725-737. https://doi.org/10.1016/j.measurement.2018.12.010

[21] Li N, Sheikh-Ahmad JY, El-Sinawi A, Krishnaraj V. Multi-objective optimization of the trimming operation of CFRPs using sensor-fused neural networks and TOPSIS. *Measurement*. 2019; 132: 252-262. https://doi.org/10.1016/j.measurement.2018.09.057

[22] Yu T, Yang L, Zhao Yu, Sun J, Li B. Experimental research and multi-response multi-parameter optimization of laser Experimental research and multi-response multi-parameter optimization of laser cladding Fe313. *Opt. Laser Technol*. 2018; 108: 321-332. https://doi.org/10.1016/j.optlastec.2018.06.030

[23] Jin J, Zhou S, Zhao Y, Zhang Q, Wang X, Li W, Chen D, Zhang L. Refined microstructure

and enhanced wear resistance of titanium matrix composites produced by selective laser melting. *Opt. Laser Technol.* 2021; 134: 106644. https://doi.org/10.1016/j.optlastec.2020.106644

[24] Cheng D, Zhang J, Shi T, Li G, Shi J, Lu L, Fu G. Microstructure and mechanical properties of additive manufactured Ti-6Al-4V components by annular laser metal deposition in a semi-open environment. *Opt. Laser Technol.* 2021; 135: 106640. https://doi.org/10.1016/j.optlastec.2020.106640

[25] Chen T, Wu W, Li W, Liu D. Laser cladding of nanoparticle TiC ceramic powder: Effects of process parameters on the quality characteristics of the coatings and its prediction model. *Opt. Laser Technol.* 2019; 116: 345-355. https://doi.org/10.1016/j.optlastec.2019.03.048

[26] Shivakoti I, Kibria G, Pradhan BB. Predictive model and parametric analysis of laser marking process on gallium nitride material using diode pumped Nd:YAG laser. *Opt. Laser Technol.* 2019; 115: 58-70. https://doi.org/10.1016/j.optlastec.2019.01.035

[27] Datta S, Raza MS, Das AK, Saha P, Pratihar DK. Experimental investigations and parametric optimization of laser beam welding of NiTinol sheets by metaheuristic techniques and desirability function analysis. *Opt. Laser Technol.* 2020; 124: 105982. https://doi.org/10.1016/j.optlastec.2019.105982

[28] Gao Z, Shao X, Jiang P, Cao L, Zhou Q, Yue C, Liu Y. Parameters optimization of hybrid fiber laser-arc butt welding on 316L stainless steel using Kriging model and GA. *Opt. Laser Technol.* 2016; 83: 153-162. https://doi.org/10.1016/j.optlastec.2016.04.001

[29] Kumar C, Das M, Paul CP, Singh B. Experimental investigation and metallographic characterization of fiber laser beam welding of Ti-6Al-4V alloy using response surface method. *Opt Lasers Eng.* 2017; 95: 52-68. https://doi.org/10.1016/j.optlaseng.2017.03.013

126

[30] Wang X, Chen H, Liu H, Li P, Yan Z, Huang C, Zhao Z, Gu Y. Simulation and optimization of continuous laser transmission welding between PET and titanium through FEM, RSM, GA and experiments. *Opt Lasers Eng*. 2013; 51(11): 1245-1254. https://doi.org/10.1016/j.optlaseng.2013.04.021

[31] Rong Y, Zhang Z, Zhang G, Yue C, Gu Y, Huang Y, Wang C, Shao X. Parameters optimization of laser brazing in crimping butt using Taguchi and BPNN-GA. *Opt Lasers Eng*. 2015; 67: 94-104. https://doi.org/10.1016/j.optlaseng.2014.10.009

[32] Weisheit A, Rittinghaus S, Dutta A, Majumdar JD. Studies on the effect of composition and pre-heating on microstructure and mechanical properties of direct laser clad titanium aluminide. *Opt Lasers Eng*. 2020; 131: 106041. https://doi.org/10.1016/j.optlaseng.2020.106041

[33] Marshall GJ, Young WJ, Thompson SM, Shamsaei N, Daniewicz SR, Shao S. Understanding the microstructure formation of Ti-6Al-4V during direct laser deposition via in-situ thermal monitoring. *J. Occup. Med*. 2016; 68(3): 778–790. https://doi.org/10.1007/s11837-015-1767-z

[34] Bandyopadhyay A, Espana F, Balla VK, Bose S, Ohgami Y, Davies NM. Influence of porosity on mechanical properties and in vivo response of Ti6Al4V implants. *Acta Biomater*. 2010; 6(4): 1640–1648. https://doi.org/10.1016/j.actbio.2009.11.011

[35] Qiu C, Ravi GA, Dance C, Ranson A, Dilworth S, Attallah MM. Fabrication of large Ti–6Al–4V structures by direct laser deposition. *J. Alloy. Comp*. 2015; 629: 351–361. https://doi.org/10.1016/j.jallcom.2014.12.234

[36] Sterling AJ, Torries B, Shamsaei N, Thompson SM, Seely DW. Fatigue behavior and failure mechanisms of direct laser deposited Ti–6Al–4V. *Mater. Sci. Eng. A*. 2016; 655: 100–112.

https://doi.org/10.1016/j.msea.2015.12.026

[37] Manjaiah M, Narendranath S and Basavarajappa S 2014 A review on machining of titanium based alloys using EDM and WEDM. *Rev. Adv. Mater. Sci*. 36: 89-111

[38] Bose S, Nandi T. Microstructural characterization and measurement of laser responses of lens developed novel titanium matrix composite. *Eur. Phys. J. Plus*. 2021; 136: 978. https://doi.org/10.1140/epjp/s13360-021-01951-6

[39] Bose S, Nandi T. A novel optimization algorithm on surface roughness of WEDM on titanium hybrid composite. *Sādhanā*. 2020; 45(1): 236. https://doi.org/10.1007/s12046-020-01472-5

[40] Bose S, Nandi T. Novel approach in experimental and statistical investigations on titanium matrix composite. *Bull Mater Sci*. 2021; 44(1): 46. https://doi.org/10.1007/s12034-020-02330-0

[41] Abidi MH, Al-Ahmari AM, Umer U, Rasheed MS. Multi-objective optimization of micro-electrical discharge machining of nickel-titanium-based shape memory alloy using MOGA-II. *Measurement*. 2018; 125: 336-349. https://doi.org/10.1016/j.measurement.2018.04.096

[42] Kumar SPL. Measurement and uncertainty analysis of surface roughness and material removal rate in micro turning operation and process parameters optimization. *Measurement*. 2019; 140: 538-547. https://doi.org/10.1016/j.measurement.2019.04.029

[43] Kumar SPL. Experimental investigations and empirical modeling for optimization of surface roughness and machining time parameters in micro end milling using Genetic Algorithm. *Measurement*. 2018; 124: 386-394. https://doi.org/10.1016/j.measurement.2018.04.056

[44] Nwobi-Okoye CC, Uzochukwu CU. RSM and ANN modeling for production of Al 6351/ egg shell reinforced composite: Multi objective optimization using genetic algorithm. *Mater.*

Today Commun. 2020; 22: 100674. https://doi.org/10.1016/j.mtcomm.2019.100674

[45] Iqbal M, Naeem UA, Ahmad A, Ghani U, Farid T. Relating groundwater levels with meteorological parameters using ANN technique. *Measurement*. 2020; 164: 108163. https://doi.org/10.1016/j.measurement.2020.108163

[46] Mondal N, Mandal S, Mandal MC. FPA based optimization of drilling burr using regression analysis and ANN model. *Measurement*. 2020; 152: 108163: 107327. https://doi.org/10.1016/j.measurement.2019.107327

[47] Adineh VR, Aghanajafi C, Dehghan GH, Jelvani S. Optimization of the operational parameters in a fast axial flow $CWCO_2$ laser using artificial neural networks and genetic algorithms. *Opt. Laser Technol*. 2008; 40(8): 1000-1007. https://doi.org/10.1016/j.optlastec.2008.03.003

[48] Singh B, Misra JP. Surface finish analysis of wire electric discharge machined specimens by RSM and ANN modeling. Measurement. 2019; 137: 225-237. https://doi.org/10.1016/j.measurement.2019.01.044

[49] Mouralova K, Kovar J, Klakurkova L, Blazik P, Kalivoda M, Kousal P. Analysis of surface and subsurface layers after WEDM for Ti-6Al-4V with heat treatment. *Measurement*. 2018; 116: 556-564. https://doi.org/10.1016/j.measurement.2017.11.053

[50] Mouralova K, Kovar J, Klakurkova L, Bednar J, Benes L, Zahradnicek R. Analysis of surface morphology and topography of pure aluminium machined using WEDM. *Measurement*. 2018; 114: 169-176. https://doi.org/10.1016/j.measurement.2017.09.040

[51] Mouralova K, Kovar J, Klakurkova L, Prokes T, Horynova M. Comparison of morphology and topography of surfaces of WEDM machined structural materials. *Measurement*. 2017; 104: 12-20. https://doi.org/10.1016/j.measurement.2017.03.009

[52] Kumar SS, Uthayakumar M, Kumaran ST, Parameswaran P, Mohandas E, Kempulraj G, Ramesh Babu BS, Natarajan SA. Parametric optimization of wire electrical discharge machining on aluminium based composites through grey relational analysis. *J. Manuf.* 2015; 20(1): 33-39. https://doi.org/10.1016/j.jmapro.2015.09.011

[53] Kavimani V, Soorya Prakash K, Thankachan T. Multi-objective optimization in WEDM process of graphene – SiC-magnesium composite through hybrid techniques. *Measurement*. 2019; 145: 335–349. https://doi.org/10.1016/j.measurement.2019.04.076

[54] Ramesh S, Viswanathan R, Ambika S. Measurement and optimization of surface roughness and tool wear via grey relational analysis, TOPSIS and RSA techniques. *Measurement*. 2016; 78: 63-72. https://doi.org/10.1016/j.measurement.2015.09.036

[55] Hwang CL, Yoon K. Multiple Attribute Decision Making Methods and Applications. Springer, Berlin Heidelberg, 1981. http://dx.doi.org/10.1007/978-3-642-48318-9

[56] Majumder H, Maity K. Prediction and optimization of surface roughness and micro-hardness using GRNN and MOORA-fuzzy-a MCDM approach for nitinol in WEDM. *Measurement*. 2018; 118: 1-13. https://doi.org/10.1016/j.measurement.2018.01.003

[57] Mandal P, Mondal SC. Multi-objective optimization of Cu-MWCNT composite electrode in electro discharge machining using MOPSO-TOPSIS. *Measurement*. 2020; 169: 108347. https://doi.org/10.1016/j.measurement.2020.108347

[58] Dewangan S, Gangopadhyay S, Biswas CK. Study of surface integrity and dimensional accuracy in EDM using Fuzzy TOPSIS and sensitivity analysis. *Measurement*. 2015; 63: 364-376. https://doi.org/10.1016/j.measurement.2014.11.025

[59] Gok A. A new approach to minimization of the surface roughness and cutting force via fuzzy TOPSIS, multi-objective grey design and RSA. *Measurement*. 2015; 70: 100-109.

https://doi.org/10.1016/j.measurement.2015.03.037

[60] Biswas R, Das MC, Bhattacharyya S, Kuar AS, Mitra S. Selection of Nd:YAG laser beam micro-drilling parameters using multi-criteria decision making methods. *Opt. Laser Technol*. 2019; 119: 105596. https://doi.org/10.1016/j.optlastec.2019.105596

[61] Zadeh LA. Fuzzy sets. *Information Control*. 1965; 8(3): 338–353. https://doi.org/10.1016/S0019-9958(65)90241-X

[62] Nădăban S, Dzitac S, Dzitac I. Fuzzy TOPSIS: A General View. *Procedia Computer Science*. 2016; 91: 823-831. https://doi.org/10.1016/j.procs.2016.07.088

[63] Nourbakhsh F, Rajurkar KP, Malshe AP, et al. Wire electro-discharge machining of titanium alloy. *Procedia CIRP.* 2013; 5: 13–18.

[64] Hsieh SF, Chen SL, Lin HC, et al. The machining characteristics and shape recovery ability of Ti–Ni–X (X=Zr,Cr) ternary shape memory alloys using the wire electro-discharge machining. *Int J Mach Tool Manu.* 2009; 49: 509-514.

[65] Kuriakose S and Shunmugam MS. Multi-objective optimization of wire-electro discharge machining process by non-dominated sorting algorithm. *J. Mater. Process. Technol.* 2005; 170: 133–141.

[66] Han F, Jiang J and Yu D. Influence of machining parameters on surface roughness in finish cut of WEDM. *Int J Adv Manuf Technol.* 2007; 34: 538–546.

[67] Sharma A, Garg MP and Goyal KK. Prediction of Optimal Conditions for WEDM of Al 6063/ $ZrSiO_{4(p)}$ MMC. *Procedia Mater. Sci.* 2014; 6: 1024-1033.

[68] Bose S, Nandi, T. Experimental investigation of WEDM on titanium hybrid composite reinforced with boron powder: a novel approach. *Eur. Phys. J. Plus*. 2020; 135: 914. https://doi.org/10.1140/epjp/s13360-020-00904-9

[69] Bose S, Nandi, T. Statistical and experimental investigation using a novel multi-objective optimization algorithm on a novel titanium hybrid composite developed by lens process. *Proc IMechE, Part C: J Mechanical Engineering Science*. 2020; 235(16): 2911-2933. https://doi.org/10.1177/0954406220959101

[70] Bose S, Samanta S, Mandal N, De S, Mistry NS, Koley P, Nandi T. A novel approach in comparison and experimentation of Hybrid Metal Matrix Composites using advanced MCDM methods. *IOP Conf. Series: Mat. Sci. Eng*. 2019; 653: 012003. doi:10.1088/1757-899X/653/1/012003

[71] Bose S, Mandal N, Nandi T. Selection and Experimentation of the Best Hybrid Green Composite Using Advanced MCDM Methods for Clean Sustainable Energy Recovery: A Novel Approach. *Int. J. Math. Eng. Management Sci*. 2020; 5(3): 556-566. https://doi.org/10.33889/IJMEMS.2020.5.3.046

[72] Bose S, Mandal N, Nandi T. Comparative and Experimental study on Hybrid Metal Matrix Composites using Additive Ratio Assessment and Multi-Attributive Border Approximation area Comparison methods varying the different Weight Percentage of the Reinforcements. *Mater. Today Proceedings*. 2020; 22: 1745–1754. https://doi.org/10.1016/j.matpr.2020.03.007

[73] Shandilya P, Rouniyar AK and Saikiran D. Multi-objective parametric optimization on machining of Inconel-825 using wire electrical discharge machining. *Proc IMechE, Part C: J Mechanical Engineering Science* 2020. https://doi.org/10.1177/0954406220917706

[74] Bisaria H and Shandilya P. The machining characteristics and surface integrity of Ni-rich NiTi shape memory alloy using wire electric discharge machining. *Proc IMechE, Part C: J Mechanical Engineering Science* 2019; 233: 1068–1078.

[75] Asghari SAA, Sarband AS and Habibnia M. Optimization of multiple quality characteristics in two-point incremental forming of aluminum 1050 by grey relational analysis. *Proc IMechE, Part C: J Mechanical Engineering Science* 2018; 232: 1–15.

[76] Sharma N, Raj T and Jangra KK. Parameter optimization and experimental study on wire electrical discharge machining of porous Ni40Ti60 alloy. *Proc IMechE, Part B: J Engineering Manufacture* 2015; 231: 956–970.

[77] Rao RV and Pawar PJ. Modelling and optimization of process parameters of wire electrical discharge machining. *Proc IMechE, Part C: J Mechanical Engineering Science* 2009; 223: 1431–1440.

[78] Somashekhar KP, Mathew J and Ramachandran N. Multi-objective optimization of micro wire electric discharge machining parameters using grey relational analysis with Taguchi method. *Proc IMechE, Part C: J Mechanical Engineering Science* 2011; 225: 1742-1753.

[79] Shayan AV, Afza RA and Teimouri R. Parametric study along with selection of optimal solutions in dry wire cut machining of cemented tungsten carbide (WC-Co). *J. Manuf.* 2013; 15: 644-658.

[80] Castañeda A, Castaño VM. Smart frost measurement for anti-disaster intelligent control in greenhouses via embedding IoT and hybrid AI methods. *Measurement*. 2020; 164: 108043. https://doi.org/10.1016/j.measurement.2020.108043

[81] Motahari M, Jafari SM. ANFIS System for Prognosis of Dynamometer High-Speed Ball Bearing Based on Frequency Domain Acoustic Emission Signals. *Measurement*. 2020; 164: 108154. https://doi.org/10.1016/j.measurement.2020.108154

[82] Abedini S, Dong C, Davies IJ. Multi-objective particle swarm optimization of multilayer functionally graded coating systems for improved interfacial delamination resistance. *Mater.*

Today Commun. 2020; 101202. In Press. https://doi.org/10.1016/j.mtcomm.2020.101202

[83] Suresh S, Sujit PB, Rao AK. Particle swarm optimization approach for multi-objective composite box-beam design. *Compos. Struct.* 2007; 81(4): 598-605. https://doi.org/10.1016/j.compstruct.2006.10.008

[84] Wu X, Liang J, Mei J, et al. Microstructures of laser-deposited Ti–6Al–4V. *Mater. Des.* 2004; 25: 137–144.

[85] Yildiz AR. A novel hybrid whale–Nelder–Mead algorithm for optimization of design and manufacturing problems. *Int J Adv Manuf Technol.* 2019; 105: 5091–5104.

[86] Yildiz AR, Mirjalili S, Yildiz BS, et al. A new hybrid Harris hawks-Nelder-Mead optimization algorithm for solving design and manufacturing problems. *Mater Test.* 2019; 61: 735-743.

[87] Champasak P, Panagant N, Pholdee N, et al. Self-adaptive many objective meta-heuristic based on decomposition for many-objective conceptual design of a fixed wing unmanned aerial vehicle. *Aerosp Sci Technol.* 2020; 100: 1-11.

[88] Kurtuluş E, Yildiz AR, Sait SM, et al. A novel hybrid Harris hawks-simulated annealing algorithm and RBF-based metamodel for design optimization of highway guardrails. *Mater Test.* 2020; 62: 251-260.

[89] Yildiz AR, Abderazek H and Mirjalili S. A Comparative Study of Recent Non-traditional Methods for Mechanical Design Optimization. *Arch Computat Methods Eng.* 2019; (in print). https://doi.org/10.1007/s11831-019-09343-x

[90] Meng Z, Li G, Wang X, et al. A Comparative Study of Metaheuristic Algorithms for Reliability-Based Design Optimization Problems. *Arch Computat Methods Eng.* 2020; (in print). https://doi.org/10.1007/s11831-020-09443-z

[91] Yildiz BS. Optimal design of automobile structures using moth-flame optimization algorithm and response surface methodology. *Mater Test.* 2020; 62: 371-377.

[92] Yildiz BS. The mine blast algorithm for the structural optimization of electrical vehicle components. *Mater Test.* 2020; 62: 497-501.

[93] Özkaya H, Yildiz M, Yildiz AR, et al. The equilibrium optimization algorithm and the response surface-based metamodel for optimal structural design of vehicle components. *Mater Test.* 2020; 62: 492-496.

[94] Yildiz AR, Yildiz BS, Sait SM, et al. The Harris hawks, grasshopper and multi-verse optimization algorithms for the selection of optimal machining parameters in manufacturing. *Mater Test.* 2019; 61: 725-733.

[95] Yildiz BS and Yildiz AR. The Harris hawks optimization algorithm, salp swarm algorithm, grasshopper optimization algorithm and dragonfly algorithm for structural design optimization of vehicle components. *Mater Test.* 2019; 61: 744-748.

[96] Yildiz BS. The spotted hyena optimization algorithm for weight-reduction of automobile brake components. *Mater Test.* 2020; 62: 383-388.

[97] Yildiz BS, Yildiz AR, Albak Eİ, et al. Butterfly optimization algorithm for optimum shape design of automobile suspension components. *Mater Test.* 2020; 62: 365-370.

[98] Yildiz BS and Yildiz AR. Comparison of grey wolf, whale, water cycle, ant lion and sine-cosine algorithms for the optimization of a vehicle engine connecting rod. *Mater Test.* 2018; 60: 311–315.

[99] Abderazek H, Yildiz AR and Mirjalili S. Comparison of recent optimization algorithms for design optimization of a cam-follower mechanism. *Knowl-Based Syst.* 2020; 191: 105237.

[100] Hamza F, Abderazek H, Lakhdar S, et al. Optimum design of cam-roller follower

mechanism using a new evolutionary algorithm. *Int J Adv Manuf Technol.* 2018; 99: 1267–1282.

[101] Yildiz BS. A comparative investigation of eight recent population-based optimisation algorithms for mechanical and structural design problems. *Int. J. Vehicle Des.* 2017; 73: 208-218.

[102] Yildiz BS. Natural frequency optimization of vehicle components using the interior search algorithm. *Mater Test.* 2017; 59: 456-458.

Soutrik Bose
26/07/22